

1 **Quantitative structural organization of bulk apical membrane traffic in pollen tubes**

2
3 Gleb Grebnev^a, Mislav Cvitkovic^{b,c,1}, Carolin Fritz^a, Giampiero Cai^d, Ana-Suncana Smith^{b,c} and
4 Benedikt Kost^{a,2}

5
6
7 ^aCell Biology, Department of Biology, Friedrich-Alexander-University Erlangen Nuremberg,
8 Erlangen, Germany

9 ^bPULS Group, Department of Physics, Friedrich-Alexander-University Erlangen Nuremberg,
10 Erlangen, Germany

11 ^cGroup for Computational Life Sciences, Division of Physical Chemistry, Ruđer Bošković Institute,
12 Zagreb, Croatia

13 ^dDepartment of Life Sciences, University of Siena, Italy

14
15 ¹Present address: Department of Physics, University of Split, Croatia

16 ²Corresponding author: benedikt.kost@fau.de

17

18

19 The author responsible for distribution of materials integral to the findings presented in this article
20 in accordance with the policy described in the Instructions for Authors (www.plantphysiol.org) is:

21

22 Benedikt Kost

23 University of Erlangen-Nuremberg

24 Staudtstrasse 5

25 91058 Erlangen, GERMANY

26 phone: +49 9131 85 28216

27

28

29 **Short title:**

30 Apical membrane traffic at the pollen tube tip

31

32

33 **Summary:**

34 Massive secretion underlying pollen tube tip growth delivers proteins and lipids to the same apical
35 plasma membrane domain and is balanced by endocytic lipid recycling in a defined subapical
36 region.

37

38 **Author contributions:**

39 GG acquired most of the experimental data and contributed to the design of the experiments, to the
40 analysis and interpretation of experimental data as well as to the writing of the manuscript; CF
41 contributed all long-term time-lapse imaging data; MC and A-SS developed, analyzed and
42 interpreted the mathematical model and contributed to the writing of the manuscript; GC
43 participated in the characterization of F-actin and TGN functions in membrane traffic; BK
44 conceived and administered the study, was responsible for data analysis/interpretation and wrote the
45 final version of the manuscript. B.K. agrees to serve as the author responsible for contact and
46 ensures communication.

47

48

49 **Funding information:**

50 This research was funded by the “German Research Foundation” (DFG) within the framework of
51 the “Research Training Group 1962” (Projects 7 [GG, BK] and 10 [MC, A-SS]), and through the
52 ERC StG MembranesAct 2013-33728 [MC, A-SS]. It was further supported by two DFG “Major

53 Equipment Grants” awarded to BK: INST90/1074-1FUGG (SP8 DIVE-FALCON microscope) and
54 INST90/1025-1FUGG (plant growth chamber facility for tobacco).
55

56 **ABSTRACT**

57 Pollen tube tip growth depends on balancing secretion of cell wall material with endocytic recycling
58 of excess material incorporated into the plasma membrane (PM). The classical model of tip growth,
59 which predicts bulk secretion occurs apically and is compensated by subapical endocytosis, has
60 been challenged in recent years. Many signaling proteins and lipids with important functions in the
61 regulation of membrane traffic underlying tip growth associate with distinct regions of the pollen
62 tube PM, and understanding the mechanisms responsible for the targeting of these regulatory factors
63 to specific PM domains requires quantitative information concerning the sites of bulk secretion and
64 endocytosis. Here, we quantitatively characterized the spatial organization of membrane traffic
65 during tip growth by analyzing steady-state distributions and dynamics of FM4-64-labeled lipids
66 and YFP-tagged transmembrane (TM) proteins in tobacco (*Nicotiana tabacum*) pollen tubes
67 growing normally or treated with Brefeldin A to block secretion. We established that 1) secretion
68 delivers TM proteins and recycled membrane lipids to the same apical PM domain, and 2) FM4-64-
69 labeled lipids, but not the analyzed TM proteins, undergo endocytic recycling within a clearly
70 defined subapical region. We mathematically modelled the steady-state PM distributions of all
71 analyzed markers to better understand differences between them and to support the experimental
72 data. Finally, we mapped subapical F-actin fringe and trans-Golgi network positioning relative to
73 sites of bulk secretion and endocytosis to further characterize functions of these structures in apical
74 membrane traffic. Our results support and further define the classical model of apical membrane
75 traffic at the tip of elongating pollen tubes.

76

77 **INTRODUCTION**

78 Pollen tube tip growth is essential for plant reproduction and is widely employed as a model to
79 investigate directional cell expansion in plants, which plays a central role in single cell as well as
80 organ morphogenesis. Pollen tubes expand very rapidly at rates of several $\mu\text{m}/\text{min}$ strictly in one
81 direction based on massive local secretion of cell wall material at the tip (Hepler et al., 2001; Kost,
82 2008; Yalovsky et al., 2008). The pollen tube cytoplasm displays extreme polarization: poorly
83 characterized cellular and molecular mechanisms are responsible for the massive accumulation of
84 vesicles containing cell wall material within an inverted cone-shaped apical region (“apical region
85 of vesicle accumulation”: ARVA), behind which all other cell organelles are located (Derksen et al.,
86 1995; Hepler et al., 2001; Cheung and Wu, 2007; Lancelle and Hepler, 1992). These organelles
87 include a detached trans-Golgi network (TGN) compartment, which depending on interactions with
88 a subapical cortical F-actin fringe, is stably positioned directly behind the ARVA and may generate
89 the secretory vesicles observed within this region (Stephan et al., 2014). The F-actin fringe is
90 essential for tip growth (Bou Daher and Geitmann, 2011; Dong et al., 2012; Rounds et al., 2014;

91 Stephan et al., 2014), possibly because of additional direct functions in the transport of secretory
92 vesicles (Cardenas et al., 2008; Bou Daher and Geitmann, 2011; Dong et al., 2012; Rounds et al.,
93 2014) or in local endocytic membrane internalization (Samaj et al., 2006; Galletta and Cooper,
94 2009; Moscatelli et al., 2012; Meunier and Gutierrez, 2016; Li et al., 2018). Most other cytoplasmic
95 organelles are rapidly transported along longitudinally oriented F-actin cables back and forth
96 between the two ends of elongating pollen tubes (“cytoplasmic streaming”) (Hepler et al. 2001;
97 Cheung and Wu 2006; Cai et al., 2015).

98

99 Cell wall biogenesis at the tip of growing pollen tubes requires secretion at an 8-10x higher rate
100 than required for plasma membrane (PM) extension (Picton and Steer, 1983; Derksen et al., 1995;
101 Bove et al., 2008; Ketelaar et al., 2008). Assuming that secretory vesicles completely fuse with the
102 PM rather than delivering their cargo based on temporary “kiss-and-run” fusion, this implies that
103 secretion results in massive incorporation of excess material into the PM, which needs to be
104 endocytically recycled. “Kiss-and-run” fusion has been proposed to occur in neuronal synapses
105 decades ago, but has remained controversial as this process is difficult to experimentally investigate
106 and unequivocally demonstrate (He and Wu, 2007; Alabi and Tsien, 2013). In fact, no experimental
107 evidence for “kiss-and-run” fusion in growing pollen tubes has been reported to date. By contrast,
108 data obtained based on evanescent wave (TIRF) microscopy strongly support complete fusion of
109 FM4-64 labeled secretory vesicles with the PM of *Picea meyeri* pollen tubes (Wang et al., 2006).

110

111 The classical model of pollen tube tip growth (Steer and Steer, 1989; Derksen et al., 1995; Kost,
112 2008) is supported by compelling albeit largely circumstantial evidence and has been challenged in
113 recent years (Grebnev et al., 2017). It predicts that massive secretion required for cell wall
114 biogenesis occurs apically and is compensated by subapical endocytic recycling of excess PM
115 material. In addition to delivering material needed for cell wall construction, massive apical
116 secretion is also proposed to be essential for the coordination of signaling processes regulating tip
117 growth (Luo et al., 2017; Li et al., 2018). As the pollen tube cell wall exclusively expands within
118 the apical dome, it needs to display plasticity within this region paired with sufficient stiffness to
119 prevent cell bursting caused by turgor pressure that drives cell elongation (Bosch et al., 2005; Bosch
120 and Hepler, 2005; Zerzour et al., 2009). Specifically at the apex, the pollen tube cell wall is
121 primarily composed of methyl-esterified pectins (Bosch et al. 2005), which are synthesized in the
122 Golgi and delivered to the cell surface by secretion (Hepler et al., 2013; Mollet et al., 2013).
123 Extracellular pectin methylesterases (PMEs) as well as inhibitors of these enzymes (PMEIs) are
124 also secreted into the cell wall (Hepler et al., 2013; Mollet et al., 2013). Specific PMEI
125 accumulation at the apex (Rockel et al. 2008) appears to contribute to the restriction of PME-

126 mediated pectin de-esterification, which enhances cell wall stiffness, to lateral regions of the cell
127 wall (Hepler et al. 2013; Mollet et al. 2013).

128

129 Fluorescence recovery after photobleaching (FRAP) analysis established that after photobleaching,
130 fluorescence emitted by a secreted PME-GFP fusion protein first recovers within the pollen tube
131 cell wall at the extreme apex before it spreads to more lateral regions (Wang et al., 2013). This
132 observation is supported by *in vivo* analyses of the delivery of fluorescent proteins fused to the
133 receptor-like kinase AtPRK1 (POLLEN RECEPTOR-LIKE KINASE 1), a transmembrane (TM)
134 protein with an extracellular ligand binding domain, through the secretory endomembrane system to
135 the PM at the pollen tube tip (Lee et al., 2008; Luo et al., 2016). After photobleaching or
136 photoactivation, PM-associated fluorescence emitted by AtPRK1 fusion proteins also first appears
137 at the extreme apex, indicating that not only the delivery of extracellular proteins to the cell wall but
138 also the transport of TM proteins to the PM may be mediated by apical secretion. However, PMEs
139 and AtPRK1 both contain extracellular domains that may interact with cell wall components
140 specifically at the apex. Therefore, these proteins may be subapically secreted and subsequently
141 recruited to the pollen tube apex by specific interactions with cell wall components (McKenna et
142 al., 2009).

143

144 Coated pits, sites of clathrin-mediated endocytosis, are enriched within the subapical PM of fixed or
145 living pollen tubes, as demonstrated by numerous studies based on transmission electron
146 microscopy (TEM; Derksen et al., 1995), immunofluorescence and fluorescent protein tagging
147 (Blackbourn and Jackson, 1996; Zhao et al., 2010; Feng et al., 2016; Sekeres et al., 2017; Li et al.,
148 2018; Muro et al., 2018; Kaneda et al., 2019). Consistent with these observations, endocytosed
149 externally applied fluorescent lipid dyes (FM4-64; Parton et al., 2001) or positively charged
150 nanogold particles (Moscatelli et al., 2007) were first detected within cytoplasmic vesicles
151 specifically beneath the subapical PM using fluorescence microscopy or TEM, respectively. At a
152 later stage, both markers are not only observed within endocytic compartments (late endosomes,
153 vacuoles), but also within Golgi stacks and/or apical vesicles. These observations suggest that bulk
154 endocytosis occurs subapically, and that material internalized through this process is partially
155 recycled to the secretory endomembrane system. However, massive endocytosis may also occur at
156 the pollen tube apex based on 1) TEM analysis of the endocytic uptake of nanoparticles carrying a
157 negative rather than a positive (see above) charge (Moscatelli et al., 2007), 2) time-lapse
158 fluorescence imaging of FM4-64 internalization into pollen tubes preloaded with FM1-43 (Zonia
159 and Munnik, 2008), and 3) the investigation of mobility patterns of cytoplasmic components within

160 the apical ARVA using DIC light microscopy or FRAP analysis after FM1-43 staining (Bove et al.,
161 2008).

162

163 Many signaling proteins and lipids with important functions in the control of membrane traffic
164 during tip growth are specifically associated with strikingly distinct apical or lateral PM domains
165 not only in pollen tubes, but also in other tip-growing plant cells. These proteins and lipids include
166 a) ROP GTPases (Lin et al., 1996; Sun et al., 2015), b) upstream regulators of ROP activity (ROP-
167 GAPs [GTPase activating proteins; Klahre and Kost, 2006] and ROP-GEFs [guanine nucleotide
168 exchange factors; Gu et al., 2006; Le Bail et al., 2019]), c) different signaling lipids
169 (phosphatidylinositide 4,5-bisphosphate [Kost et al., 1999], diacyl glycerol [Helling et al., 2006]
170 and phosphatidic acid [Potocky et al., 2014]), as well as d) lipid modifying enzymes (PLCs
171 [phospholipase C; Dowd et al., 2006; Helling et al., 2006] and PIP5Ks [phosphatidylinositide 4-
172 phosphate 5-kinases; Sousa et al., 2008; Stenzel et al., 2012]). The targeting of these signaling
173 proteins and lipids to specific PM domains in tip-growing cells appears to be essential for the
174 regulation of local secretion and endocytosis, but clearly also depends on these membrane transport
175 processes. A thorough understanding of the mechanisms, which target these factors to distinct PM
176 domains and therefore play an essential role in the control of tip growth, clearly requires
177 quantitative characterization of the spatial organization of apical membrane traffic.

178

179 A key aim of the study presented here was to quantitatively determine sites of bulk secretion and
180 endocytic membrane recycling required for apical cell wall biogenesis at the tip of growing tobacco
181 (*Nicotiana tabacum*) pollen tubes. To this end, the lipid dye FM4-64 as well as different eYFP-
182 tagged TM proteins, including proteins unlikely to interact with the cell wall, were employed as *in*
183 *vivo* markers. Using fluorescence microscopy, steady-state distributions and dynamic behavior of
184 these markers were characterized in normally growing and/or in Brefeldin A (BFA)-treated tobacco
185 pollen tubes. In addition, to achieve a better understanding of remarkable differences in the
186 observed steady-state distribution patterns of some of the analyzed markers, these patterns were
187 mathematically modeled based on experimental data obtained. Finally, using eYFP-based markers,
188 subapical F-actin fringe and TGN positioning was quantitatively mapped to further characterize
189 functions of these structures in apical vesicle accumulation and membrane traffic. Together,
190 experimental and theoretical data generated: 1) quantitatively define sites of bulk secretion and
191 endocytosis within apical and subapical PM regions at the tip of tobacco pollen tubes, respectively;
192 2) establish the exact subapical positions of the cortical F-actin fringe and of a detached TGN
193 compartment relative to these sites; 3) demonstrate that within the identified subapical region of
194 bulk endocytosis, constitutive recycling of membrane lipids occurs, which generally excludes TM

195 proteins and appears to depend on the subapical TGN compartment but not on the F-actin fringe;
196 and 4) suggest particularly slow diffusion of TM proteins and lipids with the apical region of bulk
197 secretion, a finding that warrants further investigation.

198

199 **RESULTS**

200 **Different TM proteins serving as *in vivo* markers for membrane traffic display distinct** 201 **steady-state distribution patterns in tobacco pollen tubes**

202 Three different TM proteins, which are transported through the secretory endomembrane system to
203 the PM (endoplasmic reticulum [ER] > Golgi > TGN > secretory vesicles), were fused to an
204 enhanced yellow fluorescent protein (eYFP) and used as markers to investigate membrane traffic at
205 the tip of tobacco pollen tubes. To enable the discovery of general principles underlying this process
206 in addition to marker-specific targeting mechanisms, the following TM proteins with highly diverse
207 characteristics were selected: NtINT4, AtRCI2a and AtPRK1. NtINT4 (INOSITOL
208 TRANSPORTER4) is an endogenous tobacco pollen tube inositol transporter closely related to
209 AtINT4 (Schneider et al., 2006), is composed of 582 amino acids (aa) and contains 12 TM domains
210 (Figure 1A). By contrast, AtRCI2a (RARE COLD-INDUCIBLE PROTEIN 2A) is a small 54-aa
211 Arabidopsis (*Arabidopsis thaliana*) protein containing only two TM domains that are connected via
212 a very short (6 aa) linker and are positioned between even shorter N- and C-terminal extensions (5
213 and 2 aa respectively; Figure 1A). Although AtRCI2a functions are poorly understood to date
214 (Capel et al., 1997; Medina et al., 2001), this protein is commonly used as a non-invasive PM
215 marker in plants (Cutler et al., 2000; Serna, 2005; Thompson and Wolniak, 2008). Finally, AtPRK1
216 (POLLEN RECEPTOR-LIKE KINASE 1) is a 662 aa Arabidopsis pollen tube receptor-like kinase
217 (RLK) that contains a single central TM domain, which separates an N-terminal extracellular
218 leucine-rich repeats (LRR) ligand-binding domain from an intracellular protein kinase domain
219 (PKD) (Figure 1A). The closely related RLK AtPRK2 (96 % sequence identity at the aa level) plays
220 an important role in the control of Rac/ROP signaling in pollen tubes (Zhang and McCormick,
221 2007; Chang et al., 2013; Zhao et al., 2013; Miyawaki and Yang, 2014). Fluorescent AtPRK1
222 fusion proteins have previously been employed to investigate apical membrane dynamics in tobacco
223 (Lee et al., 2008) and Arabidopsis (Luo et al., 2016) pollen tubes. To generate fluorescent markers
224 for membrane traffic, eYFP was attached to a predicted cytoplasmic terminus of each of the three
225 selected proteins (NtINT4 and AtPRK1: C-terminus; AtRCI2a: N-terminus [Thompson and
226 Wolniak, 2008]), of which only AtPRK1 contains an N-terminal ER-import signal peptide (SP)
227 (Figure 1A).

228

229 Steady-state distribution patterns of NtINT4::eYFP, eYFP::AtRCI2a and AtPRK1::eYFP transiently
230 or stably expressed under the control of the LAT52 promoter (Twell et al., 1990) in cultured
231 tobacco pollen tubes were imaged using confocal microscopy (Figure 1B). Only images of normally
232 growing pollen tubes that after confocal imaging continued to elongate at a rate of at least 3 $\mu\text{m}/\text{min}$
233 (Supplemental Figure 1A; Klahre and Kost, 2006; Sun et al., 2015; Montes-Rodriguez and Kost,
234 2017) are shown (left panel; Figure 1B) and were statistically analyzed to generate line plots
235 displaying average intensities of PM-associated eYFP fluorescence at different meridional distances
236 (measured along the curved pollen tube PM) from the apex (right panel; Figure 1B).

237

238 As expected, all three TM protein markers primarily labeled the PM as well as the inverted cone-
239 shaped cytoplasmic ARVA (Lancelle and Hepler, 1992; Derksen et al., 1995; Bove et al., 2008).
240 However, interestingly the three markers displayed clearly distinct distribution patterns within the
241 PM (Figure 1B; right panel), as well as equally clear differences in the relative intensity of PM
242 versus apical vesicle labeling (Figure 1B; left panel). Whereas NtINT4::eYFP labeled all regions of
243 the PM as well as apical vesicles essentially evenly, eYFP::AtRCI2a accumulated to highest levels
244 in a lateral PM domain (Stephan et al., 2014) and AtPRK1::eYFP was strongly enriched in the PM
245 within the apical dome as previously described (Lee et al., 2008). Interestingly, the apical PM
246 domain most strongly labeled by AtPRK1::eYFP extended to a subapical region spanning a
247 meridional distance of about 3-5 μm from the extreme apex ($X = 0 \mu\text{m}$), within which the level of
248 PM association of all other markers also appears to markedly change or to display noticeable
249 discontinuity (Figure 1 B).

250

251 Differences in the dynamic behavior of each of the three analyzed TM protein makers, which may
252 be caused in part by differential interactions with unequally distributed membrane or cell wall
253 components (Martiniere et al., 2012; Trimble and Grinstein, 2015), presumably contribute to the
254 distinct distribution patterns displayed by these makers. In fact, a truncated AtPRK1 Δ SP-
255 LRR::eYFP fusion protein, which was missing the entire N-terminus of AtPRK1 (aa 1-229)
256 including the SP and the extracellular LRR ligand-binding domain (Figure 1A), displayed an
257 essentially even distribution in the PM and in apical vesicles similar to NtINT4::eYFP (Figure 1B).
258 This strongly suggests that specific interactions of the LRR domain with the apical cell wall, which
259 by contrast to all other regions of the pollen tube cell wall is mostly composed of esterified pectin
260 (Geitmann and Parre, 2004; Bosch et al., 2005; Parre and Geitmann, 2005; Rockel et al., 2008;
261 Chebli et al., 2012), may be responsible for the observed specific accumulation of full length
262 AtPRK1::eYFP within the PM at the apex. In the absence of the N-terminal SP of full-length
263 AtPRK1 (Figure 1A), the TM domain of AtPRK1 Δ SP-LRR::eYFP appears to mediate ER

264 recruitment and subsequent membrane insertion of this truncated fusion protein (Shao and Hegde,
265 2011; Kim and Hwang, 2013).

266

267 In addition to differential interactions with membrane or cell wall components, differences in the
268 rates of 1) intramembrane diffusion, which depends on protein size, density and number of TM
269 domains (Saffman et al., 1975; Kusumi et al., 1993; Frick et al., 2007; Goose and Sansom, 2013;
270 Weiß et al., 2013), 2) exocytosis, 3) endocytic uptake and/or 4) degradation may also contribute to
271 the distinct distribution patterns displayed by the three analyzed markers. These possibilities were
272 further explored by additional experiments and theoretical modeling as described below.

273

274 **FRAP analyses of the dynamic behavior of TM protein markers for membrane traffic** 275 **demonstrate apical secretion**

276 To identify major sites of secretion, at which TM proteins are incorporated into the PM, FRAP
277 analysis was employed to investigate the dynamic behavior of NtINT4::eYFP, eYFP::AtRCI2a and
278 AtPRK1::eYFP at the tip of growing pollen tubes. After complete photobleaching of eYFP
279 fluorescence at the tip of transiently or stably transformed pollen tubes expressing each of these
280 markers, fluorescence recovery was observed by time-lapse confocal imaging of individual pollen
281 tubes (Figure 2). PM labeling by all three markers first recovered in the same region within the
282 apical dome 30-49 s after photobleaching (Figure 2A; third row: arrowheads; Figure 2B), before the
283 typical steady-state distributions of each of the markers were largely reestablished after about 120 s
284 (Figure 2; fourth row). Interestingly, the apical PM region in which labeling by all markers first
285 recovered appears to largely overlap with the membrane domain displaying highest levels of steady-
286 state AtPRK1::eYFP labeling (0 to about 3 μm meridional distance from the extreme apex; Figure
287 1B). Larger sets of confocal time-lapse images showing fluorescence recovery in each of the pollen
288 tubes displayed in figure 2 at higher time resolution are provided as supplemental data
289 (Supplemental Figures 2, 3 and 4). All analyzed pollen tubes grew normally at rates of at least 3
290 $\mu\text{m}/\text{min}$ during post-bleach time-lapse imaging ($t = 0$ to 116-124 s) (Supplemental Figure 5).

291

292 Interestingly, substantial fluorescence recovery was not observed within lateral regions of the PM
293 (more than about 3 μm meridional distance from the extreme apex), which were photobleached
294 together with the apical dome (Figure 2A; third and fourth row: asterisks; Figure 2B). To
295 investigate this more thoroughly, large regions of NtINT4::eYFP-, eYFP::AtRCI2a- or
296 AtPRK1::eYFP-expressing pollen tubes positioned just behind the apical dome were completely
297 photobleached. In these experiments, even after an extended post-bleach period of 360 s, very little
298 recovery of PM-associated fluorescence was observed within the bleached regions (Supplemental

299 Figure 6A, third row: asterisks; Supplemental Figure 6B) although all analyzed pollen tubes grew
300 normally at rates of at least 3 $\mu\text{m}/\text{min}$ during post-bleach time-lapse imaging ($t = 0$ to 360 s)
301 (Supplemental Figure 7). Furthermore, in control experiments NtINT4::eYFP-, eYFP::AtRCI2a- or
302 AtPRK1::eYFP-expressing pollen tubes were preincubated with BFA (Brefeldin A), a drug that
303 disrupts membrane traffic and blocks tip growth (Supplemental Figure 8), before they were
304 completely photobleached at the tip. These experiments showed that BFA treatment effectively
305 prevented recovery of apical PM labeling by each of these markers (Supplemental Figure 9) in all
306 analyzed pollen tubes. Together, these observations demonstrate that after photobleaching, rapid
307 and effective recovery of PM labeling by fluorescent TM protein markers is confined to a small
308 region within the apical dome and depends on active membrane traffic.

309

310 In summary, the results presented in this section establish that three different TM proteins serving
311 as markers for membrane traffic are specifically delivered to the same small PM domain within the
312 apical dome of normally growing pollen tubes, strongly suggesting that this PM domain represents
313 a major site of secretion.

314

315 **Analysis of the establishment of steady-state PM labeling by FM4-64, a fluorescent lipid** 316 **marker for membrane traffic, supports apical secretion**

317 As described in the literature, the fluorescent lipophilic dye FM4-64 becomes red fluorescent upon
318 incorporation into the pollen tube PM and is subsequently endocytosed (Parton et al., 2001; Parton
319 et al., 2003; Bolte et al., 2004; Van Gisbergen et al., 2008). Consistent with the requirement of
320 pollen tube tip growth for massive membrane recycling (see introduction), a large proportion of the
321 endocytosed FM4-64-labeled PM material is rapidly recycled back to the secretory endomembrane
322 system, whereas only a small proportion of this material enters the endocytic endomembrane system
323 and eventually (about 24 hours after dye application) detectably labels endosomal and vacuolar
324 compartments (Parton et al., 2001).

325

326 Confocal time-course imaging was performed to carefully investigate changes in FM4-64 labeling
327 patterns during the first 60 min after dye application to cultured tobacco pollen tubes (Figure 1C).
328 Immediately after application (0-5 min), FM4-64 exclusively and evenly labeled the PM (Figure
329 1C; first row). Subsequently, dye redistribution was observed as a consequence of membrane
330 traffic, which resulted about 40 min after dye application in the establishment of a steady-state
331 labeling pattern that remained stable for the rest of the observation period (41-60 min). At this
332 steady-state stage, FM4-64 specifically and evenly labeled not only the PM but also apical vesicles
333 (Figure 1C; third row). These observations are consistent with data reported in the literature (Parton

334 et al., 2001). However, particularly informative was the imaging of pollen tubes 6-40 min after
335 FM4-64 application, during which dye redistribution resulting from endocytic uptake and recycling
336 to the secretory endomembrane system was observed. At this dye redistribution stage, which was
337 not carefully investigated in previous studies, FM4-64 most strongly labeled a small PM domain
338 within the apical dome (Figure 1C; second row). Interestingly, this domain appeared to largely
339 overlap with the apical membrane region, which displays steady-state AtPRK1::eYFP accumulation
340 at highest levels (0 to about 3 μm meridional distance from the extreme apex; Figure 1B), and in
341 which labeling by all TM protein markers first recovered in FRAP time-lapse experiments (Figure
342 2). Figure 1C shows images of normally growing pollen tubes (left panel) that after confocal
343 imaging continued to elongate at a rate of at least 3 $\mu\text{m}/\text{min}$ (Supplemental Figure 1B), along with
344 line plots displaying average intensities of PM-associated eYFP fluorescence in such pollen tubes at
345 different meridional distances from the apex (right panel). A larger set of time-course images
346 showing changing FM4-64 labeling patterns during the first 60 min after dye application at higher
347 time resolution is provided as supplemental data (Supplemental Figure 10). Essentially the same
348 changes in the FM4-64 labeling pattern during this time period were also observed by time-lapse
349 imaging of individual pollen tubes (Supplemental Figure 11A).

350
351 Results discussed in the previous paragraph establish that in normally elongating pollen tubes, the
352 steady-state distributions of externally applied FM4-64 (Figure 1C: third row; Supplemental Figure
353 11A: right image) and of endogenously produced TM protein markers (Figure 1B), in particular of
354 NtINT4::eYFP and AtPRK1 Δ SP-LRR::eYFP, were remarkably similar. This underscores the
355 usefulness of FM4-64 and of the analyzed TM protein markers as excellent tools to investigate
356 major routes of apical trafficking of PM-associated lipids and proteins, respectively, during pollen
357 tube tip growth. Furthermore, the preferential accumulation of FM4-64 in a small PM region within
358 the apical dome at the dye redistribution stage (6-40 min after application; Figure 1C: central row;
359 Supplemental Figure 11A: central image) strongly suggests that PM-associated FM4-64 is actively
360 transported from sites of endocytic internalization to the apical major site of secretion, which was
361 identified based on FRAP analyses of the dynamic behavior of TM protein markers (Figure 2) and
362 also displayed highest levels of steady-state AtPRK1::eYFP accumulation (Figure 1B). Continued
363 endocytic FM4-64 internalization and recycling during the dye redistribution stage appears to cause
364 increasing dye saturation of apical vesicles, eventually resulting in even labeling of these vesicles
365 and of the PM at the steady-state stage. Based on this interpretation, changes in FM4-64 labeling
366 patterns observed during the first 60 min after dye application further support the identification of a
367 small PM region within the apical dome as a major site of secretion and indicate that membrane

368 traffic results in the massive delivery not only of proteins but also of recycled lipid components of
369 the PM to this site.

370

371 **Analysis of BFA-induced loss of FM4-64 PM labeling demonstrates subapical endocytosis of** 372 **PM lipids**

373 As discussed above BFA blocks pollen tube tip growth (Supplemental Figure 8) by disrupting
374 membrane traffic. More specifically, in plants a key effect of BFA treatment is the inhibition of the
375 formation of exocytic vesicles at the TGN (Geldner et al., 2001; Nebenführ et al., 2002), which in
376 these organisms is not only a key component of the secretory endomembrane system, but also
377 serves as an early and recycling endosome (Dettmer et al., 2006; Lam et al., 2007; Reyes et al.,
378 2011; Contento and Bassham, 2012; Paez Valencia et al., 2016). By contrast, endocytic uptake of
379 PM material continues in the presence of BFA (Baluska et al., 2002; Emans et al., 2002; Wang et
380 al., 2005). Consequently, in different types of plant cells (Geldner et al., 2001; Parton et al., 2001;
381 Parton et al., 2003), including tobacco pollen tubes (Helling et al., 2006; Rockel et al., 2008;
382 Stephan et al., 2014), BFA blocks the recycling of endocytosed material back to the PM and causes
383 this material to be trapped within the TGN. BFA effects on growing pollen tubes have been
384 reported to take about 20 min to fully develop (Parton et al., 2001; Parton et al., 2003; Rounds et al.,
385 2014). This drug generally induces aberrant TGN elements to fuse to so-called BFA compartments
386 (Lippincott-Schwartz et al., 1991; Nebenführ et al., 2002; Tse et al., 2006), which in pollen tubes
387 typically form a single subapical structure that becomes detectable only after prolonged (\geq 30-60
388 min) incubation (Parton et al., 2001; Parton et al., 2003; Helling et al., 2006; Stephan et al., 2014).

389

390 Based on the known BFA effects summarized in the previous paragraph, we hypothesized that BFA
391 treatment of pollen tubes displaying FM4-64 labeling (Figure 1C) should result in a reduction of
392 PM labeling selectively at major sites of endocytic uptake of membrane material. In fact, this was
393 observed by confocal time-course imaging of FM4-64 fluorescence displayed by cultured tobacco
394 pollen tubes, which had been grown for 30 min in the presence of FM4-64 (dye redistribution stage;
395 Figure 1C; second row), before the dye was washed out from the culture medium and BFA was
396 added (Figure 3A and B). Whereas the PM remained essentially evenly labeled for the first 20 min
397 after BFA application, during the following 20 min, PM-associated FM4-64 fluorescence
398 selectively decreased slightly within the apical dome and massively within a sharply defined
399 subapical region. Interestingly, 41-60 min after BFA application, FM4-64 labeling of the PM within
400 the apical dome further decreased to almost the same level as observed within this subapical region
401 (Figure 3A and B). A BFA compartment was often not clearly discernible in the analyzed pollen
402 tubes, as strong FM4-64 labeling of this compartment typically only starts to develop after 30-60

403 min in the presence of BFA (Parton et al., 2001; Parton et al., 2003). Figure 3A shows
404 representative images of different FM4-64 labeled pollen tubes recorded during the indicated time
405 periods after BFA application. A larger set of time-course images showing changes in FM4-64
406 distribution in BFA-treated pollen tubes at higher time resolution is provided as supplemental data
407 (Supplemental Figure 12). Essentially the same changes in FM4-64 labeling patterns within the first
408 60 min after BFA application were also observed by time-lapse imaging of individual pollen tubes
409 (Supplemental Figure 11B: first row). Figure 3B shows the results of a quantitative and statistical
410 analysis of changes in the intensity of PM-associated FM4-64 fluorescence in all pollen tubes
411 analyzed by time-course imaging in the apical dome, the subapical region and the shank.
412 Furthermore, the exact average length and position of the subapical region displaying massive loss
413 of PM-associated fluorescence 21-40 min after BFA application was determined in these pollen
414 tubes (Figure 3C; FM4-64 BFA).

415
416 In summary, data presented in figure 3A, B and C, as well as in supplemental figure 11B, identify a
417 subapical region of the tobacco pollen tube PM as a major site of endocytic uptake of FM4-64-
418 labeled lipid material. This region extends between proximal and distal ends positioned at an
419 average meridional distance of 3.6 and 12.6 μm , respectively, from the extreme apex ($X=0 \mu\text{m}$).
420 Ongoing endocytic uptake massively reduces FM4-64 labeling of the PM within this region 21-40
421 min after BFA treatment, apparently because this drug blocks recycling of internalized dye via the
422 secretory endomembrane system back to the apical PM. The delayed massive reduction of PM
423 labeling also within the apical dome 41-60 min after BFA treatment appears to be caused by FM4-
424 64 diffusion from this PM domain to the subapical major site of endocytosis followed by dye
425 internalization at this site. By contrast, a reduction of FM4-64 labeling of the PM in the shank was
426 not detected within 60 min after BFA application, presumably because the dye pool in this region of
427 the PM was much larger.

428
429 **The PM association pattern of AtAP180::eYFP, a marker for clathrin-mediated endocytosis**
430 **at the PM, supports subapical endocytosis**

431 AtAP180 is a component of the clathrin machinery (Barth and Holstein, 2004), which is required
432 for the formation of endocytic vesicles at the PM during clathrin-mediated endocytosis, the most
433 prominent form of endocytosis in plants (Dhonukshe et al., 2007; Perez-Gomez and Moore, 2007;
434 Fan et al., 2015). Fluorescent AtAP180 fusion proteins have been employed to identify endocytic
435 PM domains in different types of cells including tobacco pollen tubes (Stavrou and O'Halloran,
436 2006; Zhao et al., 2010; Kaneda et al., 2019). Consistent with previously reported observations
437 (Zhao et al., 2010; Kaneda et al., 2019), confocal imaging of essentially normally growing tobacco

438 pollen tubes transiently expressing an AtAP180::eYFP fusion protein established that this fusion
439 protein accumulated at the PM specifically in a subapical region (Figure 3D), which largely
440 overlapped with the major domain of endocytic uptake of membrane lipids that was identified based
441 on BFA treatment after FM4-64 labeling (Figure 3A, B and C; Supplemental Figure 11B). Figure
442 3D shows a representative image of an AtAP180::eYFP-expressing pollen tube. All analyzed pollen
443 tubes continued to grow at a normal rate of at least 3 $\mu\text{m}/\text{min}$ after confocal imaging, although they
444 displayed a slight but statistically significant reduction in average growth rate as compared to
445 control pollen tubes expressing free eYFP (Supplemental Figure 13). The exact average length and
446 position of the subapical PM domain at which AtAP180::eYFP accumulated is indicated in Figure
447 3C. As shown in this figure, the subapical PM domains identified based on AtAP180::eYFP
448 imaging and on the analysis of loss of FM4-64 PM labeling after BFA treatment shared an identical
449 length (ca. 9 μm) and were largely overlapping. However, the AtAP180::eYFP labeled domain was
450 positioned 2.3 μm more distally (further away from the apex). AtAP180::eYFP was imaged in
451 normally elongating pollen tubes, whereas analysis of loss of FM4-64 PM labeling was performed
452 after BFA treatment, which effectively blocks pollen tube tip growth. This may be responsible for
453 the 2.3 μm shift between the two domains, as PM domains at the pollen tube tip typically shift
454 towards the apex upon inhibition of pollen tube growth (Helling et al., 2006; Zhao et al., 2010;
455 Potocky et al., 2014). Unfortunately, this hypothesis could not be experimentally verified as for
456 unknown reasons AtAP180::eYFP did not detectably accumulate at the PM of pollen tubes treated
457 with BFA to block FM4-64 recycling, or with other drugs that inhibit pollen tube tip growth.

458
459 In any case, data resulting from confocal AtAP180::eYFP imaging provide compelling support for
460 the presence of an about 9 μm long major domain of endocytic uptake of lipid material within the
461 subapical PM of tobacco pollen tubes, which was identified based on the analysis of loss of FM4-64
462 PM labeling after BFA treatment. Furthermore, the observed intracellular distribution of
463 AtAP180::eYFP 1) indicates that in normally growing pollen tubes the proximal end of the
464 identified subapical endocytic domain is positioned at a meridional distance of about 5.9 μm from
465 the extreme apex, and 2) strongly suggests that clathrin-mediated endocytosis occurs within this
466 domain.

467
468 **Unlike FM4-64 labeled lipid material, TM protein markers for membrane traffic are not**
469 **subapically endocytosed**

470 Tobacco pollen tubes expressing NtINT4::eYFP, eYFP::AtRCI2a or AtPRK1::eYFP were treated
471 with BFA to test whether in the presence of this drug, similar to FM4-64 PM labeling (Figure 3;
472 Supplemental Figure 11B: first row), PM labeling by these TM protein markers also massively

473 decreases within the apical dome and the identified subapical endocytic domain 20-60 min after
474 drug application. This would indicate that not only FM4-64 labeled lipid material but also TM
475 marker proteins are endocytically internalized within this subapical domain. To our surprise,
476 although a large number of pollen tubes expressing each of the three TM protein markers were
477 observed by confocal time-course imaging 0-180 min after BFA application, a reduction of PM-
478 associated eYFP fluorescence within the apical dome or the subapical endocytic domain was never
479 observed (Figure 4). In figure 4A, representative images of different pollen tubes expressing each of
480 the three TM marker proteins are presented, which were recorded by time-course imaging during
481 the indicated time periods after BFA application. Essentially stable labeling of the apical and
482 subapical PM by each of the TM protein markers within the first 60 min after BFA application was
483 also observed by time-lapse imaging of individual pollen tubes (Supplemental Figure 11B: rows 2-
484 4). Quantitative analysis (Figure 4B) of all NtINT4::eYFP- or eYFP::AtRCI2a-expressing pollen
485 tubes investigated by time-course imaging established that the relative intensity of PM labeling by
486 these TM protein markers within the apical dome and the subapical endocytic region (normalized
487 based on maximal intensity measured within both these two membrane domains in each analyzed
488 pollen tube) remained close to 100 % in the presence of BFA even after prolonged incubation. By
489 contrast to NtINT4::eYFP and eYFP::AtRCI2a, AtPRK1::eYFP specifically accumulated to highest
490 levels in the PM within the apical dome of untreated, normally growing tobacco pollen tubes
491 (Figure 1B). Consequently, the relative intensity of AtPRK1::eYFP PM labeling observed by time-
492 course imaging was lower within the subapical endocytic region than within the apical dome also in
493 the presence of BFA (Figure 4 A and B). However, the relative intensity of AtPRK1::eYFP PM
494 labeling did not detectably change during BFA treatment in either of these two regions (Figure 4B).

495
496 The PM distribution displayed by each of the analyzed TM protein makers during normal tip
497 growth (Figure 1) substantially changed after BFA-induced inhibition of this process (Figure 4;
498 Supplemental Figure 11B). In the presence of this drug, NtINT4::eYFP and eYFP::AtRCI2a
499 displayed an essentially even distribution within the PM, whereas AtPRK1::eYFP labeling of this
500 structure increasingly assumed a dotted appearance and eventually completely disappeared in the
501 shank. High turnover of this TM protein marker predominantly in the shank, which remained
502 uncompensated because secretion was blocked, possibly contributed to this behavior. In any case,
503 data shown in figure 4 and in supplemental figure 11 demonstrate that by contrast to FM4-64-
504 labeled lipid material, none of the analyzed TM protein markers was detectably internalized within
505 the subapical endocytic PM region after BFA application.

506

507 Although in some pollen tubes imaged (as described in the previous paragraph) a typical subapical
508 BFA compartment was visible after prolonged BFA incubation, invariably this compartment was
509 only dimly labeled as compared to the PM (Figure 4A and Supplemental Figure 11B: arrows).
510 Consistent with the persistence of TM protein marker labeling of the subapical endocytic PM
511 domain in the presence of BFA (Figure 4A and B; Supplemental Figure 11B), this observation
512 suggests that TM protein markers are not endocytosed and cannot be delivered to the BFA
513 compartment via this route. The weak labeling of the BFA compartment in some analyzed pollen
514 tubes presumably is a consequence of redistribution of TM protein markers proteins already present
515 within the secretory endomembrane system at the time of BFA application. As BFA not only blocks
516 the formation of secretory vesicles at the TGN, but also ER to Golgi transport (Jiang and Rogers,
517 1998; Nebenführ et al., 2002), newly synthesized TM protein markers were unable to reach the
518 BFA compartment in these experiments.

519
520 To confirm the data presented in figure 4 and supplemental figure 11B, NtINT4::eYFP-,
521 eYFP::AtRCI2a- or AtPRK1::eYFP-expressing pollen tubes were co-labeled for 30 min with FM4-
522 64 and treated with BFA after the dye was washed out from the culture medium. Two-channel
523 confocal time-course imaging was employed to simultaneously observe the intracellular distribution
524 of the TM protein markers (eYFP, green fluorescence) and of FM4-64 (red fluorescence) at
525 different time points for 60 min after BFA application (Figure 5). Consistent with observations
526 described above (Figure 3; Supplemental Figure 11B), BFA induced a massive decrease of FM4-64
527 labeling of the PM early (21-40 min after application) within the subapical endocytic domain and
528 later (41-60 min after application) also within the apical dome (Figure 5; “FM4-64”). By contrast,
529 no concomitant loss of PM labeling by any of the analyzed TM protein markers was detected in
530 either of these two PM regions (Figure 5; “eYFP”). Interestingly, a BFA compartment was
531 occasionally visible in individual analyzed pollen tubes, which, relative to the PM, was labeled
532 strongly by FM4-64 but only weakly by the expressed TM protein marker (Figure 5; arrows). As
533 discussed in the previous paragraph, this observation supports transport of FM4-64 but not of TM
534 protein markers to the BFA compartment via endocytosis.

535
536 Together, data presented in figures 4 and 5 and supplemental figure 11B establish that all analyzed
537 TM protein markers are excluded from the massive internalization of FM4-64-labeled material
538 observed within the subapical endocytic PM domain, which therefore appears to be specifically
539 required for the recycling of excess lipid material delivered to the apical PM via secretion in
540 tobacco pollen tubes.

541

542 **The subapical endocytic PM domain partially overlaps with a detached TGN compartment**
543 **but not with the F-actin fringe**

544 A subapically positioned VHAA1-positive (Dettmer et al., 2006) TGN compartment is postulated to
545 act as a central sorting organelle with key functions in membrane traffic and in the recycling of PM
546 material at the tip of growing tobacco pollen tubes (Stephan et al., 2014). This organelle is proposed
547 to process membrane material delivered by endocytic vesicles to its distal surface and to recycle this
548 material to secretory vesicles that are generated on its proximal surface (Stephan et al., 2014).
549 Maintenance of the subapical position of this TGN compartment within the pollen tube cytoplasm
550 depends on the F-actin fringe (Stephan et al., 2014), a cortical ring-like F-actin structure located
551 close to the pollen tube apex (Kost et al., 1998; Chen et al., 2002; Lovy-Wheeler et al., 2005;
552 Wilsen et al., 2006; Cheung et al., 2008; Vidali et al., 2009). An intact F-actin fringe appears to be
553 essential for pollen tube tip growth (Bou Daher and Geitmann, 2011; Dong et al., 2012; Rounds et
554 al., 2014; Stephan et al., 2014), possibly because of functions of this structure not only in TGN
555 positioning but also directly in apical secretion (Cardenas et al., 2008; Bou Daher and Geitmann,
556 2011; Dong et al., 2012; Rounds et al., 2014) and/or subapical endocytic membrane internalization
557 (Samaj et al., 2006; Galletta and Cooper, 2009; Moscatelli et al., 2012; Meunier and Gutierrez,
558 2016; Li et al., 2018).

559
560 To enhance our understanding of roles of the subapical TGN compartment and of the F-actin fringe
561 in the endocytic uptake of FM4-64-labeled lipid material (Figures 3 and 5; Supplemental Figure
562 11B), the exact positions of these two structures in normally growing tobacco pollen tubes were
563 mapped (Figure 6) relative to each other and to the location of the subapical endocytic PM domain
564 as determined based on AtAP180::eYFP labeling (Figure 3C and D). The two F-actin markers
565 eYFP::MTn (mouse talin; Kost et al., 1998) and lifeact::eYFP (Riedl et al., 2008; Vidali et al.,
566 2009) both enable visualization of the F-actin fringe in tobacco pollen tubes displaying normal tip
567 growth (Montes-Rodriguez and Kost, 2017). To non-invasively label the subapical VHAA1-positive
568 TGN in such pollen tubes, eYFP fused to the Rac/ROP effector NtRISAP (eYFP::NtRISAP) can be
569 employed (Stephan et al., 2014). Tobacco pollen tubes transiently expressing lifeact::eYFP,
570 eYFP::MTn or eYFP::NtRISAP at low levels under the control of the LAT52 promoter were
571 imaged using confocal microscopy. Representative images of pollen tubes expressing each of these
572 eYFP fusion proteins and growing essentially normally at a rate of at least 3 $\mu\text{m}/\text{min}$ after confocal
573 imaging (Supplemental Figure 14) are shown in figure 6A. Figure 6B presents the results of a
574 quantitative and statistical analysis of the positions of the subapical TGN compartment and of the F-
575 actin fringe in all imaged pollen tubes. The average meridional distance from the extreme apex ($X =$
576 0) of the most proximal and the most distal contact point of each of these two cytoplasmic

577 structures with the PM is indicated in this figure. To facilitate direct comparison, the same figure
578 also shows the position of the AtAP180::eYFP-labeled subapical endocytic PM domain in normally
579 growing tobacco pollen tubes, which was determined as described above (Figure 3C and D).
580 Together, data presented in figure 6 allow the following interesting conclusions: 1) independently of
581 the F-actin marker used, no overlap was observed between the F-actin fringe and the subapical
582 endocytic PM domain, strongly suggesting that the F-actin fringe is not directly required for
583 membrane internalization within this domain, 2) the F-actin fringe completely overlaps with the
584 proximal half of the subapical TGN compartment, consistent with the reported essential function of
585 the F-actin fringe in the cytoplasmic positioning of this compartment (Stephan et al., 2014), and 3)
586 the distal half of the subapical TGN compartment overlaps with a short (ca. 1.5 μm) subdomain at
587 the proximal end of the subapical endocytic PM region, a spatial arrangement that is fully consistent
588 with the proposed delivery of internalized membrane material by endocytic vesicles to the distal
589 surface of this compartment.

590

591 BFA treatment not only blocks secretion but also rapidly disrupts the subapical F-actin fringe at the
592 pollen tube tip (Rounds et al., 2014). To further investigate a possible role of the F-actin fringe in
593 membrane internalization within the subapical endocytic PM region, pollen tubes transiently
594 expressing eYFP::MTn or lifeact::eYFP were co-labeled for 30 min with FM4-64 before the dye
595 was washed out from the culture medium and BFA was applied. Two-channel confocal time-course
596 imaging was performed to simultaneously visualize F-actin organization (eYFP; green
597 fluorescence) and FM4-64 labeling (red fluorescence) at different time points during the first 60
598 min after BFA application (Figure 7). BFA treatment 1) stopped pollen tube growth (Supplemental
599 Figure 8), 2) rapidly (0-20 min after drug application) disrupted the subapical F-actin fringe (Figure
600 7; “eYFP”), and 3) as previously demonstrated (Figures 3 and 5; Supplemental Figure 11B: first
601 row) induced a massive decrease of FM4-64 labeling of the PM first (21-40 min after drug
602 application) within the subapical endocytic domain and later (41-60 min after drug application) also
603 within the apical dome (Figure 7; “FM4-64”). The same observations were also made by time-lapse
604 imaging of lifeact::eYFP-expressing and FM4-64-labeled individual pollen tubes after the
605 application of BFA either alone or in combination with the actin disrupting drug Latrunculin B
606 (LatB; Supplemental Figure 15). Combined application of BFA and LatB not only caused rapid
607 disruption of the F-actin fringe but also strongly affected longitudinally-oriented F-actin fibers.
608 Together, these findings demonstrate that internalization of FM4-64-labeled lipid material within
609 the subapical endocytic PM domain can occur in the absence of an intact F-actin fringe.

610

611 Data presented in this section firmly establish that, consistent with the observed lack of overlap
612 between the F-actin fringe and the subapical endocytic PM domain (Figure 6), drug-induced F-actin
613 fringe disruption does not affect the internalization of lipid material within this membrane domain
614 (Figure 7). The F-actin fringe therefore clearly has no direct function in this process. However,
615 previously reported (Stephan et al., 2014) key functions of the F-actin fringe in the positioning of a
616 subapical TGN compartment, as well as of this TGN compartment in the recycling of endocytosed
617 PM material, are supported by the quantitative structural data shown in figure 6. Consequently, the
618 F-actin fringe may be essential for pollen tube tip growth because it is required for apical membrane
619 recycling based on its function in maintaining the positioning of the subapical TGN compartment.

620

621 **Mathematical modeling of steady-state marker distribution within the PM**

622 To enhance our understanding of the distinct steady-state distribution patterns within the pollen tube
623 PM, which are displayed by different markers for membrane traffic (Figure 1 B and C), these
624 distribution patterns were mathematically modeled based on a number of assumptions, which are
625 discussed below and are largely derived from experimental data reported here. Some of these
626 assumptions may be considered modeling output, as they have emerged from the process of fitting
627 the model to experimental data.

628

629 The model divides the PM into the following four regions, which are positioned at the indicated
630 meridional distances from the extreme apex: apical dome (0-3.5 μm), F-actin fringe region (3.5-5.5
631 μm), subapical region (5.5-15 μm) and shank ($>15 \mu\text{m}$). The positioning of these regions emerged
632 from model fitting and is in close agreement with experimental data (Figure 6). Four processes are
633 modelled, which together determine marker dynamics and steady-state distribution within the PM.
634 The extreme pollen tube apex is defined as a reference point with a fixed position. Consequently, all
635 markers of membrane traffic within each of the four PM regions are subject to a constant retrograde
636 flux at the rate of pollen tube tip growth (process 1), which has been experimentally determined as
637 discussed above (Supplemental Figure 1). The density of individual markers can locally increase
638 (source) or decrease (sink) within the PM as a result of cytoplasmic vesicle traffic (process 2). A
639 source may result either from secretion or from local increase in TM protein marker density caused
640 by selective endocytosis of lipid material. By contrast, a sink corresponds to endocytic
641 internalization. In addition, diffusion within the PM (process 3) is expected to occur with marker
642 and region specific coefficients. Finally, fitting to experimental plots of marker distribution within
643 the PM in the shank required the model to account for marker degradation, which in the case of
644 FM4-64 is over-compensated by ongoing PM staining by residual dye present in culture medium
645 (process 4).

646

647 To compute distribution profiles of all analyzed markers within the PM, model equations were
648 adjusted to account for different sets of the four processes introduced in the previous paragraph
649 occurring in each of the four different regions of the pollen tube PM (Table 1). The F-actin fringe
650 region, in which, apart from retrograde flux, only diffusion is assumed to occur, is modeled such
651 that it links the solutions of the equations describing marker distribution within the apical and the
652 subapical regions. Hence, within the F-actin fringe region the diffusion coefficient of each marker
653 undergoes transition between the apical and subapical values. No source or sink is assumed to be
654 present in the shank region. Furthermore, the diffusion coefficients of all markers in the subapical
655 region and in the shank are assumed equal. Marker degradation is also defined to occur at equal
656 rates in the subapical region and in the shank but has been assigned the value zero in the apical
657 region, in which degradation presumably is irrelevant compared to changes in marker density
658 resulting from vesicle traffic. In addition, the model implicates that ongoing PM staining by residual
659 FM4-64 is over-compensating degradation of this lipid dye in all PM regions and substantially
660 contributes to its distribution profile only in the shank. The rates or coefficients of all processes
661 other than retrograde flux (Q : source; q : sink; D : diffusion; K : marker protein degradation; R :
662 staining by residual FM4-64) are variables that can be read out after model fitting (Table 2).

663

664 To fit the model to experimental line plots displaying average intensity of PM-associated marker
665 fluorescence (Figure 1 B and C), these line plots needed to be normalized based on the values at the
666 extreme apex, which were set to the intensity level “1” (Figure 8; light blue line). Consequently, the
667 Q , q , D , K and R values read out for the different markers after model fitting (Table 2) are based on
668 relative levels of PM-associated marker fluorescence but not on absolute marker density. For all
669 analyzed markers, an excellent fit of the model (Figure 8; brown line) to the experimental data was
670 obtained, after the following marker specific adjustments were made: (i) Because fitting the model
671 to the AtPRK1::eYFP line plot indicated a much stronger source of this marker within the apical
672 dome (Q_a) than in the subapical region (Q_{sa}), Q_{sa} could not be accurately determined and was
673 defined to be zero ($Q_{sa} = 0$) for practical purposes. Hence, for AtPRK1::eYFP only Q_a and D_a
674 within the apical dome could be read out as independent values after model fitting (Table 2). (ii)
675 Furthermore, as the experimental NtINT4::eYFP distribution plot displays a distinct kink at the
676 border between the apical dome and the F-actin fringe region (Figures 1B and 8), the requirement
677 for smoothness in the marker distributions at this border was removed from the model. (iii) Finally,
678 selective endocytosis of lipid material within the subapical endocytic domain locally increases TM
679 protein marker density with a rate that is independent of this density, whereas the rate of FM4-64
680 internalization resulting from the same process obviously increases with higher dye concentrations

681 within the PM. To model FM4-64 distribution within the subapical PM, the term $q_{sa}c(x,t)$ was
682 therefore employed instead of the constant Q_{sa} that was used for TM protein modeling. By contrast,
683 TM protein degradation occurs at a concentration dependent rate, whereas the rate of ongoing PM
684 staining by residual FM4-64 present in the culture medium is not affected by the dye concentration
685 within the PM. Therefore, the term $K_s c(x,t)$ [equal to $K_{sa} c(x,t)$] was used to describe TM protein
686 degradation, whereas the concentration-independent constant R_s was employed to represent
687 membrane labeling by residual FM4-64.

688

689 The possibility to obtain an excellent fit of the model to the experimental data (Figure 8), along with
690 the signs of the Q_a , Q_{sa} and q_{sa} values read out for all analyzed markers (Table 2), are consistent
691 with and further support the following key experimental findings: 1) all markers of membrane
692 traffic are incorporated into the PM as a consequence of secretion occurring within the apical dome
693 (positive Q_a values), and 2) FM4-64 labeled PM material is endocytically recycled within the
694 subapical region (negative q_{sa} value), whereas TM protein markers are not (positive Q_{sa} values).
695 Furthermore, interactions of the extracellular LRR domain of AtPRK1 with the cell wall, which
696 were proposed to contribute to the experimentally detected accumulation of this protein to highest
697 levels within the apical dome (Figure 1B), are supported by the observation that AtPRK1 displays
698 the lowest D_a value ($0.040 \pm 0.003 \mu\text{m}^2\text{s}^{-1}$) of all TM protein markers tested, including a truncated
699 form of this protein missing the extra cellular LRR domain ($0.063 \pm 0.003 \mu\text{m}^2\text{s}^{-1}$) (Table 2).

700

701 In addition, model output summarized in table 2 allows a number of further interesting conclusions,
702 which remain to be experimentally verified. It is not possible to directly compare absolute Q_a , Q_{sa}
703 or q_{sa} values between markers, as experimental line plots were normalized for model fitting, and
704 because the correlation between marker fluorescence and density within the PM has not been
705 quantified. Distinct Q_{sa} values were therefore read out for different TM protein markers, although
706 local enrichment of all these markers resulting from selective endocytosis of lipid material within
707 the subapical region is expected to occur at the same rate. However, the Q_a/Q_{sa} or Q_a/q_{sa} ratio, as
708 well as D , K and R values are not affected by data normalization and can be directly compared
709 between markers. The particularly low Q_a/Q_{sa} ratio obtained for eYFP::AtRCI2a ($0.4561 \mu\text{m}$; Table
710 2) indicates that this protein is apically secreted at a low rate as compared to the rate of the
711 accumulation of this protein within the subapical region, which is caused by selective endocytosis
712 of lipid material. Together with relatively fast degradation in the shank ($K_s = -0.83 \pm 0.05 \cdot 10^{-2}\text{s}^{-1}$;
713 Table 2), this may explain the massive eYFP::AtRCI2a accumulation that is experimentally
714 observed within the lateral PM. Furthermore, as discussed above, model fitting required that all TM
715 marker proteins are degraded at a low rate in both the subapical and shank regions, and that constant

716 relabeling of the PM by residual FM4-64 in the culture medium compensates degradation of this
717 dye, a process that substantially contributes to the FM4-64 distribution profile specifically in the
718 shank. Finally and most interestingly, whereas within the subapical and shank regions of the PM the
719 diffusion coefficients (Table 2) of all TM proteins markers ($D_{sa} = 0.37\text{-}0.79 \mu\text{m}^2\text{s}^{-1}$), and of FM4-64
720 ($D_{sa} = 1.21 \mu\text{m}^2\text{s}^{-1}$), are within the typical range for TM proteins (Edidin, 1987; Vrljic et al., 2002;
721 Hartel et al., 2015) and membrane lipids (Edidin, 1987), respectively, diffusion of all markers
722 appears to be strikingly slow within the apical dome (0.034 to $0.085 \mu\text{m}^2\text{s}^{-1}$; Table 2). This
723 observation may be a consequence of substantial molecular crowding, possibly resulting from the
724 massive secretory activity within this PM region and certainly warrants experimental confirmation.

725

726 **DISCUSSION**

727 **Quantitative structural organization of apical membrane traffic at the pollen tube tip**

728 Our results are essentially consistent with the classical model of apical membrane traffic at the tip
729 of elongating pollen tubes. This model predicts that bulk secretion required for cell wall biogenesis,
730 as well as for the coordination of signaling processes controlling tip growth (Luo et al., 2017; Li et
731 al., 2018), occurs apically and results in the deposition of excess material in the PM, which is
732 recycled based on massive subapical endocytosis (Figure 9). Evidence presented here shows that in
733 growing tobacco pollen tubes, newly synthesized TM protein markers and endocytically recycled
734 FM4-64-labeled membrane lipids are specifically delivered by secretion to the PM within a small
735 domain at the tip, which extends from the extreme apex to the subapical F-actin fringe (meridional
736 distance from the extreme apex: 0 - ca. $3.5 \mu\text{m}$). Furthermore, we demonstrate that bulk endocytic
737 internalization of FM4-64-labeled membrane material, from which all analyzed TM protein markers
738 are excluded, occurs within a subapical PM domain located distal to the F-actin fringe (meridional
739 distance from the extreme apex in normally growing pollen tubes: 5.9 - $14.8 \mu\text{m}$).

740

741 In addition, data described here further support a previously suggested (Stephan et al., 2014)
742 important function of a subapical TGN compartment as a central sorting organelle in tobacco pollen
743 tubes, with which Golgi-derived and endocytic vesicles delivering newly synthesized or recycled
744 membrane material, respectively, may fuse at the distal end, and which may generate secretory
745 vesicles at its proximal surface (Figure 9). In addition to the typical trans-Golgi-associated TGN,
746 separate detached TGN elements are frequently observed in plant cells (Zarsky et al., 2009;
747 Uemura, 2016; Uemura et al., 2019), which in tobacco pollen tubes appear to aggregate to a single
748 subapical compartment. Presumably, a key function of this TGN compartment is to maintain the
749 massive accumulation of secretory vesicles within the cytoplasmic ARVA at the pollen tube tip, for
750 which no plausible alternative mechanism has been proposed to date. Maintenance of the

751 positioning of the subapical TGN compartment within a pollen tube region displaying rapid
752 cytoplasmic streaming requires an intact F-actin fringe (Stephan et al., 2014). Results of the exact
753 positional mapping of the endocytic PM domain, the F-actin fringe, and the TGN compartment to
754 distinct subapical regions of tobacco pollen tubes, which are presented here, are fully consistent
755 with the proposed functions of the subapical TGN compartment in membrane traffic, as well as of
756 the F-actin fringe in the subapical cytoplasmic positioning of this compartment. The proximal end
757 of the subapical TGN compartment precisely colocalizes with the F-actin fringe, whereas the distal
758 end of this compartment overlaps with a small proximal region (ca. 1.5 μm long) of the subapical
759 endocytic domain (Figures 6 and 9).

760

761 Interestingly, our results demonstrate that the F-actin fringe does not overlap at all with the
762 subapical endocytic domain and is not required for the internalization of FM4-64 labeled membrane
763 lipids within this domain. Furthermore, the structural organization at the tip of tobacco pollen tubes,
764 which emerges from data presented here, does not suggest a direct function of the F-actin fringe in
765 the transport of secretory vesicles to sites of fusion with the PM (Figure 9). An intact F-actin fringe
766 may therefore be essential for pollen tube tip growth (Bou Daher and Geitmann 2011; Dong et al.
767 2012; Rounds et al. 2014) exclusively because it is required for the maintenance of the cytoplasmic
768 positioning of the subapical TGN compartment. Fine F-actin filaments have been observed within
769 the cytoplasmic ARVA at the pollen tube tip in some studies (Lancelle and Hepler, 1992; Miller et
770 al., 1996; Fu et al., 2001; Qu et al., 2013) and are proposed to serve as tracks for the myosin-
771 mediated transport of secretory vesicles towards the PM (Fu and Yang, 2001; Kost, 2008; Qu et al.,
772 2013; Stephan et al., 2014). However, it is debatable whether such filaments can be unequivocally
773 detected using available *in vivo* markers in normally growing pollen tubes of tobacco and other
774 plant species (Figure 6A; Kost et al., 1998; Montes-Rodriguez and Kost, 2017; Qu et al., 2017). In
775 these pollen tubes the constant supply of secretory vesicles budding from the proximal surface of
776 the subapical TGN compartment may be sufficient to push these vesicles forward towards sites of
777 fusion with the apical PM (Figure 9).

778

779 **Identification of major sites of secretion and endocytosis**

780 To identify sites of bulk secretion and endocytosis in tobacco pollen tubes, different *in vivo* markers
781 for membrane traffic with highly diverse characteristics were employed in this study: the
782 fluorescent lipid dye FM4-64 as well as three TM proteins with distinct sizes, numbers of TM
783 domains, functions and origins, which all carried an eYFP tag attached to a cytoplasmic terminus.
784 Although in the case of eYFP::AtRCI2a different topology prediction tools (e.g. SPOCTOPUS
785 [Viklund et al., 2008] and Phobius [Kall et al., 2007]) indicate extracellular localization of both

786 termini, these predictions appear to be wrong (Thompson and Wolniak, 2008). The use of four
787 highly diverse membrane transport markers enabled the discovery of basic principles of protein and
788 lipid trafficking underlying tobacco pollen tube tip growth irrespective of marker-specific targeting
789 mechanism, which may include interaction with unequally distributed cell wall components. The
790 steady-state distribution patterns of three analyzed markers (FM4-64, NtINT4::eYFP,
791 eYFP::AtRCI2a) did not show PM accumulation preferentially within the apical dome. However,
792 consistent with bulk secretion occurring apically, the PM within the apical dome of pollen tubes
793 expressing each of these markers displayed similar levels of steady-state labeling as apical secretory
794 vesicles accumulating in the underlying cytoplasm (Figure 1B and C). Only the TM protein marker
795 AtPRK1::eYFP showed steady-state accumulation at clearly higher levels within the apical PM as
796 compared to other PM regions as well as to apical secretory vesicles. Interestingly, interactions of
797 the extracellular LRR domain of AtPRK1 with the apical cell wall appear to be primarily
798 responsible for this distribution pattern, as strongly suggested by the observations that truncated
799 AtPRK1::eYFP missing the LRR domain fails to specifically accumulate within the apical PM
800 (Figure 1B) and appears to display faster diffusion within this membrane region than full-length
801 AtPRK1::eYFP (Table 2). Additional imaging and modeling results strongly suggest that not only
802 marker-specific interactions with cell wall components, but also distinct rates of apical secretion,
803 subapical endocytosis and degradation are responsible for the observed striking differences in the
804 steady-state distribution patterns of some of the analyzed markers. Together, these findings
805 demonstrate that steady-state distribution patterns of markers for membrane traffic do not directly
806 indicate the location of sites of bulk secretion or endocytosis in pollen tubes.

807

808 The site of bulk secretion in tobacco pollen tubes was identified based on two completely different
809 approaches, which enabled investigation of the dynamic behavior of markers for membrane traffic
810 during normal tip growth: 1) analysis of the recovery of TM protein marker fluorescence after
811 photobleaching pollen tube tips, and 2) imaging FM4-64 redistribution after the initial even PM
812 labeling by this dye. The results of the application of these two approaches demonstrated that both
813 newly synthesized TM protein markers as well as endocytically recycled FM4-64 labeled
814 membrane lipids are incorporated into the PM specifically within the same central region of the
815 apical dome (Figure 9). Furthermore, the site of bulk endocytic membrane internalization in tobacco
816 pollen tubes was also identified using two entirely different approaches: 1) analysis of loss of
817 marker labeling of the PM after BFA treatment, which blocks secretion without preventing
818 endocytosis, and 2) *in vivo* imaging of the PM association of AtAP180::eYFP, a marker for
819 clathrin-mediated endocytosis at the PM. FM4-64-labeled membrane lipids, but none of the
820 analyzed TM protein markers, were internalized, apparently by clathrin-mediated endocytosis

821 within a clearly defined subapical PM domain (Figure 9). Consistent with this conclusion, marker
822 distribution profiles presented in figure 1 show that levels of PM-associated marker fluorescence
823 are substantially reduced within the subapical endocytic domain in FM4-64 labeled pollen tubes
824 both at the redistribution and the steady-state stage, whereas this is clearly not the case in pollen
825 tubes expressing NtINT4::eYFP and AtPRK1 Δ SP-LRR::eYFP, which otherwise display similar
826 steady-state distribution patterns as FM4-64. Subapical clathrin-mediated endocytosis during tip
827 growth is strongly supported also by previously published reports showing that not only fluorescent
828 AtAP180 fusion proteins (Zhao et al., 2010; Kaneda et al., 2019) but also other markers for clathrin-
829 mediated endocytosis, including AtDRP1C::RFP (ARABIDOPSIS DYNAMIN-RELATED
830 PROTEIN 1C) (Sekeres et al., 2017), PICALM5a::GFP, PICALM5b::GFP, EAP::RFP (AtAP180-
831 related ANTH domain-containing containing proteins) and CLC1::GFP (CLATHRIN LIGHT
832 CHAIN1) (Muro et al., 2018; Li et al., 2018) specifically accumulate at the subapical PM in
833 elongating tobacco and/or Arabidopsis pollen tubes.

834

835 **Internalization of membrane lipids and, possibly, selected proteins by subapical endocytosis**

836 As discussed above, FM4-64-labeled structural lipid components of the membrane of secretory
837 vesicles appear to be incorporated in excess amounts into the PM as a consequence of apical
838 secretion required for cell wall biogenesis, and therefore need to be constitutively recycled by
839 subapical endocytic internalization, which was observed not only in BFA-treated tobacco pollen
840 tubes (Figures 3, 5 and 7; Supplemental Figures 11B, 12 and 15), but also during normal tip growth
841 (Figure 1). Perhaps it is not surprising that by contrast to FM4-64-labeled lipids none of the
842 analyzed TM protein markers were internalized within the subapical endocytic PM domain. Many
843 TM proteins presumably have functions all along the pollen tube cell and are delivered by apical
844 secretion to the PM at a rate determined by expression level, which ensures maintenance of
845 adequate protein activity as required for tip growth. Subapical endocytic recycling of such proteins
846 would not serve any apparent purpose, although these proteins of course are expected to be turned-
847 over just like every other cellular factor. In fact, fitting mathematically modeled intracellular
848 distributions of analyzed TM protein makers to experimental data required the assumption that
849 these markers are degraded within the pollen tube shank (Table 2).

850

851 However, endocytic recycling plays a key role in polarizing the accumulation of some TM proteins
852 within specific PM domains in different types of plant cells (e.g. PIN auxin efflux carriers; Geldner
853 et al., 2003; Paciorek et al., 2005). Although our data show that apical AtPRK1 accumulation in
854 tobacco pollen tubes does not depend on subapical endocytosis but requires interactions with the
855 apical cell wall, observations reported in the literature strongly suggest that subapical endocytic

856 internalization is essential for the preferential accumulation of other proteins at the pollen tube
857 apex. The pectin methylesterase inhibitor AtPMEI2, a secreted soluble protein that specifically
858 accumulates within the apical cell wall of tobacco pollen tubes, was detected in BFA compartments
859 in these cells, indicating that this protein is subapically endocytosed (Rockel et al., 2008).
860 Furthermore, the specific accumulation of the receptor-like kinase ANXUR, which contains a single
861 TM domain, within the PM at the apex of Arabidopsis pollen tubes requires subapical clathrin-
862 mediated endocytic uptake, which depends on the AtAP180-related ANTH domain-containing
863 proteins PICALM5a and PICALM5b (Muro et al., 2018). Interestingly, the study by these authors
864 showed that by contrast to ANXUR the apical accumulation of another receptor-like kinase with a
865 single TM domain (AtPRK6) was not affected in *picalm5* mutants, confirming that apical
866 accumulation of TM proteins in pollen tubes can depend on different mechanisms. In any case,
867 subapical endocytic internalization responsible for apical polarization of pollen tube TM or cell wall
868 proteins is expected to depend on specific signals, which appear to be absent from all TM protein
869 markers analyzed in the study presented here. In fact, specific interaction with the WD40 protein
870 At-REN4 was recently proposed to induce subapical clathrin-mediated endocytic internalization of
871 active At-ROP1, which appears to contribute to the maintenance of the specific accumulation of this
872 protein at the pollen tube apex (Li et al., 2018). At-ROP1 is a prenylated peripheral membrane
873 protein, which belongs to the ROP GTPase family and plays a key role in the control of tip growth
874 (Qin and Yang, 2011).

875

876 **Drift and diffusion of PM components**

877 Membrane traffic at the pollen tube tip (Figure 9) is proposed to result in constant retrograde drift of
878 PM material from the apical site of secretion to the subapical endocytic domain (Kost, 2008;
879 Grebnev et al., 2017). Consistent with this hypothesis, in BFA-treated tobacco pollen tubes FM4-
880 64-labeled membrane lipids appear to drift or diffuse from the apical dome to the lateral endocytic
881 domain, where they are endocytosed (Figures 3, 5 and 7; Supplemental Figures 11B, 12 and 15).
882 Furthermore, after photoconversion at the apex of Arabidopsis pollen tubes, red fluorescent
883 AtPRK1::Dendra2 also appears to move within the PM from the apical dome to lateral regions (Luo
884 et al., 2016). Interestingly, results of mathematical modeling of TM protein marker and FM4-64
885 distributions, which are presented here, indicate that both TM proteins and membrane lipids display
886 typical diffusion coefficients within the PM in all regions of tobacco pollen tubes with the exception
887 of the apical dome. Within the apical PM, diffusion of both types of PM components appears to be
888 much slower (Table 2), an effect that can perhaps be attributed to molecular crowding resulting
889 from massive apical secretion (Goose and Sansom, 2013). To thoroughly understand apical
890 membrane traffic underlying tip growth the diffusion coefficients of different types of membrane

891 components (TM proteins, FM4-64-labeled lipids) in all regions of the pollen tube PM need to be
892 experimentally determined. To this end, photoconversion (Luo et al., 2016) along with other
893 techniques, such as fluorescence correlation spectroscopy (Li et al., 2016) or single particle tracking
894 (Cui et al., 2018) can be applied.

895

896 For reasons that are not entirely clear, investigating diffusion of pollen tube PM components based
897 on regular FRAP analyses appears to be challenging. Surprisingly little recovery of PM-associated
898 TM protein marker fluorescence was observed even after prolonged post-bleach incubation within
899 photobleached areas in subapical regions or in the shank of tobacco pollen tubes both here as well
900 as in previously reported experiments (Lee et al., 2008). While this observation confirms that
901 substantial secretion of the analyzed markers for membrane traffic is confined to the apical dome, it
902 appears inconsistent with results of modeling steady-state distribution patterns of these markers,
903 which indicate that they display typical diffusion coefficients within the PM of tobacco pollen tubes
904 outside of the apical dome (Table 2). Photobleaching generates ROS (reactive oxygen species),
905 including free radicals, that can damage analyzed fluorophores (Dixit and Cyr, 2003; Icha et al.,
906 2017). Damaged TM protein markers may form stable aggregates within photobleached regions of
907 the tobacco pollen tube PM, which possibly are highly resistant to both degeneration and
908 penetration by freely diffusible native marker proteins present in adjacent membrane domains.

909

910 **Additional sites of secretion and endocytosis**

911 Although results of the study presented here support the classical model of tip growth, suggesting
912 that bulk secretion required for cell wall biogenesis occurs apically and is compensated by massive
913 subapical endocytic recycling of membrane material, additional secretory and endocytic pathways
914 with roles e.g. in the subcellular targeting or degradation of specific proteins are likely to contribute
915 to membrane trafficking in elongating pollen tubes.

916

917 In a previous study, red-fluorescent FM4-64 labeling was analyzed by confocal time-lapse imaging
918 during the first 10 min after dye application (redistribution stage defined in the study presented
919 here) to tobacco pollen tubes, which already displayed steady-state labeling with pre-loaded FM1-
920 43, a closely related green-fluorescent styryl dye (Zonia and Munnik, 2008). Confocal images
921 simultaneously recorded in the green and red channels were superimposed using an unspecified
922 procedure to generate overlay images indicating regions of dye co-localization by yellow color-
923 coding. Results obtained indicated dye co-localization shortly after FM4-64 application specifically
924 at the interface between the PM within the apical dome and apical vesicles accumulating directly
925 underneath. As proposed by the authors, these observations may indicate that massive FM4-64

926 endocytosis also occurs within the apical dome of tobacco pollen tubes. However, our analysis of
927 FM4-64 redistribution within the tobacco pollen tube PM (Figure 1C) demonstrates that during the
928 first 10 min after application (redistribution stage) this dye preferentially accumulates at the apex,
929 whereas it displays a much more even distribution later at the steady-state stage. Conceivably,
930 depending on the procedure employed, superimposition of images showing redistribution and
931 steady-state stage styryl dye labeling in tobacco pollen tubes (Figure 1C), as was essentially done
932 by Zonia and Munnik (2008), may result in overlay images similar to those presented the study
933 published by these authors.

934

935 Bove et al. (2008) also proposed that massive endocytosis may occur at the extreme pollen tube
936 apex based on patterns of mobility displayed by cytoplasmic components, which these authors
937 observed at the tip of *Lilium longiflorum* pollen tubes using time-lapse differential interference
938 contrast transmitted light microscopy as well as FRAP analysis of FM1-43-stained endomembrane
939 compartments. Whereas the characterization and analysis of the observed mobility patterns
940 definitely were highly informative with regards to cytoplasmic transport processes, this approach
941 obviously can only provide indirect evidence with regards to sites of bulk endocytic PM
942 internalization.

943

944 Visualization of the internalization of externally applied positively charged nanogold particles into
945 tobacco pollen tubes using electron microscopy (Moscatelli et al., 2007) confirmed subapical
946 clathrin-mediated bulk endocytic uptake of such particles, which, consistent with established FM4-
947 64 transport routes, were either rapidly recycled to the secretory system or transported to the
948 vacuole. However, using this technique an additional minor pathway was identified, through which
949 positively charged nanogold particles appear to be subapically endocytosed in a clathrin-
950 independent manner before they are transported exclusively to the vacuole (Moscatelli et al., 2007).
951 Interestingly, the same study also generated evidence suggesting that negatively charged nanogold
952 particles undergo clathrin-mediated endocytosis within the apical dome rather than subapically and
953 are also subsequently transported exclusively to the vacuole (Moscatelli et al., 2007).

954

955 Apical bulk secretion required for cell wall biogenesis at the pollen tube tip may also be
956 complemented by additional conventional or unconventional secretory pathways (Wang et al.,
957 2017). The vascular sorting receptor (VSR), a TM protein that typically accumulates to highest
958 levels on the surface of endocytic endomembrane compartments, also reached the surface of
959 tobacco pollen tubes, possibly as a consequence of temporary local fusion of prevacuolar
960 compartments with the PM (Wang et al., 2011). Furthermore, the pectin methylesterase NtPPME1,

961 a soluble protein that is secreted at the pollen tube apex, is proposed to bypass the classical TGN on
962 its way to the apical cell wall in tobacco pollen tubes (Wang et al., 2016).

963

964 **CONCLUSIONS**

965 Results of the study presented here establish that bulk secretion required for cell wall biogenesis
966 occurs within a small apical domain (0-3.5 μm from the apex) at the extreme tip of tobacco pollen
967 tubes and is compensated by massive constitutive endocytic recycling, specifically of PM lipids,
968 which is restricted to a clearly defined (5.9-14.8 μm from the apex) subapical region. The subapical
969 F-actin fringe is not required for subapical endocytic lipid recycling but colocalizes with a detached
970 TGN compartment, which is ideally positioned to integrate endocytic and secretory membrane
971 traffic and to generate the secretory vesicles that are accumulating within the ARVA. Different lipid
972 and TM protein markers for membrane traffic displayed surprisingly diverse steady distribution
973 patterns within the pollen tube PM apparently as a consequence of marker-specific a) rates of
974 secretion, endocytosis, diffusion and degradation, as well as b) interactions with cell wall
975 components. Together, these findings provide an essential structural basis for the characterization of
976 molecular mechanisms responsible for the maintenance of the specific accumulation of different
977 regulatory proteins and lipids with important functions in the control of directional cell expansion
978 within clearly distinct domains of the PM at the tip of tobacco pollen tubes. To support and enhance
979 results of the study presented here, it will be important to further characterize the *in vivo* dynamics
980 of the investigated markers based on photoactivation or photoconversion studies, fluorescence
981 correlation spectroscopy and single particle imaging.

982

983 **MATERIALS AND METHODS**

984 **Plasmids**

985 Construction and analysis of recombinant plasmid DNA (pDNA) was performed using standard
986 methods (Snapp, 2005; Sambrook and Russell, 2014). All PCR products and junctions between
987 ligated fragments were verified based on sequencing. For small- or large-scale pDNA purification,
988 the mi-Plasmid Miniprep Kit (Metabion International AG) and the JetStar 2.0 Maxiprep kit
989 (Genomed; Lohne, Germany) were employed, respectively.

990

991 Expression plasmids containing an eYFP (enhanced yellow fluorescent protein) cDNA (BD
992 Biosciences-Clontech; San Jose, United States) fused in frame to cDNA sequences coding for full-
993 length or truncated forms of the following proteins were generated: tobacco (*Nicotiana tabacum*)
994 inositol transporter 4 (NtINT4; Sierra et al., 2014), Arabidopsis (*Arabidopsis thaliana*) rare cold
995 inducible protein 2a (AtRCI2a; Capel et al., 1997), Arabidopsis pollen receptor-like kinase 1

996 (AtPRK1; Kazusa et al., 2000), and Arabidopsis clathrin coat assembly protein AP180 (AtAP180;
997 Barth and Holstein, 2004). To generate plasmids for transient expression experiments, cDNA
998 sequences coding for NtINT4, AtPRK1, AtPRK1 lacking the first 229 N-terminal amino acids
999 (AtPRK1 Δ SP-LRR), or AtAP180 were cloned into a pUCAP-based vector (pHD32:
1000 LAT52::MCS::5xGA::eYFP::NOS; Klahre et al., 2006) using a multiple cloning site (MCS) located
1001 at the 5'-end of a cDNA encoding eYFP with a flexible 5x Glycine-Alanine (5xGA) linker attached
1002 at the N-terminus, which was positioned between a LAT52 promoter (Twell et al., 1990) and a NOS
1003 polyA+ signal (derived from pBI121; Jefferson et al., 1987). The NtINT4 and AtAP180 cDNAs
1004 were inserted into this pUCAP-based vector such that the sequence encoding the 5xGA linker was
1005 eliminated. By contrast, the AtRCI2a cDNA was inserted into the MCS of another pUCAP-based
1006 vector (pWEN240: LAT52::eYFP::5GA::MCS::NOS; Klahre et al., 2006) using a MCS located at
1007 the 3'-end of a cDNA encoding eYFP with a 5xGA linker attached at the C-terminus, which was
1008 also positioned between the same LAT52 promoter and NOS polyA+ signal. Finally, the
1009 LAT52::NtINT4::eYFP::NOS and LAT52::eYFP::5xGA::AtRCI2a::NOS expression cassettes
1010 generated as described above were transferred into the binary vector pPZP212 (Hajdukiewicz et al.,
1011 1994) to enable stable plant transformation.

1012
1013 Besides the constructs cloned as indicated in the previous paragraph, additional plasmids already
1014 described in the literature were used in this study, which were also generated based on the vectors
1015 pWEN240 or pHD32 and contained between the LAT52 promoter and the NOS polyA+ signal
1016 cDNA sequences coding for one of the following eYFP fusion proteins: eYFP::5xGA::NtRISAP
1017 (NtRISAP: tobacco RAC5 interacting subapical pollen tube protein; Stephan et al., 2014),
1018 lifeact::5xGA::eYFP (lifeact: N-terminal 17 amino acids of yeast (*Saccharomyces cerevisiae*) actin
1019 binding protein 140 [ScAbp140¹⁻¹⁷]; Riedl et al., 2008; Montes-Rodriguez and Kost, 2017) and
1020 eYFP::5xGA::MTn (MTn: C-terminal 197 amino acids of mouse (*Mus musculus*) talin 1
1021 [MmTalin1²³⁴⁵⁻²⁵⁴¹]; Kost et al., 1998; Montes-Rodriguez and Kost, 2017). Supplemental table 1
1022 contains a complete list of all plasmids employed for the work presented here.

1023

1024 **Plant material**

1025 To establish a constant supply of fresh pollen, wild-type tobacco (*N. tabacum* Petit Havana SR1)
1026 plants were grown from seeds at regular intervals (ca. 1 month) and maintained from seed
1027 germination to flowering in the same growth chamber under the following conditions: 16 hours of
1028 illumination (200-250 $\mu\text{mol m}^{-2} \text{s}^{-1}$) at 24 °C followed by 8 hours of darkness at 18 °C with a
1029 constant relative humidity of 60-65%. Seeds were germinated on sowing soil (ProfiFlor GmbH;
1030 Pulheim, Germany), and emerging seedlings were transferred after 2-3 weeks to type T soil

1031 (ProfiFlor GmbH), on which plants were subsequently grown until flowering. Fresh pollen
1032 collected from mature wild-type tobacco plants was used for all transient expression experiments.
1033 Transgenic pollen collected from transformed plants, which were grown as described above for
1034 wild-type plants, was either used fresh or was preserved by collecting mature anthers, which were
1035 immediately shock-frozen in liquid nitrogen and stored at – 80 °C.

1036

1037 **Stable plant transformation**

1038 Transgenic tobacco plants containing LAT52::NtINT4::eYFP::NOS or
1039 LAT52::eYFP::5xGA::AtRCI2a::NOS expression cassettes were generated by *Agrobacterium*
1040 *tumefaciens*-mediated transformation essentially as described (Horsch and Klee, 1986). To this end,
1041 pPZP212 (Hajdukiewicz et al., 1994) derived binary plasmids (pFAU656 or pFAU302) containing
1042 these cassettes were transformed into chemically competent *A. tumefaciens* AGL1 bacteria (Lazo et
1043 al., 1991).

1044

1045 **Pollen tube culture and transient transformation**

1046 Fresh or preserved (at -80 °C) wild-type or transgenic pollen was transferred onto “pollen tube *N.*
1047 *tabacum*” (PTNT) medium (Read et al., 1993, 1993) solidified with 0.25% (w/v) phytigel (Sigma-
1048 Aldrich Corporation; St. Louis, Missouri, United States) as previously described (Kost et al., 1998;
1049 Johnson and Kost, 2010). Generally, pollen collected from 2-3 flowers was used to prepare two 55
1050 mm plates each containing 3.5 ml solid PTNT medium. For pollen germination and pollen tube
1051 culture, plates were placed in an incubator providing 22 °C in complete darkness.

1052

1053 For transient transformation, immediately after plating on solid PTNT medium wild-type pollen
1054 was bombarded with pDNA-coated gold particles using a PDS 1000/He biolistic gun (Bio-Rad,
1055 Munich, Germany) as previously described (Kost et al., 1998; Johnson and Kost, 2010). pDNA
1056 coating was performed by adding to each batch of washed particles 25 µl 2.5 M CaCl₂, 10 µl 1%
1057 protamine sulfate (Sigma-Aldrich Corporation) and 3 µg pDNA.

1058

1059 Stably or transiently transformed pollen tubes were cultured for 2.5 h before analysis by laser
1060 scanning confocal microscopy.

1061

1062 **FM4-64 labeling and BFA treatment of cultured pollen tubes**

1063 Stock solutions containing either 10 mM FM4-64 (Thermo Fisher Scientific; Waltham,
1064 Massachusetts, USA) or 10 mM BFA (Brefeldin A; Thermo Fisher Scientific) in DMSO (100%
1065 v/v) were prepared and stored at - 20 °C. FM4-64 and BFA were applied to cultured pollen tubes as

1066 described by Stephan et al. (2014). In brief, for time-course imaging 200 µl liquid PTNT medium
1067 containing 50 µM FM4-64 or 70 µM BFA was added to pollen tubes that had been growing for 2.5
1068 hours on the surface of 3.5 ml solid PTNT medium under the conditions described in the previous
1069 section. Consequently, treated pollen tubes were exposed to final concentrations of 2.7 µM FM4-64
1070 and 0.027% DMSO, or 3.8 µM BFA and 0.0378% DMSO. After FM4-64 or BFA application,
1071 pollen tubes were either returned to culture or immediately imaged. Equally treated pollen tubes, to
1072 which 200 µl liquid PTNT containing just DMSO has been added (final DMSO concentration:
1073 0.0378%), served as controls. For time-lapse imaging of individual pollen tubes (Supplemental
1074 Figures 11 and 15), 200 µl liquid PTNT medium containing 15 µM FM4-64 or 50 µM BFA was
1075 added to pollen tubes growing on the surface of 3.5 ml solid PTNT medium, and samples were
1076 prepared for microscopy (as described in next paragraph) immediately after dye or drug application.
1077

1078 **Laser scanning confocal microscopy and growth rate measurement**

1079 Single square sections (1-2.25 cm² in size) of solid PTNT medium were cut out with a scalpel from
1080 plates containing transformed and/or FM4-64-labeled pollen tubes, transferred onto a 76 x 26 x 1
1081 mm glass slide and covered with a 24 x 50 mm No. 1.5 cover slip (Marienfeld Superior; Lauda-
1082 Königshofen, Germany), which was placed directly onto the growing pollen tubes. Medial optical
1083 sections through analysed pollen tubes were acquired using upright or inverted TCS SP5 II or SP8
1084 DIVE-FALCON laser scanning confocal microscope (Leica Microsystems; Wetzlar, Germany),
1085 either through an HCX PL APO CS 63.0x/1.20 NA water immersion or an HCX PL APO CS
1086 63.0x/1.30 NA glycerol immersion objective (Leica Microsystems). Excitation at 514 nm and
1087 emission detection in the range of 525-565 nm or 650-795 nm, respectively, were employed to
1088 image eYFP and FM4-64. The same excitation and emission detection parameters were also used
1089 for simultaneous two-channel eYFP and FM4-64 imaging based on sequential line-by-line
1090 scanning. All images except those generated during FRAP experiments (see next section) were
1091 recorded with the pinhole set to a diameter of 1 Airy unit, at a resolution of 1024 x 1024 pixels and
1092 a dynamic range of 8 bit, using argon laser excitation, a scan rate of 400 Hz and 3x line averaging.
1093 Other imaging parameters (photomultiplier gain and offset, AOTF transmission) were always set to
1094 maximally exploit the available dynamic range. To assess the viability of each analyzed pollen tube,
1095 its growth rate after confocal fluorescence imaging was determined by recording two time-lapse
1096 images at an interval of 1 min in the transmitted light bright-field mode and by measuring the
1097 distance between the positions of the extreme pollen tube apex on the two images. ImageJ software
1098 (Abràmoff et al., 2004) was employed to import the two time-lapse images and to apply a straight-
1099 line measuring tool.

1100

1101 **Fluorescence recovery after photobleaching (FRAP)**

1102 To investigate fluorescence recovery after photobleaching, the same hardware as described in the
1103 previous paragraph and the FRAP module of the “Leica Application Suite Advanced Fluorescence
1104 (LAS AF)” image acquisition software were employed. For photobleaching, the “zoom in” and “set
1105 background to zero” functions of the FRAP module were used, and samples were exposed for 4-5
1106 consecutive frames to argon laser excitation with AOTF transmission set to 100% for all three laser
1107 lines (488, 496, and 514 nm). Post-bleach fluorescence recovery was observed using the same
1108 imaging settings as described in the previous section with the following exceptions: time-lapse
1109 imaging was performed at a resolution of 512 x 512 pixels without line averaging. To assess the
1110 viability of each analyzed pollen tube after photobleaching, its growth rate during post-bleach time-
1111 lapse imaging was determined by measuring the distance between the positions of the extreme
1112 pollen tube apex on first and the last image recorded. To this end, ImageJ software was employed as
1113 described in the previous section.

1114

1115 **Time-lapse and time-course imaging**

1116 Time-lapse imaging was executed by recording serial images of individual pollen tubes at regular
1117 time intervals (Figures 2, Supplemental Figures 2-4, 6, 9, 11 and 15). For several reasons, time-
1118 lapse imaging of pollen tubes for periods longer than a couple of minutes (Supplemental Figures 11
1119 and 15) represented a major challenge: 1) ambient temperature and humidity on the microscope
1120 stage gradually affected pollen tube cultures, 2) observed pollen tubes often grew against an
1121 obstacle (i.e. another pollen tube), or into the medium out of reach of high-magnification lenses
1122 with short working distances, and 3) repeated imaging of the individual pollen tube resulted in
1123 phototoxicity. These problems were largely avoided by time-course imaging, which was performed
1124 without keeping track of individual pollen tubes by recording images of large numbers of different
1125 pollen tubes during each of the indicated time periods after FM4-64 or BFA application (Figures
1126 1C, 3A, 4A, 5 and 7; Supplemental Figures 10 and 12). This allowed time-effective imaging of
1127 many pollen tubes under optimal conditions.

1128

1129 **Quantitative analysis of plasma membrane-associated marker fluorescence**

1130 To quantify TM protein marker (eYFP) or FM4-64 fluorescence associated with distinct regions of
1131 the plasma membrane (PM) at different meridional distances from the extreme apex (Figure 1B and
1132 C: 0-32.6 μm ; Figure 2: extreme apex or center of the lateral bleached region; Figures 3 and 4: 0-
1133 3.6 μm [“Apex”], 3.6-12.6 μm [“Subapex”] or 12.6-32.6 μm [“Shank”]; Supplemental Figure 6:
1134 center of the lateral bleached region), ImageJ software (Abràmoff et al., 2004) was employed to
1135 import unprocessed confocal images and to roughly trace a segmented line with a width of 4 pixels

1136 along each membrane region to be analyzed. Subsequently, the “spline fit” function was employed
1137 to adjust the curvature of each segmented line such that it completely covered the analyzed
1138 membrane region, and a plot profile was read out providing an intensity value for each pixel of the
1139 segmented line. From these intensity values the mean background intensity determined in a circular
1140 region of each image showing no fluorescence was subtracted. All sample and background intensity
1141 values were imported and processed using Mathematica 10.0 (Wolfram Research Inc.; Champaign,
1142 USA) or Excel software (Microsoft Corporation; Redmond, USA), respectively, to generate the line
1143 plots displayed in figure 1, or the charts presented in figures 2, 3 and 4, as well as in supplemental
1144 figure 6. Whereas line plots in figure 1 represent absolute intensity values, figures 2, 3 and 4, as
1145 well as supplemental figure 6, show normalized data. Mean intensity values obtained for the
1146 different PM regions indicated in figures 3 and 4 were normalized for each individual imaged
1147 pollen tube to enable statistical analysis of relative levels of PM-associated marker fluorescence in
1148 the distinct regions irrespective of variability in the overall labeling intensity between different
1149 pollen tubes. To this end, the mean intensity values obtained for each pollen tube were normalized
1150 based on the highest value measured in any of the analysed PM regions in this particular pollen
1151 tube, which was set to 100 %. If possible, both sides of individual pollen tubes were separately
1152 analyzed using the described procedure, such that each pollen tube could potentially provide two
1153 independent measurements for each membrane region and time point. To quantify recovery of PM
1154 labeling in FRAP experiments, intensity values obtained for each individual analysed pollen tube
1155 were normalized based on the pre-bleach value measured at the extreme apex (Figure 2) or in the
1156 centre of the lateral bleached regions (Supplemental Figure 6), which was set to 100%.

1157

1158 **Quantitative analysis of the length and position of PM domains**

1159 To determine the meridional distance from the extreme pollen tube apex of proximal and distal
1160 endpoints of PM domains, ImageJ software (Abràmoff et al., 2004) was employed essentially as
1161 described in the previous section. In imported images, the PM between the extreme apex and each
1162 of the two domain endpoints was roughly traced with a segmented line whose curvature was
1163 subsequently adjusted to fit the PM using the “spline fit” function. After calibration, the length of
1164 the adjusted segmented lines could be directly read out providing exact information about domain
1165 length and position. If possible, both sides of individual pollen tubes were separately analyzed as
1166 described, such that each pollen tube could potentially provide two independent measurements of
1167 the position of a membrane domain.

1168

1169 **Statistical analysis**

1170 Mean and standard deviation of all data sets generated were calculated using Mathematica 10.0
 1171 (Wolfram Research Inc.; Champaign, USA; Figure 1; line plots) or Excel software (Microsoft
 1172 Corporation; Redmond, Washington, USA; all other data sets), whereas the statistical significance
 1173 of differences between data sets was analysed using GraphPad Prism software (GraphPad Software;
 1174 La Jolla, California, USA). A “Student’s *t*-test” (Student, 1908; unpaired, parametric and two-
 1175 tailed) or an “analysis of variance (ANOVA)” test (Fisher, 1918; parametric, non-repeated and one-
 1176 way) was performed to assess the statistical significance of differences between the means of two or
 1177 more data sets, respectively. The ANOVA Dunnett’s (Dunnett, 1955) and Tukey’s (Tukey, 1949)
 1178 post-hocs were employed to analyze data sets with or without a reference data set, respectively. The
 1179 95 % confidence level corresponding to *p*-values of less than or equal to 0.05 ($p\text{-value} \leq 0.05$) was
 1180 defined to indicate statistical significance.

1181

1182 **Mathematical modeling**

1183 The steady-state distribution profiles of TM protein markers (TMP) and of FM4-64 within the
 1184 pollen tube PM (Figure 1 B and C) were mathematically expressed in the form of the following
 1185 basic Fokker-Planck equations:

$$\begin{array}{ccccccc}
 & & \text{term 1} & & \text{term 2} & & \text{term3} & & \text{term4} & & \\
 \text{TMP} & & D \frac{\partial^2 c(x, t)}{\partial x^2} & - & v_0 \frac{\partial c(x, t)}{\partial x} & + & Q & + & Kc(x, t) & = & \frac{\partial c(x, t)}{\partial t} = 0 \quad [1]
 \end{array}$$

$$\begin{array}{ccccccc}
 \text{FM4-64} & & D \frac{\partial^2 c(x, t)}{\partial x^2} & - & v_0 \frac{\partial c(x, t)}{\partial x} & + & Q & + & R & = & \frac{\partial c(x, t)}{\partial t} = 0 \quad [2] \\
 \text{(apical)} & & & & & & & & & &
 \end{array}$$

$$\begin{array}{ccccccc}
 \text{FM4-64} & & D \frac{\partial^2 c(x, t)}{\partial x^2} & - & v_0 \frac{\partial c(x, t)}{\partial x} & + & qc(x, t) & + & R & = & \frac{\partial c(x, t)}{\partial t} = 0 \quad [3] \\
 \text{(subapical)} & & & & & & & & & &
 \end{array}$$

1186

1187 These equations define local marker concentrations $c(x, t)$ within the PM as a function of x , which is
 1188 the meridional distance from the extreme pollen tube apex, and t , which represents time. $c(x, t)$ is
 1189 considered proportional to the experimentally determined intensity of marker fluorescence
 1190 (Soboleski et al., 2005; Lo et al., 2015). As steady-state marker distributions are modeled,
 1191 $\partial c(x, t) / \partial t$ needs to equal 0. The first term of all equations accounts for marker diffusion with the
 1192 coefficient D (results section: process 3). The second term represents constant retrograde marker
 1193 drift at velocity v_0 , which corresponds to pollen tube growth rate and has a negative sign, as all
 1194 markers drift backwards from the pollen tube apex (results section: process 1). The third term
 1195 represents local increase (source Q : positive sign, independent of marker density) or decrease (sink
 1196 $qc(x, t)$: negative sign, proportional to marker density) in marker density within the PM (results
 1197 section: process 2). Finally, the fourth term represents marker degradation ($Kc(x, t)$: negative sign,

1198 proportional to marker density), or ongoing PM staining by residual FM4-64 (R : positive sign,
 1199 independent of marker density) (results section: process 4).

1200

1201 As discussed in detail in the results section, 1) the model divides the PM into four regions (apical a ,
 1202 F-actin fringe, subapical sa , shank s) and 2) the basic Fokker-Planck equations [1]-[3] were adjusted
 1203 to account for different sets of the four processes introduced in the previous paragraph occurring in
 1204 each region (see Table 1), as well as to incorporate additional model assumptions. Briefly
 1205 summarized, the following assumption were made: 1) v_0 is equal in all regions, 2) in the F-actin
 1206 fringe region, apart from retrograde flux only diffusion occurs with marker-specific coefficients
 1207 undergoing transition from apical to the subapical values, 3) in the shank region, $Q_s = 0$ and $q_s = 0$,
 1208 4) in the subapical region and in the shank $D_{sa} = D_s$ and $K_{sa} = K_s$, 5) in the apical dome, $K_a = 0$ and
 1209 $R_a = 0$, and 5) in the subapical region, $R_{sa} = 0$. Consequently, the following modified Fokker-Planck
 1210 equations were obtained, which describe TMP and FM4-64 concentrations within the apical dome
 1211 $c_a(x)$, the subapical region $c_{sa}(x)$ and the shank $c_s(x)$:

1212

$$c_a(x): \text{TMP/FM4-64} \quad D_a \frac{d^2 c_a(x)}{dx^2} - v_0 \frac{dc_a(x)}{dx} = 0 \quad [4]$$

$$c_{sa}(x): \text{TMP} \quad D_{sa} \frac{d^2 c_{sa}(x)}{dx^2} - v_0 \frac{dc_{sa}(x)}{dx} + Q_{sa} + K_{sa} c_{sa}(x) = 0 \quad [5]$$

$$c_{sa}(x): \text{FM4-64} \quad D_{sa} \frac{d^2 c_{sa}(x)}{dx^2} - v_0 \frac{dc_{sa}(x)}{dx} + q_{sa} c_{sa}(x) = 0 \quad [6]$$

$$c_s(x): \text{TMP} \quad D_s \frac{d^2 c_s(x)}{dx^2} - v_0 \frac{dc_s(x)}{dx} + K_s c_s(x) = 0 \quad [7]$$

$$c_s(x): \text{FM4-64} \quad D_s \frac{d^2 c_s(x)}{dx^2} - v_0 \frac{dc_s(x)}{dx} + R_{sa} = 0. \quad [8]$$

1213

1214 In addition, the general boundary conditions [9] and [10], in which a and b denote the boundary
 1215 between the apical and subapical regions, or between the subapical and shank regions, respectively,
 1216 were applied to equations [4] – [8] to represent the assumption that marker distribution is
 1217 continuous [9] and smooth [10] at the borders between the four defined PM regions. Within the
 1218 apical dome, Q_a was modeled as the total flux of membrane material across the border to the
 1219 adjacent F-actin fringe region, and hence was not directly reflected in the Fokker-Planck equations,
 1220 but was included in the model as a specific boundary condition for this region [11].

1221

$$c_a(a) = c_{sa}(a) \quad \text{and} \quad c_{sa}(b) = c_s(b) \quad [9]$$

$$\left. \frac{dc_a}{dx} \right|_{x=a} = \left. \frac{dc_{sa}}{dx} \right|_{x=a} \quad \text{and} \quad \left. \frac{dc_{sa}}{dx} \right|_{x=b} = \left. \frac{dc_s}{dx} \right|_{x=b} \quad [10]$$

$$v_0 c_a(0) - D_a \left. \frac{dc_a(x)}{dx} \right|_{x=0} = Q_a \quad [11]$$

1222

1223 The solutions of equations [4] – [8] reflecting all boundary conditions [9] – [11] and containing the
 1224 constants $\sigma, \sigma', c_\infty, c'_\infty, A, A', B, B', C, C'$ or E' , which are defined in supplementary data set 1, take
 1225 the following form:

1226

$$c_s(x): \text{TMP/FM4-64} \quad c_a(x) = \frac{Q_a}{v_0} + \left(c_0 - \frac{Q_a}{v_0} \right) \exp\left(\frac{v_0}{D_a} x\right) \quad [12]$$

$$c_{sa}(x): \text{TMP} \quad c_{sa}(x) = c_\infty - \frac{Q_{sa}}{K_{sa}} + A \exp\left(\frac{v_0(\sigma + 1)}{2D_{sa}} x\right) + B \exp\left(-\frac{v_0(\sigma - 1)}{2D_{sa}} x\right) \quad [13]$$

$$c_{sa}(x): \text{FM4-64} \quad c_{sa}(x) = c'_\infty + A' \exp\left(\frac{v_0(\sigma' + 1)}{2D_{sa}} x\right) + B' \exp\left(\frac{v_0(\sigma' - 1)}{2D_{sa}} x\right) \quad [14]$$

$$c_s(x): \text{TMP} \quad c_s(x) = c_\infty + C \exp\left(-\frac{v_0(\sigma - 1)}{2D_s} x\right) \quad [15]$$

$$c_s(x): \text{FM4-64} \quad c'_s(x) = \frac{R_s}{v_0} x + C' \exp\left(\frac{v_0}{D_s} x\right) + E' \quad [16]$$

1227

1228 Modeling experimental line plots displaying average intensity of PM-associated marker
 1229 fluorescence (Figure 1B and C) required normalization of these line plots using the following
 1230 equation:

1231

$$f_i(x) = \frac{F_i(x)}{F_i(0)} = \frac{c_i(x)}{c_i(0)} \quad [17]$$

1232

1233

1234 As discussed in detail in the results section, to optimize the fitting of solutions [12] – [16] to
 1235 normalized experimental data, the following marker-specific adjustments were introduced into the
 1236 model: 1) for AtPRK1::eYFP, Q_{sa} was assigned the value 0 resulting in $A = 0, B = C$ and $c_{sa}(x) \rightarrow$
 1237 $c_s(x)$. Consequently, for this marker, D_{sa} and $\sigma - 1$ in solution [13] did not decouple and the only
 1238 value revealed by fitting was $\frac{\sigma-1}{D_{sa}}$; 2) for NtINT4::eYFP, boundary condition [10] was released,
 1239 whereas boundary condition [9] was maintained.

1240

1241 Fitting of the solutions [12] – [16] adjusted as described in the previous paragraph to the normalized
 1242 experimental line plots (Figure 8; light blue line) was performed for each marker independently
 1243 using the “NonlinearModelFit” function of Mathematica 10.0 (Wolfram Research, Inc., Champaign,
 1244 USA). For each marker, the three region-specific solutions were simultaneously fitted to the
 1245 corresponding experimental data, such that all constants contained in these solutions could be

1246 simultaneously read out (Table 2). Because the model was fit to normalized experimental data,
1247 read-out representing zeroth-order constants (Q_a, Q_{sa}, R_s) only had relative physical meaning. By
1248 contrast, read-out representing diffusion coefficients ($D_a, D_{sa} = D_s$) and first-order constants ($K_s =$
1249 K_{sa}, q_{sa}) were not affected by data normalisation and maintained absolute physical meaning.

1250

1251 **ACCESSION NUMBERS**

1252 The amino acid sequences of all proteins employed as markers in this study can be found in the
1253 GenBank database using the indicated accession numbers: eYFP, AAX97736; NtINT4,
1254 XP_016480732; AtRCI2a, AAD17302; AtPRK1, NP_198389; AtAP180, Q9ZVN6; NtRISAP,
1255 AHX26274; ScAbp140, AJT97542.1, and MmTalin1, NP_035732.2.

1256

1257 **SUPPLEMENTAL DATA**

1258 **Supplemental Figure S1.** Mean growth rates of tobacco pollen tubes after confocal imaging of
1259 intracellular TM protein marker distribution or of FM4-64 labeling.

1260 **Supplemental Figure S2.** FRAP time-lapse analysis of NtINT4::eYFP dynamics at the tip of
1261 tobacco pollen tubes.

1262 **Supplemental Figure S3.** FRAP time-lapse analysis of eYFP::AtRCI2a dynamics at the tip of
1263 tobacco pollen tubes.

1264 **Supplemental Figure S4.** FRAP time-lapse analysis of AtPRK1::eYFP dynamics at the tip of
1265 tobacco pollen tubes.

1266 **Supplemental Figure S5.** Mean growth rates during post-bleach time-lapse imaging of tobacco
1267 pollen tubes subjected to FRAP analysis of TM protein marker dynamics at the tip.

1268 **Supplemental Figure S6.** FRAP time-lapse analysis of TM protein marker dynamics behind the
1269 apical dome of tobacco pollen tubes.

1270 **Supplemental Figure S7.** Mean growth rates during post-bleach time-lapse imaging of tobacco
1271 pollen tubes subjected to FRAP analysis of TM protein marker dynamics behind the apical
1272 dome.

1273 **Supplemental Figure S8.** Brefeldin A (BFA) blocks tobacco pollen tube tip growth.

1274 **Supplemental Figure S9.** FRAP time-lapse analysis of TM protein marker dynamics at the tip
1275 of tobacco pollen tubes pre-treated with BFA.

1276 **Supplemental Figure S10.** Time-course analysis of changes in FM4-64 labeling patterns in
1277 normally growing tobacco pollen tubes during the first 60 min after dye application.

1278 **Supplemental Figure S11.** Time-lapse analysis of PM labeling by different markers in
1279 individual tobacco pollen tubes.

1280 **Supplemental Figure S12.** Time-course analysis of BFA-induced loss of FM4-64 PM labeling
1281 in tobacco pollen tubes.

1282 **Supplemental Figure S13.** Mean growth rate of tobacco pollen tubes analyzed to determine the
1283 intracellular distribution of a transiently expressed AtAP180::eYFP fusion protein.

1284 **Supplemental Figure S14.** Mean growth rate of tobacco pollen tubes transiently expressing
1285 eYFP fusion proteins serving as TGN or F-actin markers at non-invasive levels.

1286 **Supplemental Figure S15.** Simultaneous time-lapse analysis of FM4-64 PM labeling and of
1287 non-invasively visualized F-actin structures in individual tobacco pollen tubes treated with BFA
1288 either alone or in combination with Latrunculin B.

1289 **Supplemental Table S1.** List of all plasmids used in this study.

1290 **Supplemental Data Set S1.** Definition of the constants σ/σ' , c_∞/c'_∞ , A/A' , B/B' , C/C' and E' in
1291 the solutions of the Fokker-Planck equations describing marker distributions within the PM.

1292

1293 **ACKNOWLEDGEMENTS**

1294 The authors would like to thank Stephanie Scholz, Sylwia Schulmeister, Jennifer Schuster and
1295 Martin Schuster for outstanding technical support as well as Susanne Holstein (University of
1296 Heidelberg, Germany), Chris Sommerville (University of California [Berkeley], USA), Zhenbiao
1297 Yang (University of California [Riverside], USA) and Norbert Sauer (University of Erlangen-
1298 Nuremberg, Germany) for providing cDNAs encoding AtAP180, AtRCI2a, AtPRK1, and NtINT4,
1299 respectively. Stefan Terjung (ALMF, EMBL Heidelberg, Germany) and Nan Luo (University of
1300 California [Riverside], USA) are acknowledged for invaluable help with the development of FRAP
1301 techniques employed in this study. We are also grateful for excellent scientific and technical
1302 support received from Cecilia Del Casino (University of Siena, Italy), Claudia Faleri (University of
1303 Siena, Italy) and the “Optical Imaging Center Erlangen” (OICE). This research was funded by the
1304 “German Research Foundation” (DFG) within the framework of the “Research Training Group
1305 1962” (Projects 7 [GG, BK] and 10 [MC, A-SS]), and through the ERC StG MembranesAct 2013-
1306 33728 [MC, A-SS]. It was further supported by two DFG “Major Equipment Grants” awarded to

1307 BK: INST90/1074-1FUGG (SP8 DIVE-FALCON microscope) and INST90/1025-1FUGG (plant
1308 growth chamber facility for tobacco).

1309

1310 TABLES

1311 **Table 1.** Processes assumed by the model to substantially contribute to marker distribution profiles
1312 within the indicated regions of the pollen tube PM (marked by “+”).

1313

region	retrograde flux (v_0)	source/sink (Q, q)	diffusion (D)	marker protein degradation (K) staining by residual FM4-64 (R)	
				(K)	(R)
apical (a)	+	+	+		
F-actin fringe	+		+		
subapical (sa)	+	+	+	+	
Shank (s)	+		+	+	+

1314

1315 Table 2.

1316 Read-out after model fitting to experimental data.

1317

region	parameter	unit	NtINT4	AtRCI2a	AtPRK1	AtPRK1 Δ SP-LRR	FM4-64
apical	Q_a	$\mu\text{m}^{-1}\text{s}^{-1}$	6.0 ± 0.3	2.6 ± 0.2	8.3 ± 0.6	6.3 ± 0.3	10.0 ± 0.5
	D_a	$\mu\text{m}^2\text{s}^{-1}$	0.085 ± 0.004	0.051 ± 0.003	0.040 ± 0.003	0.063 ± 0.003	0.034 ± 0.002
subapical	Q_{sa} (TMP) ¹	$\mu\text{m}^{-2}\text{s}^{-1}$	0.31 ± 0.02	5.7 ± 0.4	<i>n.a.</i>	1 ± 0.2	
	q_{sa} (FM4-64) ²	s^{-1}					$-(0.21\pm 0.01)$
	D_{sa} ³	$\mu\text{m}^2\text{s}^{-1}$	0.37 ± 0.05	0.79 ± 0.05	<i>n.a.</i>	0.45 ± 0.05	1.21 ± 0.06
	Q_a/Q_{sa} (TMP)	μm	19.3548	0.4561	<i>n.a.</i>	6.3	
	Q_a/q_{sa} (FM4-64)	μm^{-1}					-47.6190
shank	K_s ⁴ (TMP) ²	10^{-2}s^{-1}	$-(0.72\pm 0.04)$	$-(0.83\pm 0.05)$	<i>n.a.</i>	$-(0.36\pm 0.06)$	
	R_s (FM4-64) ¹	$\mu\text{m}^{-2}\text{s}^{-1}$					0.40 ± 0.02

1318 ¹concentration independent; ²concentration dependent; ³ $D_{sa} = D_s$; ⁴ $K_s = K_{sa}$; TMP: transmembrane proteins.

1319

1320 FIGURE LEGENDS

1321 **Figure 1.** Distribution patterns of TM proteins and FM4-64 serving as markers for membrane
1322 traffic in normally growing tobacco pollen tubes.

1323

1324 (A) Domain structure of the indicated TM protein markers. Protein and domain sizes are drawn to
1325 scale. SP: signal peptide; TM: transmembrane domain; LRR: leucine-rich repeats; PKD: protein
1326 kinase domain.

1327

1328 (B) Left: medial confocal optical sections through representative pollen tubes transiently
1329 (NtINT4::eYFP, AtPRK1::eYFP or AtPRK1 Δ SP-LRR::eYFP) or stably (eYFP::AtRCI2a)
1330 expressing the indicated TM protein marker. Growth rates of the individual pollen tubes shown

1331 (after confocal imaging): 6.8 $\mu\text{m}/\text{min}$ (NtINT4::eYFP), 3.6 $\mu\text{m}/\text{min}$ (eYFP::AtRCI2a), 3.8 $\mu\text{m}/\text{min}$
1332 (AtPRK1::eYFP), or 4.8 $\mu\text{m}/\text{min}$ (AtPRK1 Δ SP-LRR::eYFP). Scale bar: 10 μm .

1333

1334 Right: line plots displaying the intensity of PM-associated eYFP fluorescence at different
1335 meridional distances from the apex ($X=0 \mu\text{m}$) in analyzed pollen tubes ($n = 17$ [NtINT4::eYFP, 3
1336 independent experiments], 29 [eYFP::AtRCI2a, 5 independent experiments], 31 [AtPRK1::eYFP, 5
1337 independent experiments], or 37 [AtPRK1 Δ SP-LRR::eYFP, 5 independent experiments]). Light
1338 blue lines: average intensity; dark blue lines: standard deviation; all other lines: individual line
1339 plots.

1340

1341 (C) Left: medial confocal optical sections through different representative pollen tubes labeled with
1342 the fluorescent lipophilic dye FM4-64 (applied at 50 μM in 200 μl PTNT) for the indicated time
1343 period (initial stage: 0-5 min, redistribution stage: 6-40 min, steady-state stage: 41-60 min). Growth
1344 rates of the individual pollen tubes shown (after confocal imaging): 3.4 $\mu\text{m}/\text{min}$ (0-5 min), 4.8
1345 $\mu\text{m}/\text{min}$ (6-40 min), or 3.8 $\mu\text{m}/\text{min}$ (41-60 min). Scale bar: 10 μm .

1346

1347 Right: line plots displaying the intensity of PM-associated FM4-64 fluorescence at different
1348 meridional distances from the apex ($X=0 \mu\text{m}$) in all analyzed pollen tubes ($n = 6$ [0-5 min], 68 [6-
1349 40 min], or 41 [41-60 min]; 4 independent experiments). Light blue lines: average intensity; dark
1350 blue lines: standard deviation; all other lines: individual line plots.

1351

1352

1353 **Figure 2.** FRAP time-lapse analysis of TM protein marker dynamics at the tip of normally growing
1354 tobacco pollen tubes.

1355

1356 (A) Medial confocal optical sections through representative pollen tubes transiently (NtINT4::eYFP
1357 or AtPRK1::eYFP) or stably (eYFP::AtRCI2a) expressing the indicated TM protein marker, which
1358 were recorded before (row 1; pre-bleach) or after complete photobleaching of eYFP fluorescence
1359 within the dashed box indicated in row 2. t: time elapsed after photobleaching; arrowheads: apical
1360 PM domain within which fluorescence recovery was first observed; *: bleached lateral PM domain
1361 showing no fluorescence recovery. Scale bar: 10 μm .

1362

1363 During post-bleach time-lapse imaging ($t = 0$ to 116-124 s), the growth rate of the individual pollen
1364 tubes shown was: 4.2 $\mu\text{m}/\text{min}$ (NtINT4::eYFP), 8.7 $\mu\text{m}/\text{min}$ (eYFP::AtRCI2a), and 5.1 $\mu\text{m}/\text{min}$
1365 (AtPRK1::eYFP). In total, 7 (NtINT4::eYFP, 2 independent experiments), 10 (eYFP::AtRCI2a, 2

1366 independent experiments) or 12 (AtPRK1::eYFP, 3 independent experiments) TM protein marker
1367 expressing pollen tubes were analyzed. Each TM protein marker displayed essentially the same
1368 fluorescence recovery pattern and kinetics in all analyzed pollen tubes.

1369

1370 **(B)** Quantification of PM labelling by the indicated TM protein marker in the bleached region either
1371 at the extreme apex (0 μm meridional distance from the extreme apex; arrow heads in (A); open
1372 squares) or in the center of a lateral domain (more than 3 μm meridional distance from the extreme
1373 apex; asterisks in (A); open circles) immediately before ($t = -6.5$ s) and after ($t = 0$ s)
1374 photobleaching, as well as after different recovery periods (13s, 26s, 39s, 52s, 65s and 78s). The
1375 indicated average levels of PM labeling were computed from data obtained from all analyzed pollen
1376 tubes (A) after normalization based on pre-bleach levels of PM labeling at the extreme apex, which
1377 were set to 100%.

1378

1379

1380 **Figure 3.** Time-course analysis of BFA-induced loss of FM4-64 PM labeling and investigation of
1381 AtAP180::eYFP distribution in tobacco pollen tubes.

1382

1383 **(A)** Medial confocal optical sections through different representative pollen tubes, which were
1384 grown in the presence of FM4-64 (applied at 50 μM in 200 μl PTNT) for 30 min, before the dye
1385 was washed out from the culture medium and BFA was applied for the indicated time period (70
1386 μM in 200 μl PTNT). Scale bar: 5 μm .

1387

1388 As a result of the BFA treatment, tip growth of all analyzed pollen tubes was completely inhibited
1389 (Supplemental Figure 8). All pollen tubes analysed during each time period after BFA application
1390 ($n = 10$ [0-20 min], 22 [21-40 min], and 35 [41-60 min]; 3 independent experiments) displayed very
1391 similar FM4-64 labeling patterns.

1392

1393 **(B)** Quantitative analysis of the average relative intensity of PM-associated FM4-64 fluorescence in
1394 all pollen tubes analyzed as described in (A) within the apical dome (“Apex”; meridional distance
1395 from the apex: 0-3.6 μm), within a subapical region displaying massive loss of FM4-64 PM labeling
1396 in the presence of BFA (“Subapex”; meridional distance from the apex: 3.6-12.6 μm), and in the
1397 shank (“Shank”; meridional distance from the apex: 12.6-32.6 μm). The borders between these
1398 three PM regions were determined as described in (C). The intensity of PM-associated FM4-64
1399 fluorescence was normalized in each analyzed pollen tube based on the highest measured value (0-
1400 32.6 μm meridional distance from the apex), which was set to 100 %.

1401

1402 The statistical significance of differences in the average intensity of PM-associated FM4-64
1403 fluorescence between the three different PM regions during each time period after BFA application
1404 was assessed using ANOVA (Tukey's test, one way). **: $p \leq 0.01$; ****: $p \leq 0.0001$; ns: not
1405 significantly different ($p > 0.05$). Error bars: standard deviation.

1406

1407 (C) Quantitative analysis of the exact length and position of the subapical PM domains, which
1408 displayed massive loss of FM4-64 PM labeling 21-40 min after BFA application (A) or were
1409 associated with an AtAP180::eYFP fusion protein serving as a marker for sites of clathrin-mediated
1410 endocytosis (D). The average meridional distances from the extreme apex ($x = 0$) of both ends of
1411 these domains in all analysed pollen tubes ($n = 22$ [FM4-64 BFA], or 22 [AtAP180::eYFP]) are
1412 indicated. Exact extensions of domains shown: 5.9 ± 0.91 to 14.8 ± 2.8 μm (AtAP180::eYFP);
1413 3.6 ± 0.61 to 12.6 ± 2.0 μm (FM4-64 BFA).

1414

1415 The statistical significance of differences between the average meridional distances of both the
1416 proximal and the distal ends of the FM4-64 BFA and AtAP180::eYFP domains was assessed using
1417 a Student's *t*-test (two-tailed, type II). ***: $p \leq 0.001$; ****: $p \leq 0.0001$. Error bars: standard
1418 deviation.

1419

1420 (D) Medial confocal optical section through a representative normally growing pollen tube
1421 transiently expressing an AtAP180::eYFP fusion protein that serves as a marker for sites of clathrin-
1422 mediated endocytosis. In total, 25 essentially normally growing pollen tubes were analyzed in 2
1423 independent experiments, which displayed very similar AtAP180::eYFP distribution patterns.
1424 Growth rate of the pollen tube shown (after confocal imaging): 4.8 $\mu\text{m}/\text{min}$. Scale bar: 5 μm .

1425

1426

1427 **Figure 4.** Time-course analysis of PM labeling by TM protein markers in tobacco pollen tubes after
1428 BFA application.

1429

1430 (A) Medial confocal optical sections through different representative pollen tubes transiently
1431 (AtPRK1::eYFP) or stably (NtINT4::eYFP; eYFP::AtRCI2a) expressing the indicated TM protein
1432 marker recorded after treatment with BFA (applied at 70 μM in 200 μl PTNT) for the indicated
1433 time period. Arrows: BFA compartment. Scale bar: 10 μm .

1434

1435 As a result of the BFA treatment, tip growth of all analyzed pollen tubes was completely inhibited
1436 (Supplemental Figure 8). During each time period after BFA application, all imaged pollen tubes
1437 expressing the same TM protein marker displayed highly similar PM labeling patterns
1438 (NtINT4::eYFP [3 independent experiments]: n = 78 [0-60 min], 61 [61-120 min], or 37 [121-180];
1439 eYFP::AtRCI2a [5 independent experiments]: n = 85 [0-60 min], 82 [61-120 min], or 97 [121-180
1440 min]; AtPRK1::eYFP [3 independent experiments]: n = 46 [0-60 min], 37 [61-120 min], or 31 [121-
1441 180 min]).

1442

1443 **(B)** Quantitative analysis of the average relative intensity of PM-associated TM protein marker
1444 fluorescence in all pollen tubes analyzed as described in (A) within the apical dome (“Apex”;
1445 meridional distance from the apex: 0-3.6 μm) and within the subapical endocytic region, which was
1446 identified based on BFA treatment of FM4-64-labeled pollen tubes as described in figure 3
1447 (“Subapex”; meridional distance from the apex: 3.6-12.6 μm). The intensity of PM-associated
1448 marker fluorescence was normalized in each analyzed pollen tube based on the maximal intensity
1449 measured with these two membrane domains (0-12.6 μm meridional distance from the apex), which
1450 was set to 100 %.

1451

1452 For each TM protein marker, the statistical significance of differences in the average intensity of
1453 PM-associated marker fluorescence during different time periods after BFA application was
1454 assessed separately within the apical dome and the subapical endocytic region using ANOVA
1455 (Dunnett’s test, one-way). ns: not significantly different ($p > 0.05$). Error bars: standard deviation.

1456

1457

1458 **Figure 5.** Simultaneous time-course analysis of FM4-64 and TM protein marker PM labeling in
1459 BFA-treated tobacco pollen tubes.

1460

1461 Medial confocal optical sections through different representative pollen tubes transiently
1462 (AtPRK1::eYFP) or stably (NtINT4::eYFP, eYFP::AtRCI2a) expressing the indicated TM protein
1463 marker, which had been grown in the presence of FM4-64 (applied at 50 μM in 200 μl PTNT) for
1464 30 min before the dye was washed out from the culture medium and BFA was applied for the
1465 indicated time period (70 μM in 200 μl PTNT). eYFP fusion proteins serving as TM protein
1466 markers (green fluorescence; “eYFP”) and FM4-64 (red fluorescence; “FM4-64”) were
1467 simultaneously imaged in separate channels. Arrow: BFA compartment Scale bar: 10 μm .

1468

1469 As a result of the BFA treatment, tip growth of all analyzed pollen tubes was completely inhibited
1470 (Supplemental Figure 8). During each of the indicated time periods, all imaged pollen tubes
1471 displayed essentially the same patterns of FM4-64 and of TM marker protein specific eYFP labeling
1472 of the PM (NtINT4::eYFP [2 independent experiments]: n=11 [0-20 min], 22 [21-40 min], or 19
1473 [41-60 min]; eYFP::AtRCI2a [2 independent experiments]: n= 10 [0-20 min], 22 [21-40 min], or 22
1474 [41-60 min]; AtPRK1::eYFP [4 independent experiments]: n = 10 [0-20 min], 16 [21-40 min], or 23
1475 [41-60 min]).

1476

1477 The BFA compartment visible in the NtINT4::eYFP-expressing pollen tube shown (21-40 min after
1478 BFA application) was clearly more strongly labelled by FM4-64 than by NtINT4::eYFP (ratio
1479 between the average fluorescence intensities displayed by the BFA compartment and by the apical
1480 plasma membrane: 1.39 [FM4-64] and 0.65 [NtINT4::eYFP]).

1481

1482

1483 **Figure 6.** Positional mapping of a detached TGN compartment and of the F-actin fringe relative to
1484 each other and to the subapical endocytic PM domain in tobacco pollen tubes.

1485

1486 **(A)** Medial confocal optical sections through representative essentially normally growing pollen
1487 tubes transiently expressing the TGN marker eYFP::NtRISAP (n = 13, 4 independent experiments),
1488 or one of the F-actin markers lifeact::eYFP (n = 17, 3 independent experiments) or eYFP::MTn (n =
1489 19, 3 independent experiments). All pollen tubes expressing the same marker displayed highly
1490 similar eYFP labeling patterns. Growth rate of the pollen tubes shown (after confocal imaging): 3.6
1491 $\mu\text{m}/\text{min}$ (eYFP::NtRISAP), 5.4 $\mu\text{m}/\text{min}$ (Lifeact::eYFP), and 4.8 $\mu\text{m}/\text{min}$ (eYFP::MTn). Scale bar:
1492 10 μm .

1493

1494 **(B)** Quantitative analysis of the meridional distance from the extreme apex ($X = 0 \mu\text{m}$) of the most
1495 proximal and the most distal contact points of the NtRISAP-associated TGN compartment, or of the
1496 F-actin fringe, with the PM in all pollen tubes analysed as described in (A). For direct comparison,
1497 the position of the AtAP180::eYFP labeled subapical endocytic PM domain, which was determined
1498 in normally growing pollen tubes as described above (Figure 3C and D), is also indicated. Exact
1499 extensions of domains shown: 3.4 ± 0.21 to $7.4 \pm 0.26 \mu\text{m}$ (TGN; eYFP::NtRISAP), 3.6 ± 0.23 to
1500 $5.5 \pm 0.25 \mu\text{m}$ (F-actin fringe; lifeact::eYFP), 3.5 ± 0.20 to $5.6 \pm 0.20 \mu\text{m}$ (F-actin fringe; eYFP::MTn)
1501 and 5.9 ± 0.91 to $14.8 \pm 2.8 \mu\text{m}$ (subapical endocytic domain; AtAP180::eYFP).

1502

1503 The statistical significance of differences between the average meridional distances of proximal and
1504 distal ends (a, a', b, b', c, d, e and f) of different PM domains were analysed as indicated using
1505 ANOVA (Tukey's test, one-way). Note that the distal end of the F-actin fringe (irrespective of the
1506 marker used) and the proximal end of the subapical endocytic domain are statistically significantly
1507 different (bc, b'c). *: $p \leq 0.05$; **: $p \leq 0.01$; ***: $p \leq 0.001$; ****: $p \leq 0.0001$; ns: not significantly
1508 different ($p > 0.05$). Error bars: standard deviation.

1509

1510

1511 **Figure 7.** Simultaneous time-course analysis of FM4-64 PM labeling and of non-invasively
1512 visualized F-actin structures in BFA-treated tobacco pollen tubes.

1513

1514 Medial confocal optical sections through different representative pollen tubes transiently expressing
1515 the indicated non-invasive F-actin markers (Lifeact::eYFP or eYFP::MTn), which had been grown
1516 in the presence of FM4-64 (applied at 50 μ M in 200 μ l PTNT) for 30 min before the dye was
1517 washed out from the culture medium and BFA was applied for the indicated time period (70 μ M in
1518 200 μ l PTNT). Lifeact::eYFP or eYFP::MTn fusion proteins (green fluorescence; "eYFP") and
1519 FM4-64 (red fluorescence; "FM4-64") were simultaneously imaged in separate channels. Scale bar:
1520 10 μ m.

1521

1522 As a result of the BFA treatment, tip growth of all analyzed pollen tubes was completely inhibited
1523 (Supplemental Figure 8). During each of the indicated time periods, all imaged pollen tubes
1524 displayed essentially the same FM4-64 PM labeling patterns ("FM4-64") and very similar F-actin
1525 structures ("eYFP") labeled by one of the two non-invasive markers (Lifeact::eYFP [3 independent
1526 experiments]: n = 13 [0-20 min], 14 [21-40 min], or 13 [41-60 min]; eYFP::MTn [4 independent
1527 experiments]: n = 16 [0-20 min], 24 [21-40 min], or 14 [41-60 min]).

1528

1529

1530 **Figure 8.** Fitting of a mathematical model of steady-state marker distributions within the pollen
1531 tube PM to experimental data.

1532

1533 The experimental line plots depicted in light blue represent the steady-state distribution of the
1534 indicated markers for membrane traffic within the PM and show the average intensity of PM-
1535 associated marker fluorescence at different meridional distances from the extreme pollen tube apex.
1536 The same line plots are also presented in figure 1B and C, but are displayed here after normalization
1537 based on the values at the extreme apex ($X = 1$). The brown lines represent output of a

1538 mathematical model of steady-state marker distribution described in detail in the text, after model
1539 fitting to the experimental line plots. The excellent fit obtained for all markers strongly supports
1540 model relevance. Table 2 summarizes model read-out obtained after fitting, which provides
1541 information concerning the rate and spatial organization of cellular processes (including secretion,
1542 endocytosis, diffusion and degeneration), which determine marker dynamics and steady-state
1543 distribution.

1544
1545

1546 **Figure 9.** Model of apical membrane traffic underlying tobacco pollen tube tip growth.

1547

1548 Secretion required for cell wall biogenesis occurs within the apical dome (0-3.5 μm meridional
1549 distance from the extreme apex) and results in the incorporation of excess lipid material into the
1550 plasma membrane (PM), which is recycled by subapical endocytosis (5.9-14.8 μm meridional
1551 distance from the extreme apex). A subapical trans-Golgi network (TGN) compartment (PM
1552 contacts: 3.4-7.4 μm meridional distance from the extreme apex) serves as a central sorting
1553 organelle with which Golgi-derived as well as endocytic vesicles fuse at the distal end, and which
1554 generates secretory vesicles at its proximal surface. The cortical F-actin fringe (3.6 – 5.6 μm
1555 meridional distance from the extreme apex) maintains the positioning of the subapical TGN
1556 compartment within a pollen tube region displaying rapid cytoplasmic streaming.

1557

1558 LITERATURE CITED

- 1559 **Abràmoff MD, Magalhães PJ, Ram SJ** (2004) Image processing with imageJ. *Biophotonics Int.*
1560 **11:** 36-41
- 1561 **Alabi AA, Tsien RW** (2013) Perspectives on kiss-and-run: role in exocytosis, endocytosis, and
1562 neurotransmission. *Annu. Rev. Physiol.* **75:** 393-422
- 1563 **Baluska F, Hlavacka A, Samaj J, Palme K, Robinson DG, Matoh T, McCurdy DW, Menzel D,**
1564 **Volkman D** (2002) F-actin-dependent endocytosis of cell wall pectins in meristematic root
1565 cells. Insights from brefeldin A-induced compartments. *Plant Physiol.* **130:** 422-431
- 1566 **Barth M, Holstein SE** (2004) Identification and functional characterization of Arabidopsis AP180,
1567 a binding partner of plant alphaC-adaptin. *Journal of cell science* **117:** 2051-2062
- 1568 **Blackbourn HD, Jackson AP** (1996) Plant clathrin heavy chain: Sequence analysis and restricted
1569 localisation in growing pollen tubes. *J. Cell Sci.* **109:** 777-786
- 1570 **Bolte S, Talbot C, Boutte Y, Catrice O, Read ND, Satiat-Jeunemaitre B** (2004) FM-dyes as
1571 experimental probes for dissecting vesicle trafficking in living plant cells. *J. Microsc.* **214:**
1572 159-173
- 1573 **Bosch M, Cheung AY, Hepler PK** (2005) Pectin methylesterase, a regulator of pollen tube
1574 growth. *Plant physiology* **138:** 1334-1346
- 1575 **Bosch M, Hepler PK** (2005) Pectin methylesterases and pectin dynamics in pollen tubes. *Plant*
1576 *Cell* **17:** 3219-3226
- 1577 **Bou Daher F, Geitmann A** (2011) Actin is involved in pollen tube tropism through redefining the
1578 spatial targeting of secretory vesicles. *Traffic* **12:** 1537-1551

- 1579 **Bove J, Vaillancourt B, Kroeger J, Hepler PK, Wiseman PW, Geitmann A** (2008) Magnitude
1580 and direction of vesicle dynamics in growing pollen tubes using spatiotemporal image
1581 correlation spectroscopy and fluorescence recovery after photobleaching. *Plant physiology*
1582 **147**: 1646-1658
- 1583 **Cai G, Parrotta L, Cresti M** (2015) Organelle trafficking, the cytoskeleton, and pollen tube
1584 growth. *J. Integr. Plant Biol.* **57**: 63-78
- 1585 **Capel J, Jarillo JA, Salinas J, Martinez-Zapater JM** (1997) Two homologous low-temperature-
1586 inducible genes from *Arabidopsis* encode highly hydrophobic proteins. *Plant physiology*
1587 **115**: 569-576
- 1588 **Cardenas L, Lovy-Wheeler A, Kunkel JG, Hepler PK** (2008) Pollen tube growth oscillations
1589 and intracellular calcium levels are reversibly modulated by actin polymerization. *Plant*
1590 *Physiol.* **146**: 1611-1621
- 1591 **Chang F, Gu Y, Ma H, Yang Z** (2013) AtPRK2 promotes ROP1 activation via RopGEFs in the
1592 control of polarized pollen tube growth. *Mol. Plant* **6**: 1187-1201
- 1593 **Chebli Y, Kaneda M, Zerzour R, Geitmann A** (2012) The cell wall of the *Arabidopsis* pollen
1594 tube--spatial distribution, recycling, and network formation of polysaccharides. *Plant*
1595 *physiology* **160**: 1940-1955
- 1596 **Chen CY, Wong EI, Vidali L, Estavillo A, Hepler PK, Wu HM, Cheung AY** (2002) The
1597 regulation of actin organization by actin-depolymerizing factor in elongating pollen tubes.
1598 *Plant Cell* **14**: 2175-2190
- 1599 **Cheung AY, Duan QH, Costa SS, de Graaf BH, Di Stilio VS, Feijo J, Wu HM** (2008) The
1600 dynamic pollen tube cytoskeleton: live cell studies using actin-binding and microtubule-
1601 binding reporter proteins. *Mol. Plant* **1**: 686-702
- 1602 **Cheung AY, Wu HM** (2007) Structural and functional compartmentalization in pollen tubes. *J.*
1603 *Exp. Bot.* **58**: 75-82
- 1604 **Contento AL, Bassham DC** (2012) Structure and function of endosomes in plant cells. *Journal of*
1605 *cell science* **125**: 3511-3518
- 1606 **Cui Y, Yu M, Yao X, Xing J, Lin J, Li X** (2018) Single-particle tracking for the quantification of
1607 membrane protein dynamics in living plant cells. *Mol. Plant* **11**: 1315-1327
- 1608 **Cutler SR, Ehrhardt DW, Griffiths JS, Somerville CR** (2000) Random GFP::cDNA fusions
1609 enable visualization of subcellular structures in cells of *Arabidopsis* at a high frequency.
1610 *Proceedings of the National Academy of Sciences of the United States of America* **97**: 3718-
1611 3723
- 1612 **Derksen J, Rutten T, Lichtscheidl IK, de Win AHN, Pierson ES, Rongen G** (1995) Quantitative
1613 analysis of the distribution of organelles in tobacco pollen tubes: implications for exocytosis
1614 and endocytosis. *Protoplasma* **188**: 267-276
- 1615 **Dettmer J, Hong-Hermesdorf A, Stierhof YD, Schumacher K** (2006) Vacuolar H⁺-ATPase
1616 activity is required for endocytic and secretory trafficking in *arabidopsis*. *Plant Cell* **18**: 715-
1617 730
- 1618 **Dhonukshe P, Aniento F, Hwang I, Robinson DG, Mravec J, Stierhof YD, Friml J** (2007)
1619 Clathrin-mediated constitutive endocytosis of PIN auxin efflux carriers in *Arabidopsis*. *Curr.*
1620 *Biol.* **17**: 520-527
- 1621 **Dixit R, Cyr R** (2003) Cell damage and reactive oxygen species production induced by
1622 fluorescence microscopy: effect on mitosis and guidelines for non-invasive fluorescence
1623 microscopy. *Plant J.*, **36**: 280-290
- 1624 **Dong H, Pei W, Haiyun R** (2012) Actin fringe is correlated with tip growth velocity of pollen
1625 tubes. *Mol. Plant* **5**: 1160-1162
- 1626 **Dowd PE, Coursol S, Skirpan AL, Kao TH, Gilroy S** (2006) *Petunia* phospholipase C1 is
1627 involved in pollen tube growth. *Plant Cell*, **18**: 1438-1453
- 1628 **Dunnnett CW** (1955) A multiple comparison procedure for comparing several treatments with a
1629 control. *J. Amer. Statist. Assoc.* **50**: 1096-1121

- 1630 **Edidin M** (1987) Rotational and lateral diffusion of membrane proteins and lipids: phenomena and
1631 function. *In* F Bronner, RD Klausner, C Kempf, Jv Renswoude, eds, Current Topics in
1632 Membranes and Transport, Vol 29. Academic Press, pp 91-127
- 1633 **Emans N, Zimmermann S, Fischer R** (2002) Uptake of a fluorescent marker in plant cells is
1634 sensitive to brefeldin A and wortmannin. *Plant Cell* **14**: 71-86
- 1635 **Fan L, Li R, Pan J, Ding Z, Lin J** (2015) Endocytosis and its regulation in plants. Trends in plant
1636 science **20**: 388-397
- 1637 **Feng Q-N, Kang H, Song S-J, Ge F-R, Zhang Y-L, Li E, Li S, Zhang Y** (2016) Arabidopsis
1638 RhoGDIs Are Critical for Cellular Homeostasis of Pollen Tubes. *Plant Physiology* **170**: 841-
1639 856
- 1640 **Fisher R** (1918) The correlation between relatives on the supposition of mendelian inheritance.
1641 Trans. Roy. Soc. Edinburgh **52**: 399-433
- 1642 **Frick M, Schmidt K, Nichols BJ** (2007) Modulation of lateral diffusion in the plasma membrane
1643 by protein density. *Curr. Biol.* **17**: 462-467
- 1644 **Fu Y, Wu G, Yang ZB** (2001) Rop GTPase-dependent dynamics of tip-localized F-actin controls
1645 tip growth in pollen tubes. *Journal of Cell Biology* **152**: 1019-1032
- 1646 **Fu Y, Yang ZB** (2001) Rop GTPase: a master switch of cell polarity development in plants. Trends
1647 in Plant Science **6**: 545-547
- 1648 **Galletta BJ, Cooper JA** (2009) Actin and endocytosis: mechanisms and phylogeny. Current
1649 opinion in cell biology **21**: 20-27
- 1650 **Geitmann A, Parre E** (2004) The local cytomechanical properties of growing pollen tubes
1651 correspond to the axial distribution of structural cellular elements. *Sexual Plant*
1652 *Reproduction* **17**: 9-16
- 1653 **Geldner N, Anders N, Wolters H, Keicher J, Kornberger W, Muller P, Delbarre A, Ueda T,**
1654 **Nakano A, Jurgens G** (2003) The Arabidopsis GNOM ARF-GEF mediates endosomal
1655 recycling, auxin transport, and auxin-dependent plant growth. *Cell* **112**: 219-230
- 1656 **Geldner N, Friml J, Stierhof YD, Jurgens G, Palme K** (2001) Auxin transport inhibitors block
1657 PIN1 cycling and vesicle trafficking. *Nature* **413**: 425-428
- 1658 **Goose JE, Sansom MSP** (2013) Reduced lateral mobility of lipids and proteins in crowded
1659 membranes. *PLoS Comp. Biol.* **9**: e1003033
- 1660 **Grebnev G, Ntefidou M, Kost B** (2017) Secretion and endocytosis in pollen tubes: models of tip
1661 growth in the spot light. *Front. Plant Sci.* **8**: 154
- 1662 **Gu Y, Li S, Lord EM, Yang Z** (2006) Members of a novel class of Arabidopsis Rho Guanine
1663 Nucleotide Exchange Factors control Rho GTPase-dependent polar growth. *Plant Cell* **18**:
1664 366-381
- 1665 **Hajdukiewicz P, Svab Z, Maliga P** (1994) The small, versatile *pPZP* family of *Agrobacterium*
1666 binary vectors for plant transformation. *Plant Mol. Biol.* **25**: 989-994
- 1667 **Hartel AJ, Glogger M, Guigas G, Jones NG, Fenz SF, Weiss M, Engstler M** (2015) The
1668 molecular size of the extra-membrane domain influences the diffusion of the GPI-anchored
1669 VSG on the trypanosome plasma membrane. *Sci. Rep.* **5**: 10394
- 1670 **He L, Wu LG** (2007) The debate on the kiss-and-run fusion at synapses. *Trends Neurosci.* **30**: 447-
1671 455
- 1672 **Helling D, Possart A, Cottier S, Klahre U, Kost B** (2006) Pollen tube tip growth depends on
1673 plasma membrane polarization mediated by tobacco PLC3 activity and endocytic membrane
1674 recycling. *Plant Cell* **18**: 3519-3534
- 1675 **Hepler PK, Rounds CM, Winship LJ** (2013) Control of cell wall extensibility during pollen tube
1676 growth. *Mol. Plant* **6**: 998-1017
- 1677 **Hepler PK, Vidali L, Cheung AY** (2001) Polarized cell growth in higher plants. *Annual Review*
1678 *of Cell and Developmental Biology* **17**: 159-187
- 1679 **Horsch RB, Klee HJ** (1986) Rapid assay of foreign gene expression in leaf discs transformed by
1680 *Agrobacterium tumefaciens*: Role of T-DNA borders in the transfer process. *Proc. Natl.*
1681 *Acad. Sci. USA* **83**: 4428-4432

1682 **Icha J, Weber M, Waters JC, Norden C** (2017) Phototoxicity in live fluorescence microscopy,
1683 and how to avoid it. *Bioessays* **39**

1684 **Jefferson RA, Kavanagh TA, Bevan MW** (1987) GUS fusions: beta-glucuronidase as a sensitive
1685 and versatile gene fusion marker in higher plants. *Embo J.* **6**: 3901-3907

1686 **Jiang L, Rogers JC** (1998) Integral membrane protein sorting to vacuoles in plant cells: evidence
1687 for two pathways. *J. Cell Biol.* **143**: 1183-1199

1688 **Johnson MA, Kost B** (2010) Pollen tube development. *Methods in Molecular Biology* **655**: 155-
1689 176

1690 **Kall L, Krogh A, Sonnhammer EL** (2007) Advantages of combined transmembrane topology and
1691 signal peptide prediction--the Phobius web server. *Nucleic Acids Res.* **35**: W429-432

1692 **Kaneda M, van Oostende-Triplet C, Chebli Y, Testerink C, Bednarek SY, Geitmann A** (2019)
1693 Plant AP180 N-Terminal Homolog Proteins Are Involved in Clathrin-Dependent
1694 Endocytosis during Pollen Tube Growth in *Arabidopsis thaliana*. *Plant Cell Physiol* **60**:
1695 1316-1330

1696 **Kazusa DNARI, The Cold Spring H, Washington University Sequencing C, The European
1697 Union Arabidopsis Genome Sequencing C, Institute of Plant G, Crop Plant R** (2000)
1698 Sequence and analysis of chromosome 5 of the plant *Arabidopsis thaliana*. *Nature* **408**: 823-
1699 826

1700 **Ketelaar T, Galway ME, Mulder BM, Emons AM** (2008) Rates of exocytosis and endocytosis in
1701 *Arabidopsis* root hairs and pollen tubes. *J. Microsc.* **231**: 265-273

1702 **Kim DH, Hwang I** (2013) Direct Targeting of Proteins from the Cytosol to Organelles: The ER
1703 versus Endosymbiotic Organelles. *Traffic* **14**: 613-621

1704 **Klahre U, Becker C, Schmitt AC, Kost B** (2006) Nt-RhoGDI2 regulates Rac/Rop signaling and
1705 polar cell growth in tobacco pollen tubes. *Plant J.* **46**: 1018-1031

1706 **Klahre U, Kost B** (2006) Tobacco RhoGTPase ACTIVATING PROTEIN1 spatially restricts
1707 signaling of RAC/Rop to the apex of pollen tubes. *Plant Cell* **18**: 3033-3046

1708 **Kost B** (2008) Spatial control of Rho (Rac-Rop) signaling in tip-growing plant cells. *Trends in Cell
1709 Biology* **18**: 119-127

1710 **Kost B, Lemichez E, Spielhofer P, Hong Y, Tolias K, Carpenter C, Chua NH** (1999) Rac
1711 homologues and compartmentalized phosphatidylinositol 4, 5-bisphosphate act in a common
1712 pathway to regulate polar pollen tube growth. *J. Cell Biol.* **145**: 317-330

1713 **Kost B, Spielhofer P, Chua N-H** (1998) A GFP-mouse talin fusion protein labels plant actin
1714 filaments *in vivo* and visualizes the actin cytoskeleton in growing pollen tubes. *Plant Journal*
1715 **16**: 393-401

1716 **Kusumi A, Sako Y, Yamamoto M** (1993) Confined Lateral Diffusion of Membrane-Receptors as
1717 Studied by Single-Particle Tracking (Nanovid Microscopy) - Effects of Calcium-Induced
1718 Differentiation in Cultured Epithelial-Cells. *Biophysical Journal* **65**: 2021-2040

1719 **Lam SK, Siu CL, Hillmer S, Jang S, An G, Robinson DG, Jiang L** (2007) Rice SCAMP1
1720 defines clathrin-coated, trans-golgi-located tubular-vesicular structures as an early
1721 endosome in tobacco BY-2 cells. *Plant Cell* **19**: 296-319

1722 **Lancelle SA, Hepler PK** (1992) Ultrastructure of freeze-substituted pollen tubes of *Lilium
1723 longiflorum*. *Protoplasma* **167**: 215-230

1724 **Lazo GR, Stein PA, Ludwig RA** (1991) A DNA transformation-competent *arabidopsis* genomic
1725 library in *agrobacterium*. *BioTechnology* **9**: 963-967

1726 **Le Bail A, Schulmeister S, Perroud PF, Ntefidou M, Rensing SA, Kost B** (2019) Analysis of the
1727 Localization of Fluorescent PpROP1 and PpROP-GEF4 Fusion Proteins in Moss
1728 Protonemata Based on Genomic "Knock-In" and Estradiol-Titratable Expression. *Front
1729 Plant Sci* **10**: 456

1730 **Lee YJ, Szumlanski A, Nielsen E, Yang Z** (2008) Rho-GTPase-dependent filamentous actin
1731 dynamics coordinate vesicle targeting and exocytosis during tip growth. *J. Cell Biol.* **181**:
1732 1155-1168

- 1733 **Li H, Luo N, Wang W, Liu Z, Chen J, Zhao L, Tan L, Wang C, Qin Y, Li C, Xu T, Yang Z**
 1734 (2018) The REN4 rheostat dynamically coordinates the apical and lateral domains of
 1735 Arabidopsis pollen tubes. *Nat. Commun.* **9**: 2573
- 1736 **Li X, Xing J, Qiu Z, He Q, Lin J** (2016) Quantification of membrane protein dynamics and
 1737 interactions in plant cells by fluorescence correlation spectroscopy. *Mol. Plant* **9**: 1229-1239
- 1738 **Lin Y, Wang Y, Zhu J-k, Yang Z** (1996) Localization of a Rho GTPase implies a role in tip
 1739 growth and movement of the generative cell in pollen tubes. *Plant Cell*, **8**: 293-303
- 1740 **Lippincott-Schwartz J, Yuan L, Tipper C, Amherdt M, Orci L, Klausner RD** (1991) Brefeldin
 1741 A's effects on endosomes, lysosomes, and the TGN suggest a general mechanism for
 1742 regulating organelle structure and membrane traffic. *Cell* **67**: 601-616
- 1743 **Lo C-A, Kays I, Emran F, Lin T-J, Cvetkovska V, Chen Brian E** (2015) Quantification of
 1744 Protein Levels in Single Living Cells. *Cell Rep.* **13**: 2634-2644
- 1745 **Lovy-Wheeler A, Wilsen KL, Baskin TI, Hepler PK** (2005) Enhanced fixation reveals the apical
 1746 cortical fringe of actin filaments as a consistent feature of the pollen tube. *Planta* **221**: 95-
 1747 104
- 1748 **Luo N, Yan A, Liu G, Guo J, Rong D, Kanaoka MM, Xiao Z, Xu G, Higashiyama T, Cui X,**
 1749 **Yang Z** (2017) Exocytosis-coordinated mechanisms for tip growth underlie pollen tube
 1750 growth guidance. *Nat. Commun.* **8**: 1687
- 1751 **Luo N, Yan A, Yang Z** (2016) Measuring exocytosis rate using corrected fluorescence recovery
 1752 after photoconversion. *Traffic* **17**: 554-564
- 1753 **Martiniere A, Lavagi I, Nageswaran G, Rolfe DJ, Maneta-Peyret L, Luu DT, Botchway SW,**
 1754 **Webb SED, Mongrand S, Maurel C, Martin-Fernandez ML, Kleine-Vehn J, Friml J,**
 1755 **Moreau P, Runions J** (2012) Cell wall constrains lateral diffusion of plant plasma-
 1756 membrane proteins. *Proc. Natl. Acad. Sci. USA* **109**: 12805-12810
- 1757 **McKenna ST, Kunkel JG, Bosch M, Rounds CM, Vidali L, Winship LJ, Hepler PK** (2009)
 1758 Exocytosis precedes and predicts the increase in growth in oscillating pollen tubes. *Plant*
 1759 *Cell* **21**: 3026-3040
- 1760 **Medina J, Catalá R, J S** (2001) Developmental and stress regulation of RCI2A and RCI2B, two
 1761 cold-inducible genes of Arabidopsis encoding highly conserved hydrophobic proteins. *Plant*
 1762 *Physiology* **125**: 1655-1666
- 1763 **Meunier FA, Gutierrez LM** (2016) Captivating new roles of F-actin cortex in exocytosis and bulk
 1764 endocytosis in neurosecretory cells. *Trends in neurosciences* **39**: 605-613
- 1765 **Miller DD, Lancelle SA, Hepler PK** (1996) Actin microfilaments do not form a dense meshwork
 1766 in *Lilium longiflorum* pollen tube tips. *Protoplasma* **195**: 123-132
- 1767 **Miyawaki KN, Yang Z** (2014) Extracellular signals and receptor-like kinases regulating ROP
 1768 GTPases in plants. *Front. Plant Sci.* **5**: 449
- 1769 **Mollet JC, Leroux C, Dardelle F, Lehner A** (2013) Cell wall composition, biosynthesis and
 1770 remodeling during pollen tube growth. *Plants* **2**: 107-147
- 1771 **Montes-Rodriguez A, Kost B** (2017) Direct comparison of the performance of commonly
 1772 employed in vivo F-actin markers (Lifeact-YFP, YFP-mTn and YFP-FABD2) in tobacco
 1773 pollen tubes. *Front. Plant Sci.* **8**: 1-14
- 1774 **Moscatelli A, Ciampolini F, Rodighiero S, Onelli E, Cresti M, Santo N, Idilli A** (2007) Distinct
 1775 endocytic pathways identified in tobacco pollen tubes using charged nanogold. *J. Cell Sci.*
 1776 **120**: 3804-3819
- 1777 **Moscatelli A, Idilli AI, Rodighiero S, Caccianiga M** (2012) Inhibition of actin polymerisation by
 1778 low concentration Latrunculin B affects endocytosis and alters exocytosis in shank and tip
 1779 of tobacco pollen tubes. *Plant biology* **14**: 770-782
- 1780 **Muro K, Matsuura-Tokita K, Tsukamoto R, Kanaoka MM, Ebine K, Higashiyama T, Nakano**
 1781 **A, Ueda T** (2018) ANTH domain-containing proteins are required for the pollen tube
 1782 plasma membrane integrity via recycling ANXUR kinases. *Commun. Biol.* **1**: 152
- 1783 **Nebenführ A, Ritzenthaler C, Robinson DG** (2002) Brefeldin A: deciphering an enigmatic
 1784 inhibitor of secretion. *Plant Physiology* **130**: 1102-1108

- 1785 **Paciorek T, Zazimalova E, Ruthardt N, Petrasek J, Stierhof YD, Kleine-Vehn J, Morris DA,**
 1786 **Emans N, Jurgens G, Geldner N, Friml J** (2005) Auxin inhibits endocytosis and promotes
 1787 its own efflux from cells. *Nature* **435**: 1251-1256
- 1788 **Paez Valencia J, Goodman K, Otegui MS** (2016) Endocytosis and endosomal trafficking in
 1789 plants. *Ann. Rev. Plant Biol.* **67**: 309-335
- 1790 **Parre E, Geitmann A** (2005) Pectin and the role of the physical properties of the cell wall in pollen
 1791 tube growth of *Solanum chacoense*. *Planta* **220**: 582-592
- 1792 **Parton RM, Fischer-Parton S, Trewavas AJ, Watahiki MK** (2003) Pollen tubes exhibit regular
 1793 periodic membrane trafficking events in the absence of apical extension. *Journal of Cell*
 1794 *Science* **116**: 2707-2719
- 1795 **Parton RM, Fischer-Parton S, Watahiki MK, Trewavas aJ** (2001) Dynamics of the apical
 1796 vesicle accumulation and the rate of growth are related in individual pollen tubes. *Journal of*
 1797 *Cell Science* **114**: 2685-2695
- 1798 **Perez-Gomez J, Moore I** (2007) Plant endocytosis: it is clathrin after all. *Curr. Biol.* **17**: R217-219
- 1799 **Picton JM, Steer MW** (1983) Membrane recycling and the control of secretory activity in pollen
 1800 tubes. *J. Cell Sci.* **63**: 303-320
- 1801 **Potocky M, Pleskot R, Pejchar P, Vitale N, Kost B, Zarsky V** (2014) Live-cell imaging of
 1802 phosphatidic acid dynamics in pollen tubes visualized by Spo20p-derived biosensor. *New*
 1803 *Phytol.* **203**: 483-494
- 1804 **Qin Y, Yang Z** (2011) Rapid tip growth: insights from pollen tubes. *Semin. Cell Dev. Biol.* **22**:
 1805 816-824
- 1806 **Qu X, Zhang H, Xie Y, Wang J, Chen N, Huang S** (2013) Arabidopsis villins promote actin
 1807 turnover at pollen tube tips and facilitate the construction of actin collars. *Plant Cell* **25**:
 1808 1803-1817
- 1809 **Qu X, Zhang H, Zhang M, Diao M, Xue Y, Huang S** (2017) Organizational innovation of apical
 1810 actin filaments drives rapid pollen tube growth and turning. *Mol. Plant* **10**: 930-947
- 1811 **Read SM, Clarke AE, Bacic A** (1993) Requirements for division of the generative nucleus in
 1812 cultured pollen tubes of *Nicotiana*. *Protoplasma* **174**: 101-115
- 1813 **Read SM, Clarke AE, Bacic A** (1993) Stimulation of growth of cultured *Nicotiana tabacum* W 38
 1814 pollen tubes by poly(ethylene glycol) and Cu(II) salts. *Protoplasma* **177**: 1-14
- 1815 **Reyes FC, Buono R, Otegui MS** (2011) Plant endosomal trafficking pathways. *Current Opinion in*
 1816 *Plant Biology* **14**: 666-673
- 1817 **Riedl J, Crevenna AH, Kessenbrock K, Yu JH, Neukirchen D, Bista M, Bradke F, Jenne D,**
 1818 **Holak TA, Werb Z, Sixt M, Wedlich-Soldner R** (2008) Lifeact: a versatile marker to
 1819 visualize F-actin. *Nat. Methods* **5**: 605-607
- 1820 **Rockel N, Wolf S, Kost B, Rausch T, Greiner S** (2008) Elaborate spatial patterning of cell-wall
 1821 PME and PME1 at the pollen tube tip involves PME1 endocytosis, and reflects the
 1822 distribution of esterified and de-esterified pectins. *Plant J.*, **53**: 133-143
- 1823 **Rounds CM, Hepler PK, Winship LJ** (2014) The apical actin fringe contributes to localized cell
 1824 wall deposition and polarized growth in the lily pollen tube. *Plant physiology* **166**: 139-151
- 1825 **Saffman PG, Delbruck M, Delbrück M** (1975) Brownian motion in biological membranes. *Proc.*
 1826 *Natl. Acad. Sci. USA* **72**: 3111-3113
- 1827 **Samaj J, Muller J, Beck M, Bohm N, Menzel D** (2006) Vesicular trafficking, cytoskeleton and
 1828 signalling in root hairs and pollen tubes. *Trends Plant Sci.* **11**: 594-600
- 1829 **Sambrook JF, Russell DW** (2014) *Molecular cloning: a laboratory manual*, Ed Fourth edi. Cold
 1830 Spring Harbor Laboratory Press
- 1831 **Schneider S, Schneidereit A, Konrad KR, Hajirezaei M-R, Gramann M, Hedrich R, Sauer N**
 1832 (2006) Arabidopsis INOSITOL TRANSPORTER4 mediates high-affinity H1 symport of
 1833 myoinositol across the plasma membrane. *Plant Physiology* **141**: 565-577
- 1834 **Sekeres J, Pejchar P, Santrucek J, Vukasinovic N, Zarsky V, Potocky M** (2017) Analysis of
 1835 exocyst subunit EXO70 family reveals distinct membrane domains in tobacco pollen tubes.
 1836 *Plant Physiol.* **173**: 1659-1675

- 1837 **Serna L** (2005) A simple method for discriminating between cell membrane and cytosolic proteins.
1838 *New Phytol.* **165**: 947-952
- 1839 **Shao S, Hegde RS** (2011) Membrane protein insertion at the endoplasmic reticulum. *Annual*
1840 *Review of Cell and Developmental Biology* **27**: 25-56
- 1841 **Sierro N, Batty JN, Ouadi S, Bakaher N, Bovet L, Willig A, Goepfert S, Peitsch MC, Ivanov**
1842 **NV** (2014) The tobacco genome sequence and its comparison with those of tomato and
1843 potato. *Nat. Commun.* **5**: 3833
- 1844 **Snapp E** (2005) Design and Use of Fluorescent Fusion Proteins in Cell Biology. *Curr. Protoc. Cell*
1845 *Biol.* **Chapter 21**: 21.24.21-21.24.13
- 1846 **Soboleski MR, Oaks J, Halford WP** (2005) Green fluorescent protein is a quantitative reporter of
1847 gene expression in individual eukaryotic cells. *FASEB J.* **19**: 440-442
- 1848 **Sousa E, Kost B, Malho R** (2008) Arabidopsis Phosphatidylinositol-4-Monophosphate 5-Kinase 4
1849 Regulates Pollen Tube Growth and Polarity by Modulating Membrane Recycling. *Plant Cell*
1850 **20**: 3050-3064
- 1851 **Stavrou I, O'Halloran T** (2006) The monomeric clathrin assembly protein, AP180, regulates
1852 contractile vacuole size in *Dictyostelium discoideum*. *Molecular Biology of the Cell* **18**:
1853 986-994
- 1854 **Steer MW, Steer JM** (1989) Pollen tube tip growth. *New Phytol.* **111**: 323-358
- 1855 **Stenzel I, Ischebeck T, Quint M, Heilmann I** (2012) Variable regions of PI4P 5-kinases direct
1856 PtdIns(4,5)P₂ towards alternative regulatory functions in tobacco pollen tubes. *Frontiers in*
1857 *Plant Science* **2**
- 1858 **Stephan O, Cottier S, Fahlen S, Montes-Rodriguez A, Sun J, Eklund DM, Klahre U, Kost B**
1859 (2014) RISAP is a TGN-associated RAC5 effector regulating membrane traffic during polar
1860 cell growth in tobacco. *Plant Cell* **26**: 4426-4447
- 1861 **Student B** (1908) The probable error of a mean. *Biometrika* **6**: 1-25
- 1862 **Sun J, Eklund DM, Montes-Rodriguez A, Kost B** (2015) In vivo Rac/Rop localization as well as
1863 interaction with RhoGAP and RhoGDI in tobacco pollen tubes: analysis by low-level
1864 expression of fluorescent fusion proteins and bimolecular fluorescence complementation.
1865 *Plant J.* **84**: 83-98
- 1866 **Thompson MV, Wolniak SM** (2008) A plasma membrane-anchored fluorescent protein fusion
1867 illuminates sieve element plasma membranes in arabidopsis and tobacco. *Plant Physiol.* **146**:
1868 1599-1610
- 1869 **Trimble WS, Grinstein S** (2015) Barriers to the free diffusion of proteins and lipids in the plasma
1870 membrane. *Journal of Cell Biology* **208**: 259-271
- 1871 **Tse YC, Lo SW, Hillmer S, Dupree P, Jiang L** (2006) Dynamic response of prevacuolar
1872 compartments to brefeldin A in plant cells. *Plant Physiology* **142**: 1442-1459
- 1873 **Tukey JW** (1949) Comparing individual means in the analysis of variance. *Biometrics* **5**: 99-99
- 1874 **Twell D, Yamaguchi J, McCormick S** (1990) Pollen-specific gene expression in transgenic plants:
1875 coordinate regulation of two different tomato gene promoters during microsporogenesis.
1876 *Development* **109**: 705-713
- 1877 **Uemura T** (2016) Physiological roles of plant post-golgi transport pathways in membrane
1878 trafficking. *Plant Cell Physiol.* **57**: 2013-2019
- 1879 **Uemura T, Nakano RT, Takagi J, Wang Y, Kramer K, Finkemeier I, Nakagami H, Tsuda K,**
1880 **Ueda T, Schulze-Lefert P, Nakano A** (2019) A Golgi-Released Subpopulation of the
1881 Trans-Golgi Network Mediates Protein Secretion in Arabidopsis. *Plant Physiol* **179**: 519-
1882 532
- 1883 **Van Gisbergen PAC, Esseling-Ozdoba A, Vos JW** (2008) Microinjecting FM4-64 validates it as
1884 a marker of the endocytic pathway in plants. *J. Microsc.* **231**: 284-290
- 1885 **Vidali L, Rounds CM, Hepler PK, Bezanilla M** (2009) Lifeact-mEGFP reveals a dynamic apical
1886 F-Actin Network in tip growing plant cells. *PLoS ONE* **4**: e5744
- 1887 **Viklund H, Bernsel A, Skwark M, Elofsson A** (2008) SPOCTOPUS: a combined predictor of
1888 signal peptides and membrane protein topology. *Bioinformatics* **24**: 2928-2929

- 1889 **Vrljic M, Nishimura SY, Brasselet S, Moerner WE, McConnell HM** (2002) Translational
1890 diffusion of individual class II MHC membrane proteins in cells. *Biophysical journal* **83**:
1891 2681-2692
- 1892 **Wang H, Zhuang X, Cai Y, Cheung AY, Jiang L** (2013) Apical F-actin-regulated exocytic
1893 targeting of NtPPME1 is essential for construction and rigidity of the pollen tube cell wall.
1894 *Plant J.*, **76**: 367-379
- 1895 **Wang H, Zhuang X, Wang X, Law AH, Zhao T, Du S, Loy MM, Jiang L** (2016) A distinct
1896 pathway for polar exocytosis in plant cell wall formation. *Plant Physiol* **172**: 1003-1018
- 1897 **Wang H, Zhuang XH, Hillmer S, Robinson DG, Jiang LW** (2011) Vacuolar sorting receptor
1898 (VSR) proteins reach the plasma membrane in germinating pollen tubes. *Mol. Plant* **4**: 845-
1899 853
- 1900 **Wang Q, Kong L, Hao H, Wang X, Lin J, Samaj J, Baluska F** (2005) Effects of Brefeldin A on
1901 pollen germination and tube growth. antagonistic effects on endocytosis and secretion. *Plant*
1902 *Physiol.* **139**: 1692-1703
- 1903 **Wang X, Chung KP, Lin W, Jiang L** (2017) Protein secretion in plants: conventional and
1904 unconventional pathways and new techniques. *J. Exp. Bot.* **69**: 21-37
- 1905 **Wang X, Teng Y, Wang Q, Li X, Sheng X, Zheng M, Samaj J, Baluska F, Lin J** (2006)
1906 Imaging of dynamic secretory vesicles in living pollen tubes of *Picea meyeri* using
1907 evanescent wave microscopy. *Plant Physiol.* **141**: 1591-1603
- 1908 **Weiß K, Neef A, Van Q, Kramer S, Gregor I, Enderlein J** (2013) Quantifying the diffusion of
1909 membrane proteins and peptides in black lipid membranes with 2-focus fluorescence
1910 correlation spectroscopy. *Biophysical Journal* **105**: 455-462
- 1911 **Wilsen KL, Lovy-Wheeler A, Voigt B, Menzel D, Kunkel JG, Hepler PK** (2006) Imaging the
1912 actin cytoskeleton in growing pollen tubes. *Sexual Plant Reproduction* **19**: 51-62
- 1913 **Yalovsky S, Bloch D, Sorek N, Kost B** (2008) Regulation of membrane trafficking, cytoskeleton
1914 dynamics, and cell polarity by ROP/RAC GTPases. *Plant Physiology* **147**: 1527-1543
- 1915 **Zarsky V, Cvrckova F, Potocky M, Hala M** (2009) Exocytosis and cell polarity in plants -
1916 exocyst and recycling domains. *New Phytol.* **183**: 255-272
- 1917 **Zerzour R, Kroeger J, Geitmann A** (2009) Polar growth in pollen tubes is associated with
1918 spatially confined dynamic changes in cell mechanical properties. *Dev. Biol.* **334**: 437-446
- 1919 **Zhang Y, McCormick S** (2007) A distinct mechanism regulating a pollen-specific guanine
1920 nucleotide exchange factor for the small GTPase Rop in *Arabidopsis thaliana*. *Proceedings*
1921 *of the National Academy of Sciences of the United States of America* **104**: 18830-18835
- 1922 **Zhao XY, Wang Q, Li S, Ge FR, Zhou LZ, McCormick S, Zhang Y** (2013) The juxtamembrane
1923 and carboxy-terminal domains of *Arabidopsis* PRK2 are critical for ROP-ind. *Journal of*
1924 *Experimental Botany* **64**: 5599-5610
- 1925 **Zhao Y, Yan A, Feijó JA, Furutani M, Takenawa T, Hwang I, Fu Y, Yang Z** (2010)
1926 Phosphoinositides regulate clathrin-dependent endocytosis at the tip of pollen tubes in
1927 *arabidopsis* and tobacco. *Plant Cell* **22**: 4031-4044
- 1928 **Zonia L, Munnik T** (2008) Vesicle trafficking dynamics and visualization of zones of exocytosis
1929 and endocytosis in tobacco pollen tubes. *Journal of Experimental Botany* **59**: 861-873

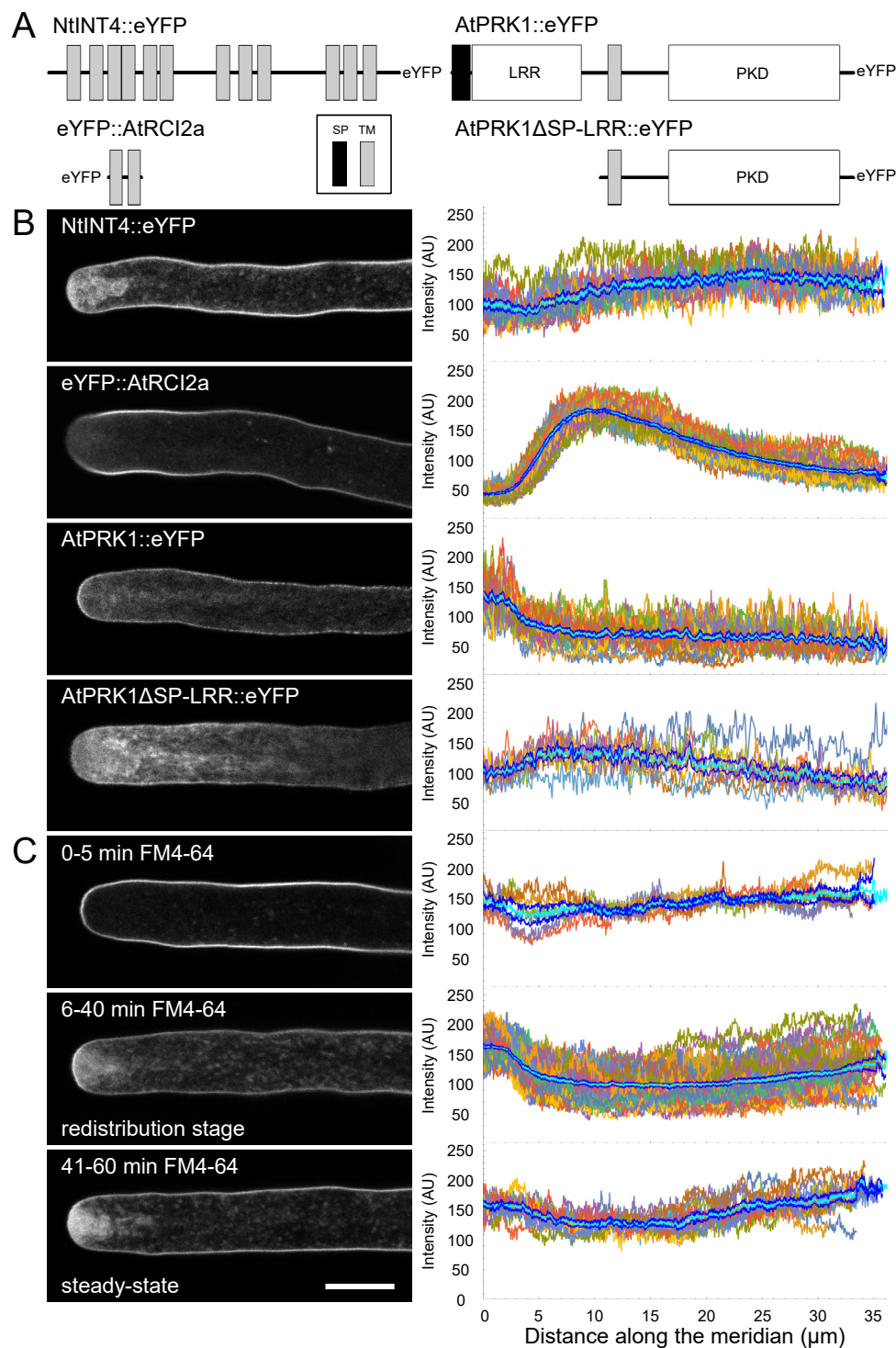


Figure 1. Distribution patterns of TM proteins and FM4-64 serving as markers for membrane traffic in normally growing tobacco pollen tubes.

(A) Domain structure of the indicated TM protein markers. Protein and domain sizes are drawn to scale. SP: signal peptide; TM: transmembrane domain; LRR: leucine-rich repeats; PKD: protein kinase domain.

(B) Left panel: medial confocal optical sections through representative pollen tubes transiently (*NtINT4::eYFP*, *AtPRK1::eYFP* or *AtPRK1ΔSP-LRR::eYFP*) or stably (*eYFP::AtRCI2a*) expressing the indicated TM protein marker. Growth rates of the individual pollen tubes shown (after confocal imaging): 6.8 μm/min (*NtINT4::eYFP*), 3.6 μm/min (*eYFP::AtRCI2a*), 3.8 μm/min (*AtPRK1::eYFP*), or 4.8 μm/min (*AtPRK1ΔSP-LRR::eYFP*). Scale bar: 10 μm.

Right panel: line plots displaying the intensity of PM-associated eYFP fluorescence at different meridional distances from the apex ($X=0 \mu\text{m}$) in all analyzed pollen tubes ($n = 17$ [NtINT4::eYFP, 3 independent experiments], 29 [eYFP::AtRCI2a, 5 independent experiments], 31 [AtPRK1::eYFP, 5 independent experiments], or 37 [AtPRK1 Δ SP-LRR::eYFP, 5 independent experiments]). Light blue lines: average intensity; dark blue lines: standard deviation; all other lines: individual line plots.

(C) Left panel: medial confocal optical sections through different representative pollen tubes labeled with the fluorescent lipophilic dye FM4-64 (applied at $50 \mu\text{M}$ in $200 \mu\text{l}$ PTNT) for the indicated period of time (initial stage: 0-5 min, redistribution stage: 6-40 min, steady-state stage: 41-60 min). Growth rates of the individual pollen tubes shown (after confocal imaging): $3.4 \mu\text{m}/\text{min}$ (0-5 min), $4.8 \mu\text{m}/\text{min}$ (6-40 min), or $3.8 \mu\text{m}/\text{min}$ (41-60 min). Scale bar: $10 \mu\text{m}$.

Right panel: line plots displaying the intensity of PM-associated FM4-64 fluorescence at different meridional distances from the apex ($X=0 \mu\text{m}$) in all analyzed pollen tubes ($n = 6$ [0-5 min], 68 [6-40 min], or 41 [41-60 min]; 4 independent experiments). Light blue lines: average intensity; dark blue lines: standard deviation; all other lines: individual line plots.

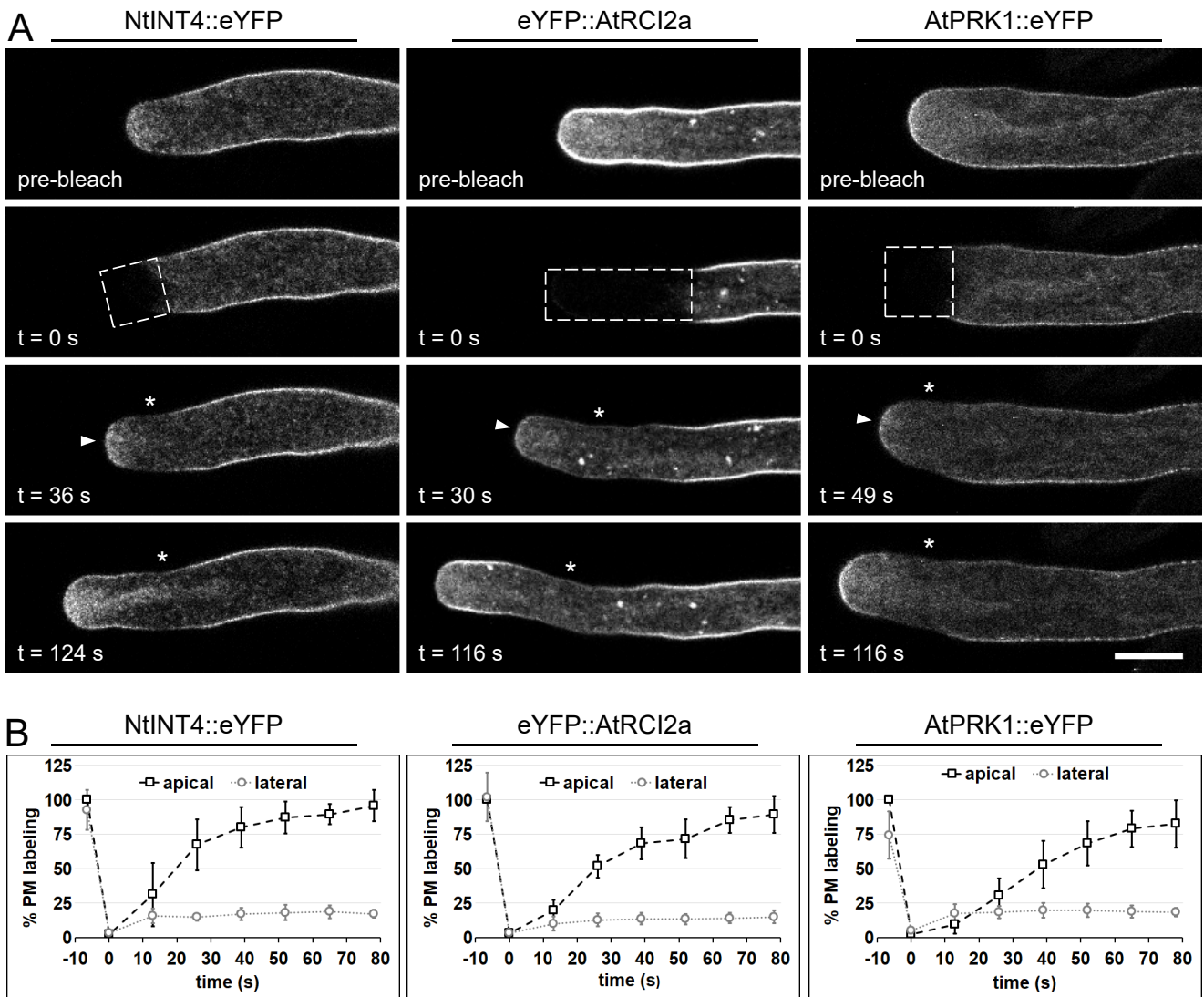


Figure 2. FRAP time-lapse analysis of TM protein marker dynamics at the tip of normally growing tobacco pollen tubes.

(A) Medial confocal optical sections through representative pollen tubes transiently (NtINT4::eYFP or AtPRK1::eYFP) or stably (eYFP::AtRCI2a) expressing the indicated TM protein marker, which were recorded before (row 1; pre-bleach) or after complete photobleaching of eYFP fluorescence within the dashed box indicated in row 2. *t*: time elapsed after photobleaching; arrowheads: apical PM domain within which fluorescence recovery was first observed; *: bleached lateral PM domain showing no fluorescence recovery. Scale bar: 10 μ m.

During post-bleach time-lapse imaging (*t* = 0 to 116-124 s), the growth rate of the individual pollen tubes shown was: 4.2 μ m/min (NtINT4::eYFP), 8.7 μ m/min (eYFP::AtRCI2a), and 5.1 μ m/min (AtPRK1::eYFP). In total, 7 (NtINT4::eYFP, 2 independent experiments), 10 (eYFP::AtRCI2a, 2 independent experiments) or 12 (AtPRK1::eYFP, 3 independent experiments) TM protein marker expressing pollen tubes were analyzed. Each TM protein marker displayed essentially the same fluorescence recovery pattern and kinetics in all analyzed pollen tubes.

(B) Quantification of PM labelling by the indicated TM protein marker within the bleached region either at the extreme apex (0 μ m meridional distance from the extreme apex; arrow heads in (A); open squares) or in the center of a lateral domain (more than 3 μ m meridional distance from the extreme apex; asterisks in (A); open circles) immediately before (*t* = -6,5 s) and after (*t* = 0 s) photobleaching, as well as after different recovery periods (13s, 26s, 39s, 52s, 65s and 78s). The indicated average levels of PM labelling were computed from data obtained from all analyzed pollen tubes (A) after normalization based on pre-bleach levels of PM labelling at the extreme apex, which were set to 100%.

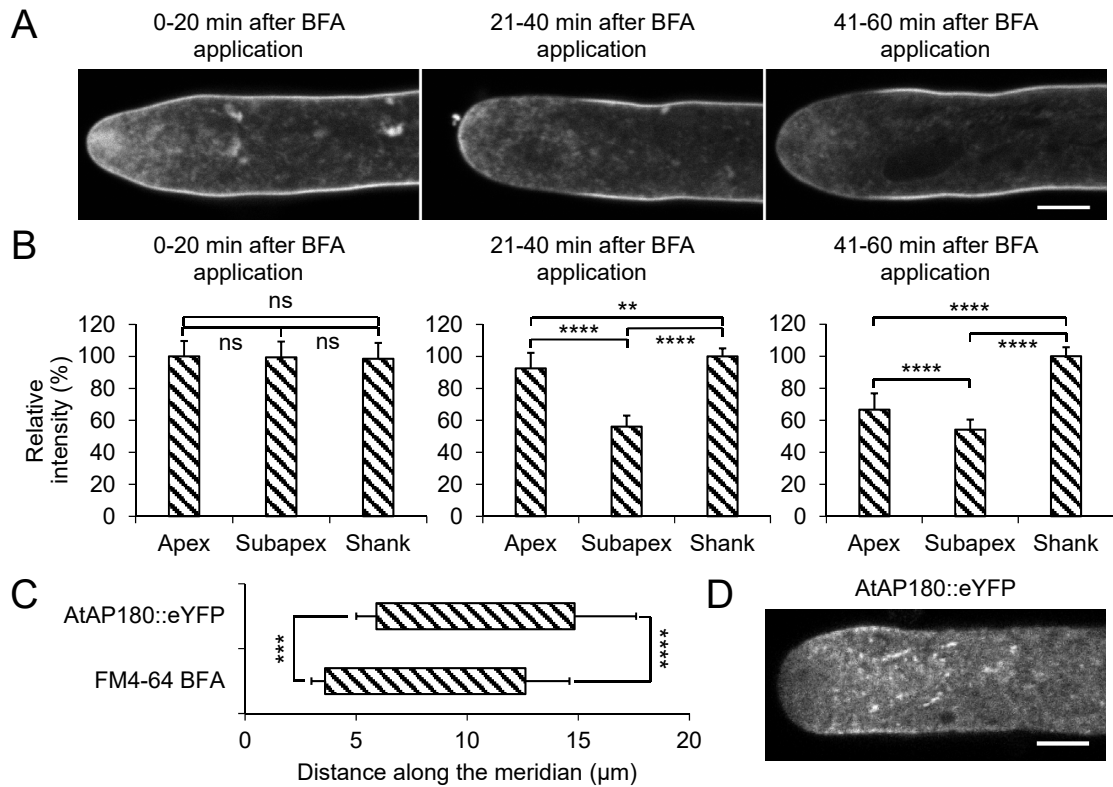


Figure 3. Time-course analysis of BFA-induced loss of FM4-64 PM labeling and investigation of AtAP180::eYFP distribution in tobacco pollen tubes.

(A) Medial confocal optical sections through different representative pollen tubes, which had been grown in the presence of FM4-64 (applied at 50 μM in 200 μl PTNT) for 30 min, before the dye was washed-out from the culture medium and BFA was applied for the indicated time period (70 μM in 200 μl PTNT). Scale bar: 5 μm .

As a result of the BFA treatment, tip growth of all analyzed pollen tubes was completely inhibited (Supplemental Figure 8). All pollen tubes analysed during each time period after BFA application ($n = 10$ [0-20 min], 22 [21-40 min], and 35 [41-60 min]; 3 independent experiments) displayed very similar FM4-64 labeling patterns.

(B) Quantitative analysis of the average relative intensity of PM-associated FM4-64 fluorescence in all pollen tubes analyzed as described in (A) within the apical dome (“Apex”; meridional distance from the apex: 0-3.6 μm), within a subapical region displaying massive loss of FM4-64 PM labeling in the presence of BFA (“Subapex”; meridional distance from the apex: 3.6-12.6 μm), and in the shank (“Shank”; meridional distance from the apex: 12.6-32.6 μm). The borders between these three PM regions were determined as described in (C). The intensity of PM-associated FM4-64 fluorescence was normalized in each analyzed pollen tube based on the highest measured value (0-32.6 μm meridional distance from the apex), which was set to 100 %.

The statistical significance of differences in the average intensity of PM-associated FM4-64 fluorescence between the three different PM regions during each time period after BFA application was assessed using ANOVA (Tukey’s test, one way). **: $p \leq 0.01$; ****: $p \leq 0.0001$; ns: not significantly different ($p > 0.05$). Error bars: standard deviation.

(C) Quantitative analysis of the exact length and position of the subapical PM domains, which display massive loss of FM4-64 PM labeling 21-40 min after BFA application (A), or are associated with an AtAP180::eYFP fusion protein serving as a marker for sites of clathrin-mediated endocytosis (D). The average meridional distances from the extreme apex ($x = 0$) of both ends of these domains in all analysed pollen tubes ($n = 22$ [FM4-64 BFA], or 22 [AtAP180::eYFP]) are indicated. Exact extensions of domains shown: 5.9 ± 0.91 to 14.8 ± 2.8 μm (AtAP180::eYFP); 3.6 ± 0.61 to 12.6 ± 2.0 μm (FM4-64 BFA).

The statistical significance of differences between the average meridional distances of both the proximal and the distal ends of the FM4-64 BFA and AtAP180::eYFP domains was assessed using a Student's *t*-test (two-tailed, type II). ***: $p \leq 0.001$; ****: $p \leq 0.0001$. Error bars: standard deviation.

(D) Medial confocal optical section through a representative normally growing pollen tube transiently expressing an AtAP180::eYFP fusion protein that serves as a marker for sites of clathrin-mediated endocytosis. In total, 25 essentially normally growing pollen tubes were analyzed in 2 independent experiments, which displayed very similar AtAP180::eYFP distribution patterns. Growth rate of the pollen tube shown (after confocal imaging): 4.8 $\mu\text{m}/\text{min}$. Scale bar: 5 μm .

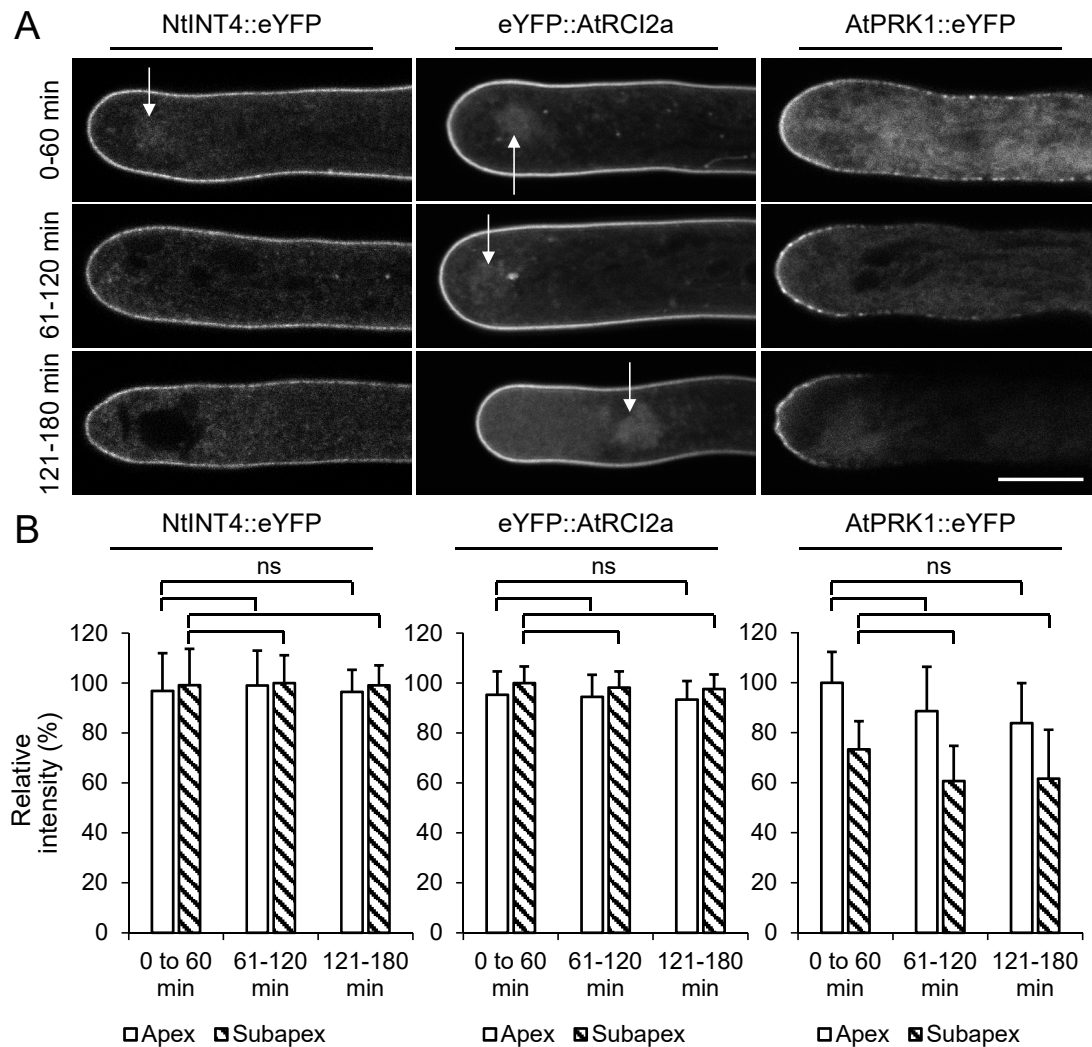


Figure 4. Time-course analysis of PM labeling by TM protein markers in tobacco pollen tubes after BFA application.

(A) Medial confocal optical sections through different representative pollen tubes transiently (AtPRK1::eYFP) or stably (NtINT4::eYFP; eYFP::AtRCI2a) expressing the indicated TM protein marker, which were recorded after treatment with BFA (applied at 70 μ M in 200 μ l PTNT) for the indicated time period. Arrows: BFA compartment. Scale bar: 10 μ m.

As a result of the BFA treatment, tip growth of all analyzed pollen tubes was completely inhibited (Supplemental Figure 8). During each time period after BFA application, all imaged pollen tubes expressing the same TM protein marker displayed highly similar PM labeling patterns (NtINT4::eYFP [3 independent experiments]: n = 78 [0-60 min], 61 [61-120 min], or 37 [121-180]; eYFP::AtRCI2a [5 independent experiments]: n = 85 [0-60 min], 82 [61-120 min], or 97 [121-180 min]; AtPRK1::eYFP [3 independent experiments]: n = 46 [0-60 min], 37 [61-120 min], or 31 [121-180 min]).

(B) Quantitative analysis of the average relative intensity of PM-associated TM protein marker fluorescence in all pollen tubes analyzed as described in (A) within the apical dome (“Apex”; meridional distance from the apex: 0-3.6 μ m) and within the subapical endocytic region, which was identified based on BFA treatment of FM4-64 labeled pollen tubes as described in figure 3 (“Subapex”; meridional distance from the apex: 3.6-12.6 μ m). The intensity of PM-associated marker fluorescence was normalized in each analyzed pollen tube based on the maximal intensity measured with these two membrane domains (0-12.6 μ m meridional distance from the apex), which was set to 100 %.

For each TM protein marker, the statistical significance of differences in the average intensity of PM-associated marker fluorescence during different time periods after BFA application was assessed separately within the apical dome and the subapical endocytic region using ANOVA (Dunnett’s test, one-way). ns: not significantly different ($p > 0.05$). Error bars: standard deviation.

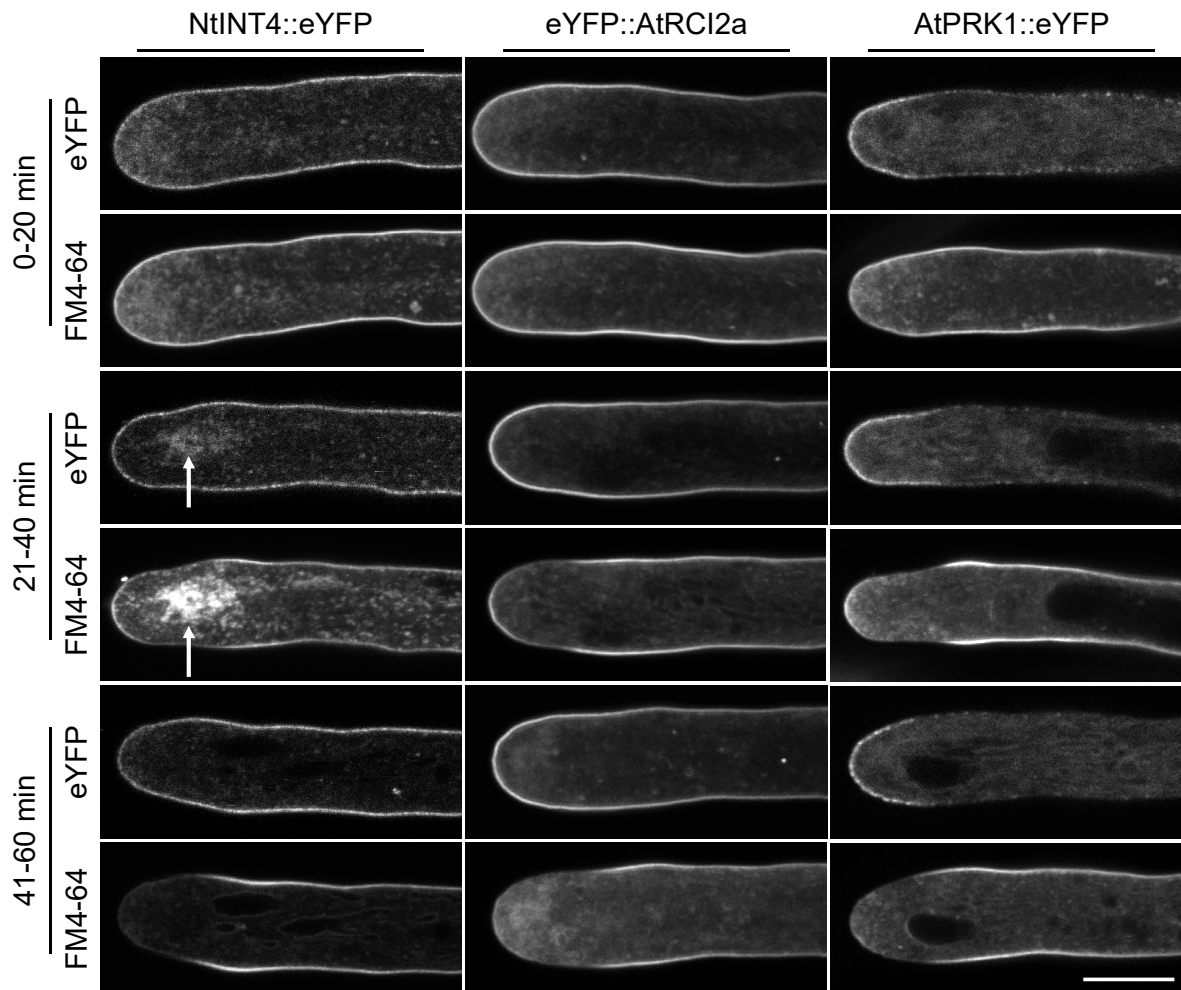


Figure 5. Simultaneous time-course analysis of FM4-64 and TM protein marker PM labeling in BFA-treated tobacco pollen tubes.

Medial confocal optical sections through different representative pollen tubes transiently (AtPRK1::eYFP) or stably (NtINT4::eYFP, eYFP::AtRCI2a) expressing the indicated TM protein marker, which had been grown in the presence of FM4-64 (applied at 50 μ M in 200 μ l PTNT) for 30 min, before the dye was washed-out from the culture medium and BFA was applied for the indicated time period (70 μ M in 200 μ l PTNT). eYFP fusion proteins serving as TM protein markers (green fluorescence; “eYFP”) and FM4-64 (red fluorescence; “FM4-64”) were simultaneously imaged in separate channels. Arrow: BFA compartment; Scale bar: 10 μ m.

As a result of the BFA treatment, tip growth of all analyzed pollen tubes was completely inhibited (Supplemental Figure 8). During each of the indicated time periods, all imaged pollen tubes displayed essentially the same patterns of FM4-64 and of TM marker protein specific eYFP labeling of the PM (NtINT4::eYFP [2 independent experiments]: n=11 [0-20 min], 22 [21-40 min], or 19 [41-60 min]; eYFP::AtRCI2a [2 independent experiments]: n= 10 [0-20 min], 22 [21-40 min], or 22 [41-60 min]; AtPRK1::eYFP [4 independent experiments]: n = 10 [0-20 min], 16 [21-40 min], or 23 [41-60 min]).

The BFA compartment visible in the NtINT4::eYFP expressing pollen tube shown (21-40 min after BFA application) was clearly more strongly labelled by FM4-64 than by NtINT4::eYFP (ratio between the average fluorescence intensities displayed by the BFA compartment and by the apical plasma membrane: 1,39 [FM4-64] and 0,65 [NtINT4::eYFP]).

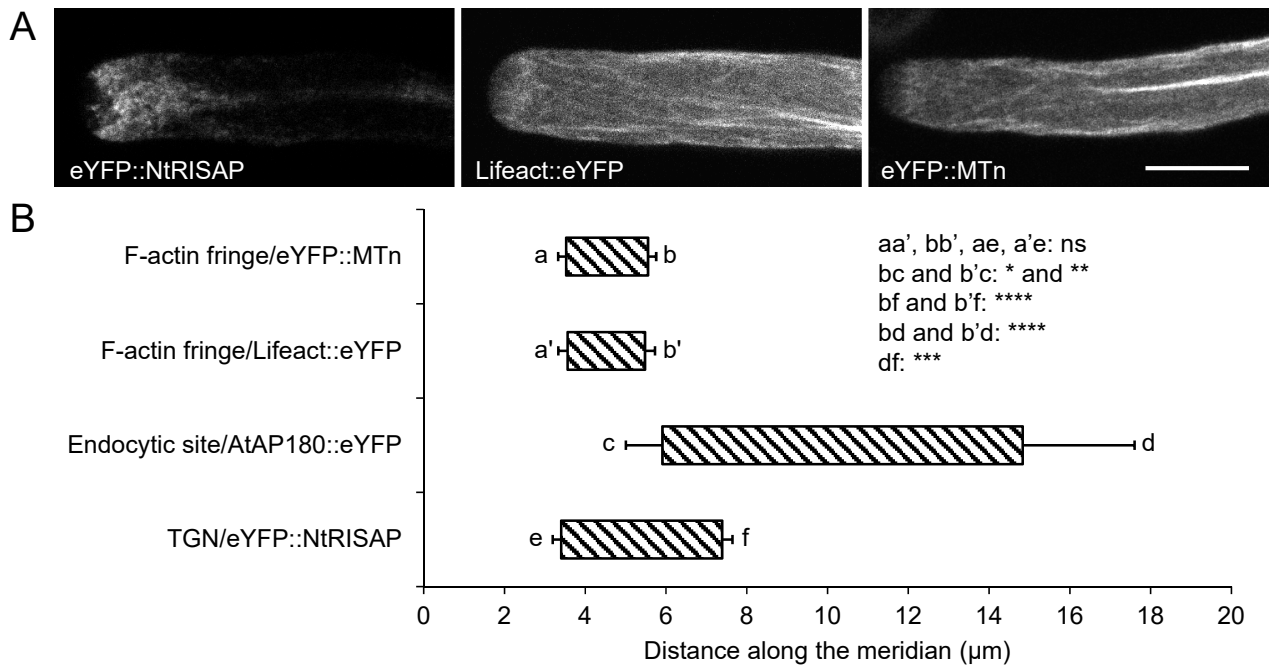


Figure 6. Positional mapping of a detached TGN compartment and of the F-actin fringe relative to each other and to the subapical endocytic PM domain in tobacco pollen tubes.

(A) Medial confocal optical sections through representative essentially normally growing pollen tubes transiently expressing the TGN marker eYFP::NtRISAP ($n = 13$, 4 independent experiments), or one of the F-actin markers lifeact::eYFP ($n = 17$, 3 independent experiments) or eYFP::MTn ($n = 19$, 3 independent experiments). All pollen tubes expressing the same marker displayed highly similar eYFP labeling patterns. Growth rate of the pollen tubes shown (after confocal imaging): $3.6 \mu\text{m}/\text{min}$ (eYFP::NtRISAP), $5.4 \mu\text{m}/\text{min}$ (Lifeact::eYFP), and $4.8 \mu\text{m}/\text{min}$ (eYFP::MTn). Scale bar: $10 \mu\text{m}$.

(B) Quantitative analysis of the meridional distance from the extreme apex ($X = 0 \mu\text{m}$) of the most proximal and the most distal contact points of the NtRISAP-associated TGN compartment, or of the F-actin fringe, with the PM in all pollen tubes analysed as described in (A). For direct comparison, the position of the AtAP180::eYFP labeled subapical endocytic PM domain, which was determined in normally growing pollen tubes as described above (Figure 3C and D), is also indicated. Exact extensions of domains shown: 3.4 ± 0.21 to $7.4 \pm 0.26 \mu\text{m}$ (TGN; eYFP::NtRISAP), 3.6 ± 0.23 to $5.5 \pm 0.25 \mu\text{m}$ (F-actin fringe; lifeact::eYFP), 3.5 ± 0.20 to $5.6 \pm 0.20 \mu\text{m}$ (F-actin fringe; eYFP::MTn) and 5.9 ± 0.91 to $14.8 \pm 2.8 \mu\text{m}$ (subapical endocytic domain; AtAP180::eYFP).

The statistical significance of differences between the average meridional distances of proximal and distal ends (a, a', b, b', c, d, e and f) of different PM domains were analysed as indicated using ANOVA (Tukey's test, one-way). Note that the distal end of the F-actin fringe (irrespective of the marker used) and the proximal end of the subapical endocytic domain are statistically significantly different (bc, b'c). *: $p \leq 0.05$; **: $p \leq 0.01$; ***: $p \leq 0.001$; ****: $p \leq 0.0001$; ns: not significantly different ($p > 0.05$). Error bars: standard deviation.

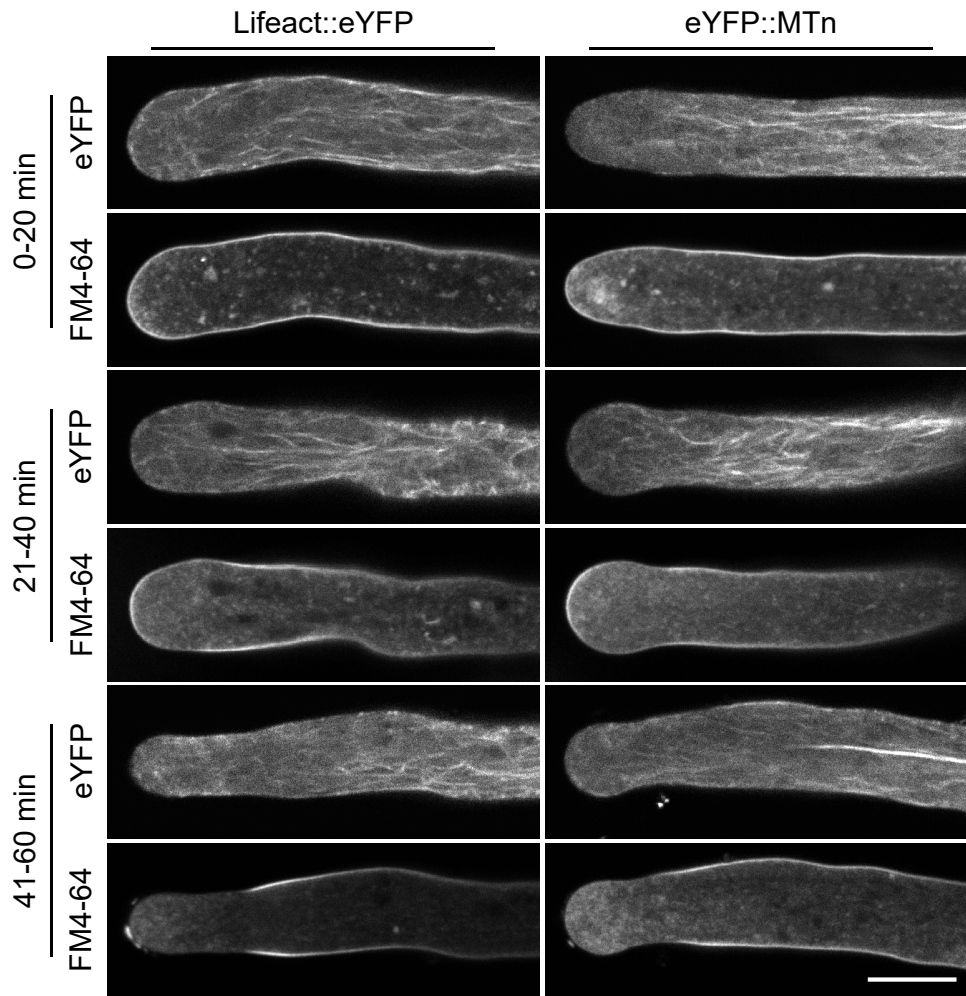


Figure 7. Simultaneous time-course analysis of FM4-64 PM labeling and of non-invasively visualized F-actin structures in BFA-treated tobacco pollen tubes.

Medial confocal optical sections through different representative pollen tubes transiently expressing the indicated non-invasive F-actin markers (Lifeact::eYFP or eYFP::MTn), which had been grown in the presence of FM4-64 (applied at 50 μ M in 200 μ l PTNT) for 30 min, before the dye was washed-out from the culture medium and BFA was applied for the indicated time period (70 μ M in 200 μ l PTNT). Lifeact::eYFP or eYFP::MTn fusion proteins (green fluorescence; “eYFP”) and FM4-64 (red fluorescence; “FM4-64”) were simultaneously imaged in separate channels. Scale bar: 10 μ m.

As a result of the BFA treatment, tip growth of all analyzed pollen tubes was completely inhibited (Supplemental Figure 8). During each of the indicated time periods, all imaged pollen tubes displayed essentially the same FM4-64 PM labeling patterns (“FM4-64”) and very similar F-actin structures (“eYFP”) labeled by one of the two non-invasive markers (Lifeact::eYFP [3 independent experiments]: n = 13 [0-20 min], 14 [21-40 min], or 13 [41-60 min]; eYFP::MTn [4 independent experiments]: n = 16 [0-20 min], 24 [21-40 min], or 14 [41-60 min]).

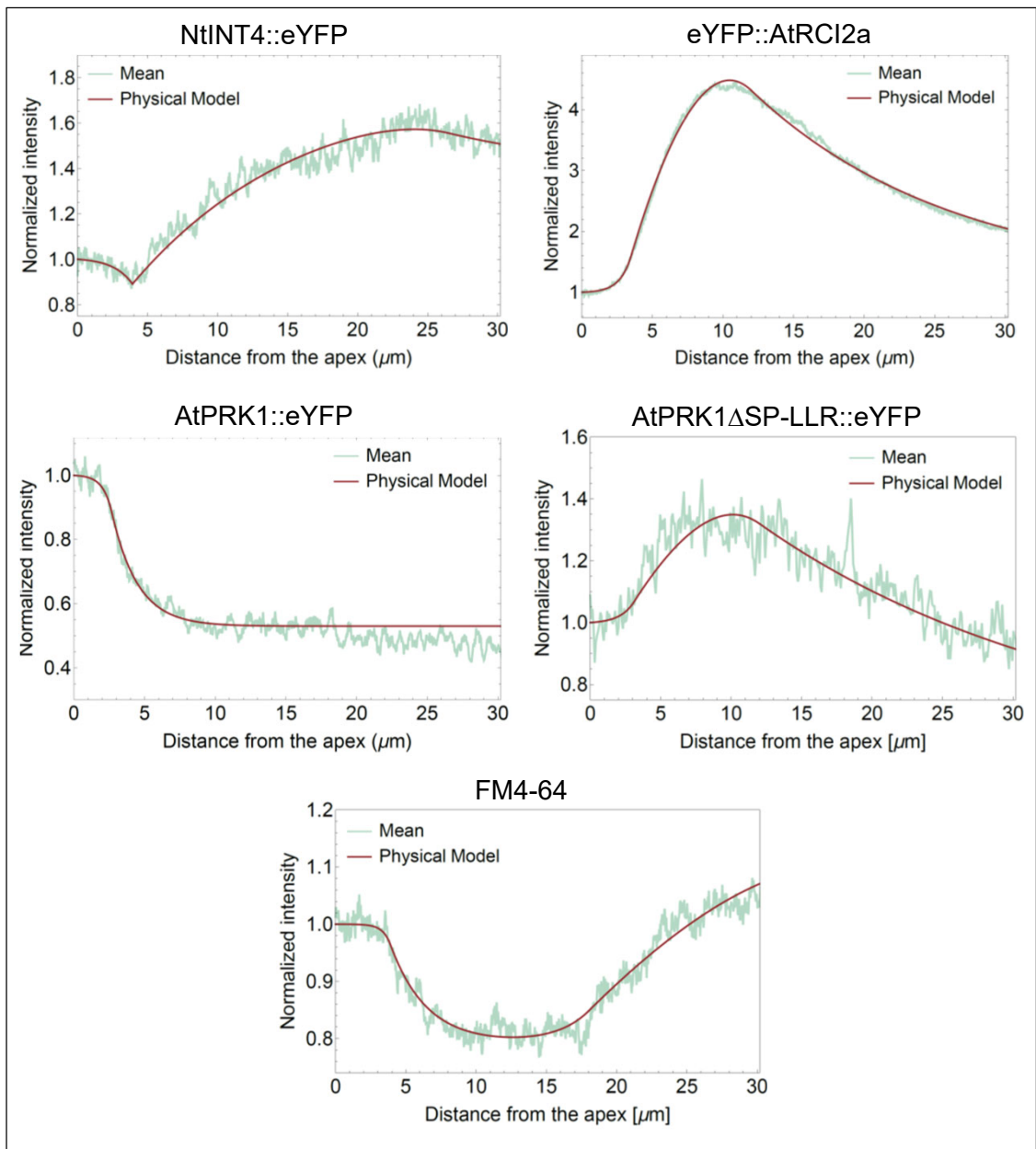


Figure 8. Fitting of a mathematical model of steady-state marker distributions within the pollen tube PM to experimental data.

The experimental line plots depicted in light blue represent the steady-state distribution of the indicated markers for membrane traffic within the PM and show the average intensity of PM-associated marker fluorescence at different meridional distances from the extreme pollen tube apex. The same line plots are also presented in figure 1B and C, but are displayed here after normalization based on the values at the extreme apex ($X = 1$). The brown lines represent output of a mathematical model of steady-state marker distribution described in detail in the text, after model fitting to the experimental line plots. The excellent fit obtained for all markers strongly supports model relevance. Table 2 summarizes model read out obtained after fitting, which provides information concerning the rate and spatial organization of cellular processes (including secretion, endocytosis, diffusion and degeneration), which are determining marker dynamics and steady-state distribution.

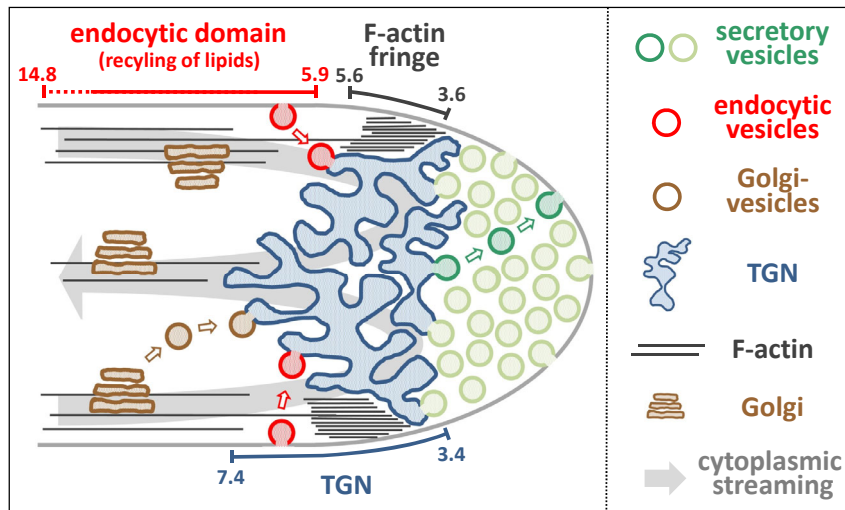


Figure 9. Model of apical membrane traffic underlying tobacco pollen tube tip growth.

Secretion required for cell wall biogenesis occurs within the apical dome (0 - 3.5 μm meridional distance from the extreme apex) and results in the incorporation of excess lipid material into the PM, which is recycled by subapical endocytosis (5.9 - 14.8 μm meridional distance from the extreme apex). A subapical TGN compartment (PM contacts: 3.4 – 7.4 μm meridional distance from the extreme apex) serves as a central sorting organelle with which Golgi-derived as well as endocytic vesicles are fusing at the distal end, and which generates secretory vesicles at its proximal surface. The cortical F-actin fringe (3.6 – 5.6 μm meridional distance from the extreme apex) maintains the positioning of the subapical TGN compartment within a pollen tube region displaying rapid cytoplasmic streaming.

Parsed Citations

Abràmoff MD, Magalhães PJ, Ram SJ (2004) Image processing with imageJ. *Biophotonics Int.* 11: 36-41

Pubmed: [Author and Title](#)

Google Scholar: [Author Only](#) [Title Only](#) [Author and Title](#)

Alabi AA, Tsien RW (2013) Perspectives on kiss-and-run: role in exocytosis, endocytosis, and neurotransmission. *Annu. Rev. Physiol.* 75: 393-422

Pubmed: [Author and Title](#)

Google Scholar: [Author Only](#) [Title Only](#) [Author and Title](#)

Baluska F, Hlavacka A, Samaj J, Palme K, Robinson DG, Match T, McCurdy DW, Menzel D, Volkmann D (2002) F-actin-dependent endocytosis of cell wall pectins in meristematic root cells. Insights from brefeldin A-induced compartments. *Plant Physiol.* 130: 422-431

Pubmed: [Author and Title](#)

Google Scholar: [Author Only](#) [Title Only](#) [Author and Title](#)

Barth M, Holstein SE (2004) Identification and functional characterization of Arabidopsis AP180, a binding partner of plant alphaC-adaptin. *Journal of cell science* 117: 2051-2062

Pubmed: [Author and Title](#)

Google Scholar: [Author Only](#) [Title Only](#) [Author and Title](#)

Blackbourn HD, Jackson AP (1996) Plant clathrin heavy chain: Sequence analysis and restricted localisation in growing pollen tubes. *J. Cell Sci.* 109: 777-786

Pubmed: [Author and Title](#)

Google Scholar: [Author Only](#) [Title Only](#) [Author and Title](#)

Bolte S, Talbot C, Boutte Y, Catrice O, Read ND, Satiat-Jeunemaitre B (2004) FM-dyes as experimental probes for dissecting vesicle trafficking in living plant cells. *J. Microsc.* 214: 159-173

Pubmed: [Author and Title](#)

Google Scholar: [Author Only](#) [Title Only](#) [Author and Title](#)

Bosch M, Cheung AY, Hepler PK (2005) Pectin methylesterase, a regulator of pollen tube growth. *Plant physiology* 138: 1334-1346

Pubmed: [Author and Title](#)

Google Scholar: [Author Only](#) [Title Only](#) [Author and Title](#)

Bosch M, Hepler PK (2005) Pectin methylesterases and pectin dynamics in pollen tubes. *Plant Cell* 17: 3219-3226

Pubmed: [Author and Title](#)

Google Scholar: [Author Only](#) [Title Only](#) [Author and Title](#)

Bou Daher F, Geitmann A (2011) Actin is involved in pollen tube tropism through redefining the spatial targeting of secretory vesicles. *Traffic* 12: 1537-1551

Pubmed: [Author and Title](#)

Google Scholar: [Author Only](#) [Title Only](#) [Author and Title](#)

Bove J, Vaillancourt B, Kroeger J, Hepler PK, Wiseman PW, Geitmann A (2008) Magnitude and direction of vesicle dynamics in growing pollen tubes using spatiotemporal image correlation spectroscopy and fluorescence recovery after photobleaching. *Plant physiology* 147: 1646-1658

Pubmed: [Author and Title](#)

Google Scholar: [Author Only](#) [Title Only](#) [Author and Title](#)

Cai G, Parrotta L, Cresti M (2015) Organelle trafficking, the cytoskeleton, and pollen tube growth. *J. Integr. Plant Biol.* 57: 63-78

Pubmed: [Author and Title](#)

Google Scholar: [Author Only](#) [Title Only](#) [Author and Title](#)

Capel J, Jarillo JA, Salinas J, Martinez-Zapater JM (1997) Two homologous low-temperature-inducible genes from Arabidopsis encode highly hydrophobic proteins. *Plant physiology* 115: 569-576

Pubmed: [Author and Title](#)

Google Scholar: [Author Only](#) [Title Only](#) [Author and Title](#)

Cardenas L, Lovy-Wheeler A, Kunkel JG, Hepler PK (2008) Pollen tube growth oscillations and intracellular calcium levels are reversibly modulated by actin polymerization. *Plant Physiol.* 146: 1611-1621

Pubmed: [Author and Title](#)

Google Scholar: [Author Only](#) [Title Only](#) [Author and Title](#)

Chang F, Gu Y, Ma H, Yang Z (2013) AtPRK2 promotes ROP1 activation via RopGEFs in the control of polarized pollen tube growth. *Mol. Plant* 6: 1187-1201

Pubmed: [Author and Title](#)

Google Scholar: [Author Only](#) [Title Only](#) [Author and Title](#)

Chebli Y, Kaneda M, Zerzour R, Geitmann A (2012) The cell wall of the Arabidopsis pollen tube--spatial distribution, recycling, and network formation of polysaccharides. *Plant physiology* 160: 1940-1955

Pubmed: [Author and Title](#)

Google Scholar: [Author Only](#) [Title Only](#) [Author and Title](#)

Chen CY, Wong EI, Vidali L, Estavillo A, Hepler PK, Wu HM, Cheung AY (2002) The regulation of actin organization by actin-depolymerizing factor in elongating pollen tubes. *Plant Cell* 14: 2175-2190

Pubmed: [Author and Title](#)

Google Scholar: [Author Only](#) [Title Only](#) [Author and Title](#)

Cheung AY, Duan QH, Costa SS, de Graaf BH, Di Stilio VS, Feijo J, Wu HM (2008) The dynamic pollen tube cytoskeleton: live cell studies using actin-binding and microtubule-binding reporter proteins. *Mol. Plant* 1: 686-702

Pubmed: [Author and Title](#)

Google Scholar: [Author Only](#) [Title Only](#) [Author and Title](#)

Cheung AY, Wu HM (2007) Structural and functional compartmentalization in pollen tubes. *J. Exp. Bot.* 58: 75-82

Pubmed: [Author and Title](#)

Google Scholar: [Author Only](#) [Title Only](#) [Author and Title](#)

Contento AL, Bassham DC (2012) Structure and function of endosomes in plant cells. *Journal of cell science* 125: 3511-3518

Pubmed: [Author and Title](#)

Google Scholar: [Author Only](#) [Title Only](#) [Author and Title](#)

Cui Y, Yu M, Yao X, Xing J, Lin J, Li X (2018) Single-particle tracking for the quantification of membrane protein dynamics in living plant cells. *Mol. Plant* 11: 1315-1327

Pubmed: [Author and Title](#)

Google Scholar: [Author Only](#) [Title Only](#) [Author and Title](#)

Cutler SR, Ehrhardt DW, Griffiths JS, Somerville CR (2000) Random GFP::cDNA fusions enable visualization of subcellular structures in cells of *Arabidopsis* at a high frequency. *Proceedings of the National Academy of Sciences of the United States of America* 97: 3718-3723

Pubmed: [Author and Title](#)

Google Scholar: [Author Only](#) [Title Only](#) [Author and Title](#)

Derksen J, Rutten T, Lichtscheidl IK, de Win AHN, Pierson ES, Rongen G (1995) Quantitative analysis of the distribution of organelles in tobacco pollen tubes: implications for exocytosis and endocytosis. *Protoplasma* 188: 267-276

Pubmed: [Author and Title](#)

Google Scholar: [Author Only](#) [Title Only](#) [Author and Title](#)

Dettmer J, Hong-Hermesdorf A, Stierhof YD, Schumacher K (2006) Vacuolar H⁺-ATPase activity is required for endocytic and secretory trafficking in *Arabidopsis*. *Plant Cell* 18: 715-730

Pubmed: [Author and Title](#)

Google Scholar: [Author Only](#) [Title Only](#) [Author and Title](#)

Dhonukshe P, Aniento F, Hwang I, Robinson DG, Mravec J, Stierhof YD, Friml J (2007) Clathrin-mediated constitutive endocytosis of PIN auxin efflux carriers in *Arabidopsis*. *Curr. Biol.* 17: 520-527

Pubmed: [Author and Title](#)

Google Scholar: [Author Only](#) [Title Only](#) [Author and Title](#)

Dixit R, Cyr R (2003) Cell damage and reactive oxygen species production induced by fluorescence microscopy: effect on mitosis and guidelines for non-invasive fluorescence microscopy. *Plant J.* 36: 280-290

Pubmed: [Author and Title](#)

Google Scholar: [Author Only](#) [Title Only](#) [Author and Title](#)

Dong H, Pei W, Haiyun R (2012) Actin fringe is correlated with tip growth velocity of pollen tubes. *Mol. Plant* 5: 1160-1162

Pubmed: [Author and Title](#)

Google Scholar: [Author Only](#) [Title Only](#) [Author and Title](#)

Dowd PE, Coursol S, Skirpan AL, Kao TH, Gilroy S (2006) *Petunia* phospholipase C1 is involved in pollen tube growth. *Plant Cell*, 18: 1438-1453

Pubmed: [Author and Title](#)

Google Scholar: [Author Only](#) [Title Only](#) [Author and Title](#)

Dunnnett CW (1955) A multiple comparison procedure for comparing several treatments with a control. *J. Amer. Statist. Assoc.* 50: 1096-1121

Pubmed: [Author and Title](#)

Google Scholar: [Author Only](#) [Title Only](#) [Author and Title](#)

Edidin M (1987) Rotational and lateral diffusion of membrane proteins and lipids: phenomena and function. In F Bronner, RD Klausner, C Kempf, Jv Renswoude, eds, *Current Topics in Membranes and Transport*, Vol 29. Academic Press, pp 91-127

Pubmed: [Author and Title](#)

Google Scholar: [Author Only](#) [Title Only](#) [Author and Title](#)

Emans N, Zimmermann S, Fischer R (2002) Uptake of a fluorescent marker in plant cells is sensitive to brefeldin A and wortmannin. *Plant Cell* 14: 71-86

Pubmed: [Author and Title](#)

Google Scholar: [Author Only](#) [Title Only](#) [Author and Title](#)

Fan L, Li R, Pan J, Ding Z, Lin J (2015) Endocytosis and its regulation in plants. *Trends in plant science* 20: 388-397

Pubmed: [Author and Title](#)

Google Scholar: [Author Only](#) [Title Only](#) [Author and Title](#)

Feng Q-N, Kang H, Song S-J, Ge F-R, Zhang Y-L, Li E, Li S, Zhang Y (2016) Arabidopsis RhoGDIs Are Critical for Cellular Homeostasis of Pollen Tubes. *Plant Physiology* 170: 841-856

Pubmed: [Author and Title](#)

Google Scholar: [Author Only](#) [Title Only](#) [Author and Title](#)

Fisher R (1918) The correlation between relatives on the supposition of mendelian inheritance. *Trans. Roy. Soc. Edinburgh* 52: 399-433

Pubmed: [Author and Title](#)

Google Scholar: [Author Only](#) [Title Only](#) [Author and Title](#)

Frick M, Schmidt K, Nichols BJ (2007) Modulation of lateral diffusion in the plasma membrane by protein density. *Curr. Biol.* 17: 462-467

Pubmed: [Author and Title](#)

Google Scholar: [Author Only](#) [Title Only](#) [Author and Title](#)

Fu Y, Wu G, Yang ZB (2001) Rop GTPase-dependent dynamics of tip-localized F-actin controls tip growth in pollen tubes. *Journal of Cell Biology* 152: 1019-1032

Pubmed: [Author and Title](#)

Google Scholar: [Author Only](#) [Title Only](#) [Author and Title](#)

Fu Y, Yang ZB (2001) Rop GTPase: a master switch of cell polarity development in plants. *Trends in Plant Science* 6: 545-547

Pubmed: [Author and Title](#)

Google Scholar: [Author Only](#) [Title Only](#) [Author and Title](#)

Galletta BJ, Cooper JA (2009) Actin and endocytosis: mechanisms and phylogeny. *Current opinion in cell biology* 21: 20-27

Pubmed: [Author and Title](#)

Google Scholar: [Author Only](#) [Title Only](#) [Author and Title](#)

Geitmann A, Parre E (2004) The local cytomechanical properties of growing pollen tubes correspond to the axial distribution of structural cellular elements. *Sexual Plant Reproduction* 17: 9-16

Pubmed: [Author and Title](#)

Google Scholar: [Author Only](#) [Title Only](#) [Author and Title](#)

Geldner N, Anders N, Wolters H, Keicher J, Kornberger W, Muller P, Delbarre A, Ueda T, Nakano A, Jurgens G (2003) The Arabidopsis GNOM ARF-GEF mediates endosomal recycling, auxin transport, and auxin-dependent plant growth. *Cell* 112: 219-230

Pubmed: [Author and Title](#)

Google Scholar: [Author Only](#) [Title Only](#) [Author and Title](#)

Geldner N, Friml J, Stierhof YD, Jurgens G, Palme K (2001) Auxin transport inhibitors block PIN1 cycling and vesicle trafficking. *Nature* 413: 425-428

Pubmed: [Author and Title](#)

Google Scholar: [Author Only](#) [Title Only](#) [Author and Title](#)

Goose JE, Sansom MSP (2013) Reduced lateral mobility of lipids and proteins in crowded membranes. *PLoS Comp. Biol.* 9: e1003033

Pubmed: [Author and Title](#)

Google Scholar: [Author Only](#) [Title Only](#) [Author and Title](#)

Grebnev G, Ntefidou M, Kost B (2017) Secretion and endocytosis in pollen tubes: models of tip growth in the spot light. *Front. Plant Sci.* 8: 154

Pubmed: [Author and Title](#)

Google Scholar: [Author Only](#) [Title Only](#) [Author and Title](#)

Gu Y, Li S, Lord EM, Yang Z (2006) Members of a novel class of Arabidopsis Rho Guanine Nucleotide Exchange Factors control Rho GTPase-dependent polar growth. *Plant Cell* 18: 366-381

Pubmed: [Author and Title](#)

Google Scholar: [Author Only](#) [Title Only](#) [Author and Title](#)

Hajdukiewicz P, Svab Z, Maliga P (1994) The small, versatile pPZP family of Agrobacterium binary vectors for plant transformation. *Plant Mol. Biol.* 25: 989-994

Pubmed: [Author and Title](#)

Google Scholar: [Author Only](#) [Title Only](#) [Author and Title](#)

Hartel AJ, Glogger M, Guigas G, Jones NG, Fenz SF, Weiss M, Engstler M (2015) The molecular size of the extra-membrane domain influences the diffusion of the GPI-anchored VSG on the trypanosome plasma membrane. *Sci. Rep.* 5: 10394

Pubmed: [Author and Title](#)

Google Scholar: [Author Only](#) [Title Only](#) [Author and Title](#)

He L, Wu LG (2007) The debate on the kiss-and-run fusion at synapses. *Trends Neurosci.* 30: 447-455

Pubmed: [Author and Title](#)

Google Scholar: [Author Only](#) [Title Only](#) [Author and Title](#)

Helling D, Possart A, Cottier S, Klahre U, Kost B (2006) Pollen tube tip growth depends on plasma membrane polarization mediated by tobacco PLC3 activity and endocytic membrane recycling. *Plant Cell* 18: 3519-3534

Pubmed: [Author and Title](#)

Google Scholar: [Author Only](#) [Title Only](#) [Author and Title](#)

- Hepler PK, Rounds CM, Winship LJ (2013) Control of cell wall extensibility during pollen tube growth. Mol. Plant 6: 998-1017**
Pubmed: [Author and Title](#)
Google Scholar: [Author Only](#) [Title Only](#) [Author and Title](#)
- Hepler PK, Vidali L, Cheung AY (2001) Polarized cell growth in higher plants. Annual Review of Cell and Developmental Biology 17: 159-187**
Pubmed: [Author and Title](#)
Google Scholar: [Author Only](#) [Title Only](#) [Author and Title](#)
- Horsch RB, Klee HJ (1986) Rapid assay of foreign gene expression in leaf discs transformed by Agrobacterium tumefaciens: Role of T-DNA borders in the transfer process. Proc. Natl. Acad. Sci. USA 83: 4428-4432**
Pubmed: [Author and Title](#)
Google Scholar: [Author Only](#) [Title Only](#) [Author and Title](#)
- Icha J, Weber M, Waters JC, Norden C (2017) Phototoxicity in live fluorescence microscopy, and how to avoid it. Bioessays 39**
Pubmed: [Author and Title](#)
Google Scholar: [Author Only](#) [Title Only](#) [Author and Title](#)
- Jefferson RA, Kavanagh TA, Bevan MW (1987) GUS fusions: beta-glucuronidase as a sensitive and versatile gene fusion marker in higher plants. Embo J. 6: 3901-3907**
Pubmed: [Author and Title](#)
Google Scholar: [Author Only](#) [Title Only](#) [Author and Title](#)
- Jiang L, Rogers JC (1998) Integral membrane protein sorting to vacuoles in plant cells: evidence for two pathways. J. Cell Biol. 143: 1183-1199**
Pubmed: [Author and Title](#)
Google Scholar: [Author Only](#) [Title Only](#) [Author and Title](#)
- Johnson MA, Kost B (2010) Pollen tube development. Methods in Molecular Biology 655: 155-176**
Pubmed: [Author and Title](#)
Google Scholar: [Author Only](#) [Title Only](#) [Author and Title](#)
- Kall L, Krogh A, Sonnhammer EL (2007) Advantages of combined transmembrane topology and signal peptide prediction--the Phobius web server. Nucleic Acids Res. 35: W429-432**
Pubmed: [Author and Title](#)
Google Scholar: [Author Only](#) [Title Only](#) [Author and Title](#)
- Kaneda M, van Oostende-Triplet C, Chebli Y, Testerink C, Bednarek SY, Geitmann A (2019) Plant AP180 N-Terminal Homolog Proteins Are Involved in Clathrin-Dependent Endocytosis during Pollen Tube Growth in Arabidopsis thaliana. Plant Cell Physiol 60: 1316-1330**
Pubmed: [Author and Title](#)
Google Scholar: [Author Only](#) [Title Only](#) [Author and Title](#)
- Kazusa DNARI, The Cold Spring H, Washington University Sequencing C, The European Union Arabidopsis Genome Sequencing C, Institute of Plant G, Crop Plant R (2000) Sequence and analysis of chromosome 5 of the plant Arabidopsis thaliana. Nature 408: 823-826**
Pubmed: [Author and Title](#)
Google Scholar: [Author Only](#) [Title Only](#) [Author and Title](#)
- Ketelaar T, Galway ME, Mulder BM, Emons AM (2008) Rates of exocytosis and endocytosis in Arabidopsis root hairs and pollen tubes. J. Microsc. 231: 265-273**
Pubmed: [Author and Title](#)
Google Scholar: [Author Only](#) [Title Only](#) [Author and Title](#)
- Kim DH, Hwang I (2013) Direct Targeting of Proteins from the Cytosol to Organelles: The ER versus Endosymbiotic Organelles. Traffic 14: 613-621**
Pubmed: [Author and Title](#)
Google Scholar: [Author Only](#) [Title Only](#) [Author and Title](#)
- Klahre U, Becker C, Schmitt AC, Kost B (2006) Nt-RhoGDI2 regulates Rac/Rop signaling and polar cell growth in tobacco pollen tubes. Plant J. 46: 1018-1031**
Pubmed: [Author and Title](#)
Google Scholar: [Author Only](#) [Title Only](#) [Author and Title](#)
- Klahre U, Kost B (2006) Tobacco RhoGTPase ACTIVATING PROTEIN1 spatially restricts signaling of RAC/Rop to the apex of pollen tubes. Plant Cell 18: 3033-3046**
Pubmed: [Author and Title](#)
Google Scholar: [Author Only](#) [Title Only](#) [Author and Title](#)
- Kost B (2008) Spatial control of Rho (Rac-Rop) signaling in tip-growing plant cells. Trends in Cell Biology 18: 119-127**
Pubmed: [Author and Title](#)
Google Scholar: [Author Only](#) [Title Only](#) [Author and Title](#)
- Kost B, Lemichez E, Spielhofer P, Hong Y, Tolia K, Carpenter C, Chua NH (1999) Rac homologues and compartmentalized phosphatidylinositol 4, 5-bisphosphate act in a common pathway to regulate polar pollen tube growth. J. Cell Biol. 145: 317-330**
Pubmed: [Author and Title](#)

Google Scholar: [Author Only](#) [Title Only](#) [Author and Title](#)

Kost B, Spielhofer P, Chua N-H (1998) A GFP-mouse talin fusion protein labels plant actin filaments in vivo and visualizes the actin cytoskeleton in growing pollen tubes. Plant Journal 16: 393-401

Pubmed: [Author and Title](#)

Google Scholar: [Author Only](#) [Title Only](#) [Author and Title](#)

Kusumi A, Sako Y, Yamamoto M (1993) Confined Lateral Diffusion of Membrane-Receptors as Studied by Single-Particle Tracking (Nanovid Microscopy) - Effects of Calcium-Induced Differentiation in Cultured Epithelial-Cells. Biophysical Journal 65: 2021-2040

Pubmed: [Author and Title](#)

Google Scholar: [Author Only](#) [Title Only](#) [Author and Title](#)

Lam SK, Siu CL, Hillmer S, Jang S, An G, Robinson DG, Jiang L (2007) Rice SCAMP1 defines clathrin-coated, trans-golgi-located tubular-vesicular structures as an early endosome in tobacco BY-2 cells. Plant Cell 19: 296-319

Pubmed: [Author and Title](#)

Google Scholar: [Author Only](#) [Title Only](#) [Author and Title](#)

Lancelle SA, Hepler PK (1992) Ultrastructure of freeze-substituted pollen tubes of Liliun longiflorum. Protoplasma 167: 215-230

Pubmed: [Author and Title](#)

Google Scholar: [Author Only](#) [Title Only](#) [Author and Title](#)

Lazo GR, Stein PA, Ludwig RA (1991) A DNA transformation-competent arabidopsis genomic library in agrobacterium. BioTechnology 9: 963-967

Pubmed: [Author and Title](#)

Google Scholar: [Author Only](#) [Title Only](#) [Author and Title](#)

Le Bail A, Schulmeister S, Perroud PF, Ntefidou M, Rensing SA, Kost B (2019) Analysis of the Localization of Fluorescent PpROP1 and PpROP-GEF4 Fusion Proteins in Moss Protonemata Based on Genomic "Knock-In" and Estradiol-Titratable Expression. Front Plant Sci 10: 456

Pubmed: [Author and Title](#)

Google Scholar: [Author Only](#) [Title Only](#) [Author and Title](#)

Lee YJ, Szumlanski A, Nielsen E, Yang Z (2008) Rho-GTPase-dependent filamentous actin dynamics coordinate vesicle targeting and exocytosis during tip growth. J. Cell Biol. 181: 1155-1168

Pubmed: [Author and Title](#)

Google Scholar: [Author Only](#) [Title Only](#) [Author and Title](#)

Li H, Luo N, Wang W, Liu Z, Chen J, Zhao L, Tan L, Wang C, Qin Y, Li C, Xu T, Yang Z (2018) The REN4 rheostat dynamically coordinates the apical and lateral domains of Arabidopsis pollen tubes. Nat. Commun. 9: 2573

Pubmed: [Author and Title](#)

Google Scholar: [Author Only](#) [Title Only](#) [Author and Title](#)

Li X, Xing J, Qiu Z, He Q, Lin J (2016) Quantification of membrane protein dynamics and interactions in plant cells by fluorescence correlation spectroscopy. Mol. Plant 9: 1229-1239

Pubmed: [Author and Title](#)

Google Scholar: [Author Only](#) [Title Only](#) [Author and Title](#)

Lin Y, Wang Y, Zhu J-k, Yang Z (1996) Localization of a Rho GTPase implies a role in tip growth and movement of the generative cell in pollen tubes. Plant Cell, 8: 293-303

Pubmed: [Author and Title](#)

Google Scholar: [Author Only](#) [Title Only](#) [Author and Title](#)

Lippincott-Schwartz J, Yuan L, Tipper C, Amherdt M, Orci L, Klausner RD (1991) Brefeldin A's effects on endosomes, lysosomes, and the TGN suggest a general mechanism for regulating organelle structure and membrane traffic. Cell 67: 601-616

Pubmed: [Author and Title](#)

Google Scholar: [Author Only](#) [Title Only](#) [Author and Title](#)

Lo C-A, Kays I, Emran F, Lin T-J, Cvetkovska V, Chen Brian E (2015) Quantification of Protein Levels in Single Living Cells. Cell Rep. 13: 2634-2644

Pubmed: [Author and Title](#)

Google Scholar: [Author Only](#) [Title Only](#) [Author and Title](#)

Lovy-Wheeler A, Wilson KL, Baskin TI, Hepler PK (2005) Enhanced fixation reveals the apical cortical fringe of actin filaments as a consistent feature of the pollen tube. Planta 221: 95-104

Pubmed: [Author and Title](#)

Google Scholar: [Author Only](#) [Title Only](#) [Author and Title](#)

Luo N, Yan A, Liu G, Guo J, Rong D, Kanaoka MM, Xiao Z, Xu G, Higashiyama T, Cui X, Yang Z (2017) Exocytosis-coordinated mechanisms for tip growth underlie pollen tube growth guidance. Nat. Commun. 8: 1687

Pubmed: [Author and Title](#)

Google Scholar: [Author Only](#) [Title Only](#) [Author and Title](#)

Luo N, Yan A, Yang Z (2016) Measuring exocytosis rate using corrected fluorescence recovery after photoconversion. Traffic 17: 554-564

Pubmed: [Author and Title](#)

Google Scholar: [Author Only](#) [Title Only](#) [Author and Title](#)

Martiniere A, Lavagi I, Nageswaran G, Rolfe DJ, Maneta-Peyret L, Luu DT, Botchway SW, Webb SED, Mongrand S, Maurel C, Martin-Fernandez ML, Kleine-Vehn J, Friml J, Moreau P, Runions J (2012) Cell wall constrains lateral diffusion of plant plasma-membrane proteins. *Proc. Natl. Acad. Sci. USA* 109: 12805-12810

Pubmed: [Author and Title](#)

Google Scholar: [Author Only](#) [Title Only](#) [Author and Title](#)

McKenna ST, Kunkel JG, Bosch M, Rounds CM, Vidali L, Winship LJ, Hepler PK (2009) Exocytosis precedes and predicts the increase in growth in oscillating pollen tubes. *Plant Cell* 21: 3026-3040

Pubmed: [Author and Title](#)

Google Scholar: [Author Only](#) [Title Only](#) [Author and Title](#)

Medina J, Catalá R, J S (2001) Developmental and stress regulation of RCI2A and RCI2B, two cold-inducible genes of Arabidopsis encoding highly conserved hydrophobic proteins. *Plant Physiology* 125: 1655-1666

Pubmed: [Author and Title](#)

Google Scholar: [Author Only](#) [Title Only](#) [Author and Title](#)

Meunier FA, Gutierrez LM (2016) Captivating new roles of F-actin cortex in exocytosis and bulk endocytosis in neurosecretory cells. *Trends in neurosciences* 39: 605-613

Pubmed: [Author and Title](#)

Google Scholar: [Author Only](#) [Title Only](#) [Author and Title](#)

Miller DD, Lancelle SA, Hepler PK (1996) Actin microfilaments do not form a dense meshwork in *Lilium longiflorum* pollen tube tips. *Protoplasma* 195: 123-132

Pubmed: [Author and Title](#)

Google Scholar: [Author Only](#) [Title Only](#) [Author and Title](#)

Miyawaki KN, Yang Z (2014) Extracellular signals and receptor-like kinases regulating ROP GTPases in plants. *Front. Plant Sci.* 5: 449

Pubmed: [Author and Title](#)

Google Scholar: [Author Only](#) [Title Only](#) [Author and Title](#)

Mollet JC, Leroux C, Dardelle F, Lehner A (2013) Cell wall composition, biosynthesis and remodeling during pollen tube growth. *Plants* 2: 107-147

Pubmed: [Author and Title](#)

Google Scholar: [Author Only](#) [Title Only](#) [Author and Title](#)

Montes-Rodriguez A, Kost B (2017) Direct comparison of the performance of commonly employed in vivo F-actin markers (Lifeact-YFP, YFP-mTn and YFP-FABD2) in tobacco pollen tubes. *Front. Plant Sci.* 8: 1-14

Pubmed: [Author and Title](#)

Google Scholar: [Author Only](#) [Title Only](#) [Author and Title](#)

Moscattelli A, Ciampolini F, Rodighiero S, Onelli E, Cresti M, Santo N, Idilli A (2007) Distinct endocytic pathways identified in tobacco pollen tubes using charged nanogold. *J. Cell Sci.* 120: 3804-3819

Pubmed: [Author and Title](#)

Google Scholar: [Author Only](#) [Title Only](#) [Author and Title](#)

Moscattelli A, Idilli AI, Rodighiero S, Caccianiga M (2012) Inhibition of actin polymerisation by low concentration Latrunculin B affects endocytosis and alters exocytosis in shank and tip of tobacco pollen tubes. *Plant biology* 14: 770-782

Pubmed: [Author and Title](#)

Google Scholar: [Author Only](#) [Title Only](#) [Author and Title](#)

Muro K, Matsuura-Tokita K, Tsukamoto R, Kanaoka MM, Ebine K, Higashiyama T, Nakano A, Ueda T (2018) ANTH domain-containing proteins are required for the pollen tube plasma membrane integrity via recycling ANXUR kinases. *Commun. Biol.* 1: 152

Pubmed: [Author and Title](#)

Google Scholar: [Author Only](#) [Title Only](#) [Author and Title](#)

Nebenführ A, Ritzenthaler C, Robinson DG (2002) Brefeldin A: deciphering an enigmatic inhibitor of secretion. *Plant Physiology* 130: 1102-1108

Pubmed: [Author and Title](#)

Google Scholar: [Author Only](#) [Title Only](#) [Author and Title](#)

Paciorek T, Zazimalova E, Ruthardt N, Petrasek J, Stierhof YD, Kleine-Vehn J, Morris DA, Emans N, Jurgens G, Geldner N, Friml J (2005) Auxin inhibits endocytosis and promotes its own efflux from cells. *Nature* 435: 1251-1256

Pubmed: [Author and Title](#)

Google Scholar: [Author Only](#) [Title Only](#) [Author and Title](#)

Paez Valencia J, Goodman K, Otegui MS (2016) Endocytosis and endosomal trafficking in plants. *Ann. Rev. Plant Biol.* 67: 309-335

Pubmed: [Author and Title](#)

Google Scholar: [Author Only](#) [Title Only](#) [Author and Title](#)

Parre E, Geitmann A (2005) Pectin and the role of the physical properties of the cell wall in pollen tube growth of *Solanum chacoense*. *Planta* 220: 582-592

Pubmed: [Author and Title](#)

Google Scholar: [Author Only](#) [Title Only](#) [Author and Title](#)

- Parton RM, Fischer-Parton S, Trewavas AJ, Watahiki MK (2003) Pollen tubes exhibit regular periodic membrane trafficking events in the absence of apical extension. Journal of Cell Science 116: 2707-2719**
Pubmed: [Author and Title](#)
Google Scholar: [Author Only](#) [Title Only](#) [Author and Title](#)
- Parton RM, Fischer-Parton S, Watahiki MK, Trewavas AJ (2001) Dynamics of the apical vesicle accumulation and the rate of growth are related in individual pollen tubes. Journal of Cell Science 114: 2685-2695**
Pubmed: [Author and Title](#)
Google Scholar: [Author Only](#) [Title Only](#) [Author and Title](#)
- Perez-Gomez J, Moore I (2007) Plant endocytosis: it is clathrin after all. Curr. Biol. 17: R217-219**
Pubmed: [Author and Title](#)
Google Scholar: [Author Only](#) [Title Only](#) [Author and Title](#)
- Picton JM, Steer MW (1983) Membrane recycling and the control of secretory activity in pollen tubes. J. Cell Sci. 63: 303-320**
Pubmed: [Author and Title](#)
Google Scholar: [Author Only](#) [Title Only](#) [Author and Title](#)
- Potocky M, Pleskot R, Pejchar P, Vitale N, Kost B, Zarsky V (2014) Live-cell imaging of phosphatidic acid dynamics in pollen tubes visualized by Spo20p-derived biosensor. New Phytol. 203: 483-494**
Pubmed: [Author and Title](#)
Google Scholar: [Author Only](#) [Title Only](#) [Author and Title](#)
- Qin Y, Yang Z (2011) Rapid tip growth: insights from pollen tubes. Semin. Cell Dev. Biol. 22: 816-824**
Pubmed: [Author and Title](#)
Google Scholar: [Author Only](#) [Title Only](#) [Author and Title](#)
- Qu X, Zhang H, Xie Y, Wang J, Chen N, Huang S (2013) Arabidopsis villins promote actin turnover at pollen tube tips and facilitate the construction of actin collars. Plant Cell 25: 1803-1817**
Pubmed: [Author and Title](#)
Google Scholar: [Author Only](#) [Title Only](#) [Author and Title](#)
- Qu X, Zhang H, Zhang M, Diao M, Xue Y, Huang S (2017) Organizational innovation of apical actin filaments drives rapid pollen tube growth and turning. Mol. Plant 10: 930-947**
Pubmed: [Author and Title](#)
Google Scholar: [Author Only](#) [Title Only](#) [Author and Title](#)
- Read SM, Clarke AE, Bacic A (1993) Requirements for division of the generative nucleus in cultured pollen tubes of Nicotiana. Protoplasma 174: 101-115**
Pubmed: [Author and Title](#)
Google Scholar: [Author Only](#) [Title Only](#) [Author and Title](#)
- Read SM, Clarke AE, Bacic A (1993) Stimulation of growth of cultured Nicotiana tabacum W 38 pollen tubes by poly(ethylene glycol) and Cu(II) salts. Protoplasma 177: 1-14**
Pubmed: [Author and Title](#)
Google Scholar: [Author Only](#) [Title Only](#) [Author and Title](#)
- Reyes FC, Buono R, Otegui MS (2011) Plant endosomal trafficking pathways. Current Opinion in Plant Biology 14: 666-673**
Pubmed: [Author and Title](#)
Google Scholar: [Author Only](#) [Title Only](#) [Author and Title](#)
- Riedl J, Crevenna AH, Kessenbrock K, Yu JH, Neukirchen D, Bista M, Bradke F, Jenne D, Holak TA, Werb Z, Sixt M, Wedlich-Soldner R (2008) Lifeact: a versatile marker to visualize F-actin. Nat. Methods 5: 605-607**
Pubmed: [Author and Title](#)
Google Scholar: [Author Only](#) [Title Only](#) [Author and Title](#)
- Rockel N, Wolf S, Kost B, Rausch T, Greiner S (2008) Elaborate spatial patterning of cell-wall PME and PME1 at the pollen tube tip involves PME1 endocytosis, and reflects the distribution of esterified and de-esterified pectins. Plant J., 53: 133-143**
Pubmed: [Author and Title](#)
Google Scholar: [Author Only](#) [Title Only](#) [Author and Title](#)
- Rounds CM, Hepler PK, Winship LJ (2014) The apical actin fringe contributes to localized cell wall deposition and polarized growth in the lily pollen tube. Plant physiology 166: 139-151**
Pubmed: [Author and Title](#)
Google Scholar: [Author Only](#) [Title Only](#) [Author and Title](#)
- Saffman PG, Delbruck M, Delbrück M (1975) Brownian motion in biological membranes. Proc. Natl. Acad. Sci. USA 72: 3111-3113**
Pubmed: [Author and Title](#)
Google Scholar: [Author Only](#) [Title Only](#) [Author and Title](#)
- Samaj J, Muller J, Beck M, Bohm N, Menzel D (2006) Vesicular trafficking, cytoskeleton and signalling in root hairs and pollen tubes. Trends Plant Sci. 11: 594-600**
Pubmed: [Author and Title](#)
Google Scholar: [Author Only](#) [Title Only](#) [Author and Title](#)

Sambrook JF, Russell DW (2014) Molecular cloning: a laboratory manual, Ed Fourth edi. Cold Spring Harbor Laboratory Press

Pubmed: [Author and Title](#)

Google Scholar: [Author Only Title Only Author and Title](#)

Schneider S, Schneidereit A, Konrad KR, Hajirezaei M-R, Gramann M, Hedrich R, Sauer N (2006) Arabidopsis INOSITOL TRANSPORTER4 mediates high-affinity H1 symport of myoinositol across the plasma membrane. Plant Physiology 141: 565-577

Pubmed: [Author and Title](#)

Google Scholar: [Author Only Title Only Author and Title](#)

Sekeres J, Pejchar P, Santrucek J, Vukasinovic N, Zarsky V, Potocky M (2017) Analysis of exocyst subunit EXO70 family reveals distinct membrane domains in tobacco pollen tubes. Plant Physiol. 173: 1659-1675

Pubmed: [Author and Title](#)

Google Scholar: [Author Only Title Only Author and Title](#)

Serna L (2005) A simple method for discriminating between cell membrane and cytosolic proteins. New Phytol. 165: 947-952

Pubmed: [Author and Title](#)

Google Scholar: [Author Only Title Only Author and Title](#)

Shao S, Hegde RS (2011) Membrane protein insertion at the endoplasmic reticulum. Annual Review of Cell and Developmental Biology 27: 25-56

Pubmed: [Author and Title](#)

Google Scholar: [Author Only Title Only Author and Title](#)

Sierro N, Battey JN, Ouadi S, Bakaher N, Bovet L, Willig A, Goepfert S, Peitsch MC, Ivanov NV (2014) The tobacco genome sequence and its comparison with those of tomato and potato. Nat. Commun. 5: 3833

Pubmed: [Author and Title](#)

Google Scholar: [Author Only Title Only Author and Title](#)

Snapp E (2005) Design and Use of Fluorescent Fusion Proteins in Cell Biology. Curr. Protoc. Cell Biol. Chapter 21: 21.24.21-21.24.13

Pubmed: [Author and Title](#)

Google Scholar: [Author Only Title Only Author and Title](#)

Soboleski MR, Oaks J, Halford WP (2005) Green fluorescent protein is a quantitative reporter of gene expression in individual eukaryotic cells. FASEB J. 19: 440-442

Pubmed: [Author and Title](#)

Google Scholar: [Author Only Title Only Author and Title](#)

Sousa E, Kost B, Malho R (2008) Arabidopsis Phosphatidylinositol-4-Monophosphate 5-Kinase 4 Regulates Pollen Tube Growth and Polarity by Modulating Membrane Recycling. Plant Cell 20: 3050-3064

Pubmed: [Author and Title](#)

Google Scholar: [Author Only Title Only Author and Title](#)

Stavrou I, O'Halloran T (2006) The monomeric clathrin assembly protein, AP180, regulates contractile vacuole size in Dictyostelium discoideum. Molecular Biology of the Cell 18: 986-994

Pubmed: [Author and Title](#)

Google Scholar: [Author Only Title Only Author and Title](#)

Steer MW, Steer JM (1989) Pollen tube tip growth. New Phytol. 111: 323-358

Pubmed: [Author and Title](#)

Google Scholar: [Author Only Title Only Author and Title](#)

Stenzel I, Ischebeck T, Quint M, Heilmann I (2012) Variable regions of PI4P 5-kinases direct PtdIns(4,5)P2 towards alternative regulatory functions in tobacco pollen tubes. Frontiers in Plant Science 2

Pubmed: [Author and Title](#)

Google Scholar: [Author Only Title Only Author and Title](#)

Stephan O, Cottier S, Fahlen S, Montes-Rodriguez A, Sun J, Eklund DM, Klahre U, Kost B (2014) RISAP is a TGN-associated RAC5 effector regulating membrane traffic during polar cell growth in tobacco. Plant Cell 26: 4426-4447

Pubmed: [Author and Title](#)

Google Scholar: [Author Only Title Only Author and Title](#)

Student B (1908) The probable error of a mean. Biometrika 6: 1-25

Pubmed: [Author and Title](#)

Google Scholar: [Author Only Title Only Author and Title](#)

Sun J, Eklund DM, Montes-Rodriguez A, Kost B (2015) In vivo Rac/Rop localization as well as interaction with RhoGAP and RhoGDI in tobacco pollen tubes: analysis by low-level expression of fluorescent fusion proteins and bimolecular fluorescence complementation. Plant J. 84: 83-98

Pubmed: [Author and Title](#)

Google Scholar: [Author Only Title Only Author and Title](#)

Thompson MV, Wolniak SM (2008) A plasma membrane-anchored fluorescent protein fusion illuminates sieve element plasma membranes in arabidopsis and tobacco. Plant Physiol. 146: 1599-1610

Pubmed: [Author and Title](#)

Google Scholar: [Author Only Title Only Author and Title](#)

- Trimble WS, Grinstein S (2015) Barriers to the free diffusion of proteins and lipids in the plasma membrane. Journal of Cell Biology 208: 259-271**
Pubmed: [Author and Title](#)
Google Scholar: [Author Only Title Only Author and Title](#)
- Tse YC, Lo SW, Hillmer S, Dupree P, Jiang L (2006) Dynamic response of prevacuolar compartments to brefeldin A in plant cells. Plant Physiology 142: 1442-1459**
Pubmed: [Author and Title](#)
Google Scholar: [Author Only Title Only Author and Title](#)
- Tukey JW (1949) Comparing individual means in the analysis of variance. Biometrics 5: 99-99**
Pubmed: [Author and Title](#)
Google Scholar: [Author Only Title Only Author and Title](#)
- Twell D, Yamaguchi J, McCormick S (1990) Pollen-specific gene expression in transgenic plants: coordinate regulation of two different tomato gene promoters during microsporogenesis. Development 109: 705-713**
Pubmed: [Author and Title](#)
Google Scholar: [Author Only Title Only Author and Title](#)
- Uemura T (2016) Physiological roles of plant post-golgi transport pathways in membrane trafficking. Plant Cell Physiol. 57: 2013-2019**
Pubmed: [Author and Title](#)
Google Scholar: [Author Only Title Only Author and Title](#)
- Uemura T, Nakano RT, Takagi J, Wang Y, Kramer K, Finkemeier I, Nakagami H, Tsuda K, Ueda T, Schulze-Lefert P, Nakano A (2019) A Golgi-Released Subpopulation of the Trans-Golgi Network Mediates Protein Secretion in Arabidopsis. Plant Physiol 179: 519-532**
Pubmed: [Author and Title](#)
Google Scholar: [Author Only Title Only Author and Title](#)
- Van Gisbergen PAC, Esseling-Ozdoba A, Vos JW (2008) Microinjecting FM4-64 validates it as a marker of the endocytic pathway in plants. J. Microsc. 231: 284-290**
Pubmed: [Author and Title](#)
Google Scholar: [Author Only Title Only Author and Title](#)
- Vidali L, Rounds CM, Hepler PK, Bezanilla M (2009) Lifeact-mEGFP reveals a dynamic apical F-Actin Network in tip growing plant cells. PLoS ONE 4: e5744**
Pubmed: [Author and Title](#)
Google Scholar: [Author Only Title Only Author and Title](#)
- Viklund H, Bernsel A, Skwark M, Elofsson A (2008) SPOCTOPUS: a combined predictor of signal peptides and membrane protein topology. Bioinformatics 24: 2928-2929**
Pubmed: [Author and Title](#)
Google Scholar: [Author Only Title Only Author and Title](#)
- Vrljic M, Nishimura SY, Bresselet S, Moerner WE, McConnell HM (2002) Translational diffusion of individual class II MHC membrane proteins in cells. Biophysical journal 83: 2681-2692**
Pubmed: [Author and Title](#)
Google Scholar: [Author Only Title Only Author and Title](#)
- Wang H, Zhuang X, Cai Y, Cheung AY, Jiang L (2013) Apical F-actin-regulated exocytic targeting of NtPPME1 is essential for construction and rigidity of the pollen tube cell wall. Plant J., 76: 367-379**
Pubmed: [Author and Title](#)
Google Scholar: [Author Only Title Only Author and Title](#)
- Wang H, Zhuang X, Wang X, Law AH, Zhao T, Du S, Loy MM, Jiang L (2016) A distinct pathway for polar exocytosis in plant cell wall formation. Plant Physiol 172: 1003-1018**
Pubmed: [Author and Title](#)
Google Scholar: [Author Only Title Only Author and Title](#)
- Wang H, Zhuang XH, Hillmer S, Robinson DG, Jiang LW (2011) Vacuolar sorting receptor (VSR) proteins reach the plasma membrane in germinating pollen tubes. Mol. Plant 4: 845-853**
Pubmed: [Author and Title](#)
Google Scholar: [Author Only Title Only Author and Title](#)
- Wang Q, Kong L, Hao H, Wang X, Lin J, Samaj J, Baluska F (2005) Effects of Brefeldin A on pollen germination and tube growth. antagonistic effects on endocytosis and secretion. Plant Physiol. 139: 1692-1703**
Pubmed: [Author and Title](#)
Google Scholar: [Author Only Title Only Author and Title](#)
- Wang X, Chung KP, Lin W, Jiang L (2017) Protein secretion in plants: conventional and unconventional pathways and new techniques. J. Exp. Bot. 69: 21-37**
Pubmed: [Author and Title](#)
Google Scholar: [Author Only Title Only Author and Title](#)
- Wang X, Teng Y, Wang Q, Li X, Sheng X, Zheng M, Samaj J, Baluska F, Lin J (2006) Imaging of dynamic secretory vesicles in living**

pollen tubes of *Picea meyeri* using evanescent wave microscopy. *Plant Physiol.* 141: 1591-1603

Pubmed: [Author and Title](#)

Google Scholar: [Author Only](#) [Title Only](#) [Author and Title](#)

Weiß K, Neef A, Van Q, Kramer S, Gregor I, Enderlein J (2013) Quantifying the diffusion of membrane proteins and peptides in black lipid membranes with 2-focus fluorescence correlation spectroscopy. *Biophysical Journal* 105: 455-462

Pubmed: [Author and Title](#)

Google Scholar: [Author Only](#) [Title Only](#) [Author and Title](#)

Wilson KL, Lovy-Wheeler A, Voigt B, Menzel D, Kunkel JG, Hepler PK (2006) Imaging the actin cytoskeleton in growing pollen tubes. *Sexual Plant Reproduction* 19: 51-62

Pubmed: [Author and Title](#)

Google Scholar: [Author Only](#) [Title Only](#) [Author and Title](#)

Yalovsky S, Bloch D, Sorek N, Kost B (2008) Regulation of membrane trafficking, cytoskeleton dynamics, and cell polarity by ROP/RAC GTPases. *Plant Physiology* 147: 1527-1543

Pubmed: [Author and Title](#)

Google Scholar: [Author Only](#) [Title Only](#) [Author and Title](#)

Zarsky V, Cvrckova F, Potocky M, Hala M (2009) Exocytosis and cell polarity in plants - exocyst and recycling domains. *New Phytol.* 183: 255-272

Pubmed: [Author and Title](#)

Google Scholar: [Author Only](#) [Title Only](#) [Author and Title](#)

Zerzour R, Kroeger J, Geitmann A (2009) Polar growth in pollen tubes is associated with spatially confined dynamic changes in cell mechanical properties. *Dev. Biol.* 334: 437-446

Pubmed: [Author and Title](#)

Google Scholar: [Author Only](#) [Title Only](#) [Author and Title](#)

Zhang Y, McCormick S (2007) A distinct mechanism regulating a pollen-specific guanine nucleotide exchange factor for the small GTPase Rop in *Arabidopsis thaliana*. *Proceedings of the National Academy of Sciences of the United States of America* 104: 18830-18835

Pubmed: [Author and Title](#)

Google Scholar: [Author Only](#) [Title Only](#) [Author and Title](#)

Zhao XY, Wang Q, Li S, Ge FR, Zhou LZ, McCormick S, Zhang Y (2013) The juxtamembrane and carboxy-terminal domains of *Arabidopsis* PRK2 are critical for ROP-ind. *Journal of Experimental Botany* 64: 5599-5610

Pubmed: [Author and Title](#)

Google Scholar: [Author Only](#) [Title Only](#) [Author and Title](#)

Zhao Y, Yan A, Feijó JA, Furutani M, Takenawa T, Hwang I, Fu Y, Yang Z (2010) Phosphoinositides regulate clathrin-dependent endocytosis at the tip of pollen tubes in *Arabidopsis* and tobacco. *Plant Cell* 22: 4031-4044

Pubmed: [Author and Title](#)

Google Scholar: [Author Only](#) [Title Only](#) [Author and Title](#)

Zonia L, Munnik T (2008) Vesicle trafficking dynamics and visualization of zones of exocytosis and endocytosis in tobacco pollen tubes. *Journal of Experimental Botany* 59: 861-873

Pubmed: [Author and Title](#)

Google Scholar: [Author Only](#) [Title Only](#) [Author and Title](#)